Calibration of Upward and Downward Looking Violet Photometers

M. Tomasko, M. Prout, and L. MacFarlane

I. Introduction

This document describes the calibration of the Upward-Looking and Downward-Looking Violet Photometers (ULV and DLV) of the flight model (SN03) of the Descent Imager/Spectral Radiometer (DISR) of the Huygens Probe on the Cassini Mission. These photometers have filtered silicon detectors behind a transmitting diffusing plate at the center of external "bears ear" baffles. The external baffles limit the field of view of the ULV and DLV to about 170 degrees in azimuth and from 5 to 90 degrees of zenith angle for the ULV and from 90 to 175 degrees zenith angle for the DLV. The diffusing plate makes the response relatively constant in azimuth and approximates a cosine function in zenith angle. The filter over the silicon detector is intended to define the response of the system to be relatively flat and limited to the region from 350 to 480 nm. The goal of the calibration is to measure the actual relative spectral response of the ULV and DLV optical systems over a range of temperatures from about 300 K to 200 K, to measure the absolute responsivity of the systems as a function of temperature over this temperature range, to measure the bias of the photometers as a function of temperature, and to measure the relative spatial response as a function of azimuth and zenith angle at room temperature.

The ULV and DLV photometers also receive light from internal calibration lamp system via quartz fibers. The fibers bounce light off the back of the diffuser plate on the ULV or DLV systems to illuminate the photometers. The response of the ULV and DLV photometers has been tracked from instrument delivery throughout the cruise to Titan using this inflight calibration system, and the results are available in our series of inflight checkout reports published after each of our cruise checkouts conducted approximately twice yearly.

This report begins with a brief description of the optical system of the ULV and DLV systems. It then summarizes the calibration of the relative spectral response of the systems as a function of temperature. This is followed by a description of the calibration of the absolute responsivity of the ULV and DLV systems as a function of temperature. We also describe the measurement of the relative spatial response of the ULV and DLV systems at room temperature. We conclude with notes of our plans to determine the upward, downward direct, downward diffuse, and net solar flux in the bandpass of the ULV/DLV systems from our measurements during the descent into Titan's atmosphere.

II. Overview of Optical System

The external "bears ear" baffles used for the ULV and DLV systems are shown in Fig. 1. The purpose of these baffles is to limit the field of view of these optical systems to 170 degrees in azimuth and 85 degrees in zenith (or nadir). The region within 5 degrees of the zenith is excluded in the ULV system to avoid seeing the parachute. The region within 5 degrees of the nadir is excluded to make the field of view of the DLV similar to that of the ULV. In fact, the ULV system shares its diffuser and bear's ear baffle with the Upward-Looking Visible Spectrometer (ULVS), and so includes the shadow bar that sometimes blocks the direct solar beam.

The optical system consists of a small transmitting diffuser measuring 4 by 5 mm at the center of the bears ear baffle. The silicon photometer covered by an interference filter is located behind the diffuser. The electrical system for reading the output of the photometer has a fixed gain for each photometer, with the gain of the DLV an order of magnitude greater than that of the ULV because of the expected relative signal levels of the upward and downward streaming ultraviolet radiation on Titan. The electrical signals are digitized using a 12-bit analog to digital (A/D) converter in the DISR sensor head. This A/D converter is the same one used for sensing temperatures and other housekeeping functions in the sensor head.

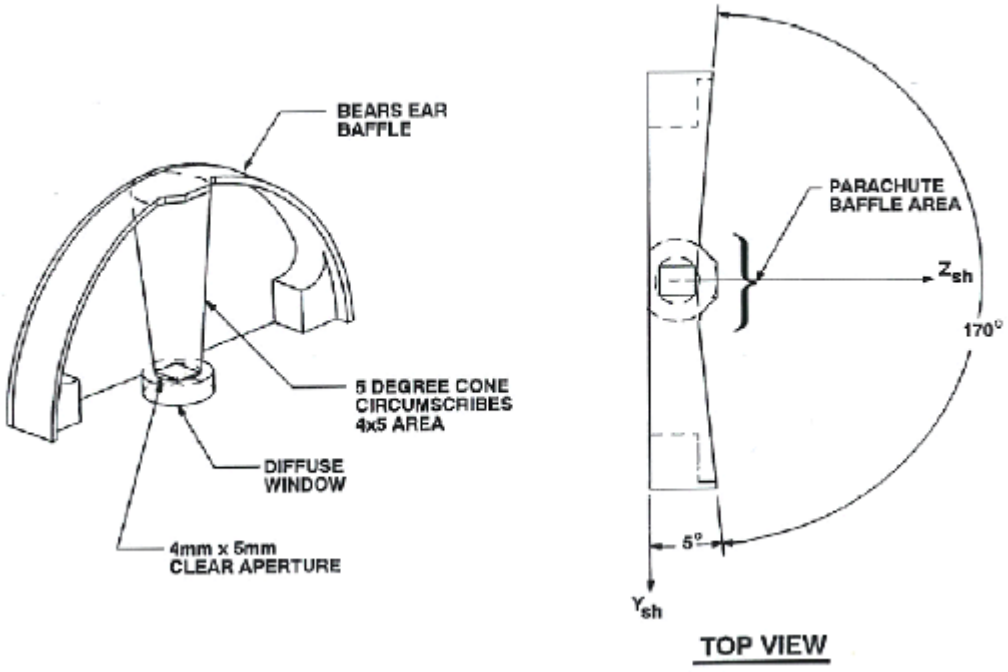

Fig. 1. The shape of the "bear's ear" baffle which surrounds the diffuse of the upward-looking infrared spectrometer to define its limit its field of view to 170° in azimuth and to the range from 5° to nearly 90° in zenith angle. The region within 5° of the zenith is masked to avoid viewing the parachute. The shape of the baffle for the DLV is the same as for the ULV.

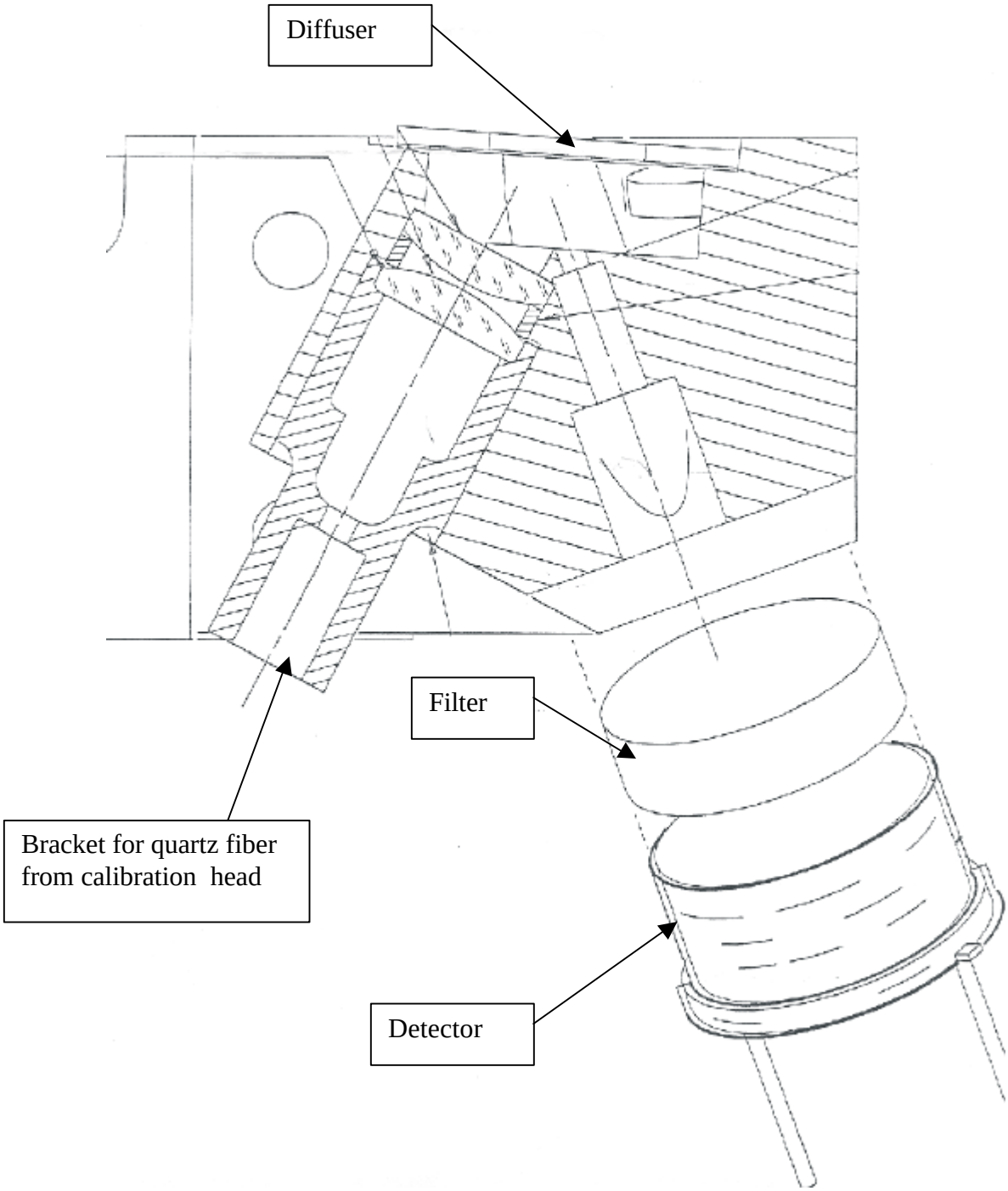

Fig. 2. Schematic view showing the detector used in the ULV system, its filter, the block holding the filter and detector in the proper location to view the diffuser mounted at the top of the drawing, and the bracket and lenses used to bring light from the inflight calibration lamp assembly via a quartz fiber.

III. Relative Spectral Response as a function of temperature

A. Method used for reduction of relative spectral measurements

The relative spectral response measurements for the ULV/DLV systems must be made over a range of temperatures from about ambient (300 K) down to some 200 K, the operating temperature deep in Titan's atmosphere. We used an integrating sphere in order to make measurements of the relative spectral response of the ULV/DLV systems with their wide spatial fields of view over a wide temperature range. This approach decreased the intensity of the light incident on the ULV/DLV systems, but permitted us to measure the relative spectral response of these systems over the required range of temperatures. The signal levels using the integrating sphere were too low to permit use of our monochrometer to illuminate the violet photometers. We used a high intensity lamp and a set of filters with nominal 10 nm full width at half maximum response to illuminate the integrating sphere. A standard silicon detector with known relative spectral response looking into one of the ports of the integrating sphere was used to determine the intensity of the wall of the integrating sphere for each of the 18 filters centered from 330 nm to 500 nm. The ULV and DLV signals were measured in the when the sphere was illuminated through each filter. For every other filter, the beam from the high intensity lamp was blocked, and the response of the ULV/DLV systems with no incident illumination was measured. Thus, the data collected at each temperature consisted of the bright and dark readings of the violet photometers, and the current produced by the standard silicon detector looking at the wall of the integrating sphere when the lamp illuminated the sphere through each of the filters. The relative spectral response of the standard detector is also available from the literature from the standard detector manufacturer (xxxx).

The data are reduced as follows. The signal on the standard detector C, is given by

$$C(i) = Resp_{std\ \det} \int I(l) T_i(l) RelSpecResp_{std\ \det}(l) dl \quad . \qquad (1.)$$

Here C(i) is the signal current measured by the standard detector with absolute responsivity $Resp_{std\ \det}(l)$, and relative spectral response $RelSpecResp_{std\ \det}(l)$. $T_i(\lambda)$ is the transmission of filter i, and I(λ) is the intensity of the lamp as a function of wavelength before it passes through the filter. The signal measured by the ULV or DLV system is given by

$$DN_{bright}(ULV) = Resp_{ULV} \int I(l) T_i(l) RelSpecResp_{ULV}(l) dl + DN_{dark}(ULV) \quad . \qquad (2.)$$

Here the absolute responsivity and relative spectral response of the ULV system is indicated, and the data number when the light passes into the sphere (DN_{bright}) includes a contribution from the bias of the violet system (DN_{dark}) produced even when no light is permitted to shine on the violet system.

In our first pass at the reduction of these data, we assume that the relative spectral response of the standard detector and of the violet photometers does not change much over the bandpass of the 10 nm full width at half maximum response of the filters used to

measure the relative spectral response of the violet system. In this case, the relative spectral response of the standard detector can be moved outside the integral in eqn. (1) and the relative spectral response of the violet photometer can be moved outside the integral in equation (2). Rearranging eqn. (1) then gives

$$\int I(\lambda)T_i(\lambda)d\lambda = C(i)/[Resp_{std\ \det} RelSpecResp_{std\ \det}(\lambda_i)]. \qquad (3.)$$

Rearranging eqn. (2) gives

$$RelSpecResp_{ULV}(\lambda_i) = \frac{DN_{bright}(ULV) - DN_{dark}(ULV)}{Resp_{ULV}\int I(\lambda)T(\lambda)d\lambda}. \qquad (4.)$$

Now substituting from eqn. (3) into eqn. (4) gives

$$RelSpecResp_{ULV}(\lambda) =$$

$$\frac{DN_{bright}(ULV) - DN_{dark}(ULV)}{C(i)}\left(\frac{Resp_{std\ \det}}{Resp_{ULV}}\right)RelSpecResp_{std\ \det}(\lambda). \qquad (5.)$$

The quantity in brackets in eqn. (5) is a constant independent of wavelength, and can be omitted so long as only the relative spectral response of the violet system is desired. After omission of this quantity, the resulting curve for the relative spectral response as a function of wavelength can be normalized to unity at the wavelength of the peak relative response. This gives

$$RelSpecResp_{ULV}(\lambda) =$$

$$\frac{DN_{bright}(ULV) - DN_{dark}(ULV)}{C(i)} RelSpecResp_{std\ \det}(\lambda) \qquad (6.)$$

before the renormalization.

However, using eqn. (6) for the relative spectral response of the violet photometer leaves open the question of the effective wavelength at which the relative spectral response has been found. There is a better approach for dealing with the integrals in eqns. (1) and (2) than simply assuming that the relative spectral response does not change much over the bandpass of the filter. Rather, if the relative spectral response can be described by a polynomial up to quadratic in wavelength over the bandpass of the filter, it is possible to define the short wavelength limit, the long wavelength limit, and the mean transmission of the filter so that the true mean relative spectral response between the short and long wavelength limits of the filter can be moved outside the integrals in eqns. (1) and (2). That is, for functions y(λ) up to quadratic in wavelength we have

$$\int_0^\infty w(\lambda)y(\lambda)d\lambda = \overline{w}\int_{\lambda 1}^{\lambda 2} y(\lambda)d\lambda \qquad (7.)$$

where

$$\lambda_1 = \tilde{\lambda} - \sqrt{3\left(\tilde{\lambda}^2 - \tilde{\lambda}\tilde{\lambda}\right)}, \qquad (8.)$$

$$\lambda_2 = \tilde{\lambda} + \sqrt{3\left(\tilde{\lambda}^2 - \tilde{\lambda}\tilde{\lambda}\right)}, \qquad (9.)$$

$$\overline{w} = \frac{\int w(\lambda)d\lambda}{\lambda_2 - \lambda_1}, \qquad (10.)$$

$$\tilde{\lambda} = \frac{\int \lambda\, w(\lambda)d\lambda}{\int w(\lambda)d\lambda}, \qquad (11.)$$

$$\tilde{\lambda}^2 = \frac{\int \lambda^2\, w(\lambda)d\lambda}{\int w(\lambda)d\lambda}. \qquad (12.)$$

Now we can use eqn. (7.) in eqns. (1) and (2) with w(λ)=*I(λ)T(λ)* to give

$$C(i) = Resp_{std\ \det}\,\overline{IT}\int_{\lambda 1}^{\lambda 2} RelSpecResp_{std\ \det}(\lambda)d\lambda\ . \qquad (13.)$$

and

$$DN_{bright}(ULV) = Resp_{ULV}\,\overline{IT}\int_{\lambda 1}^{\lambda 2} RelSpecResp_{ULV}(\lambda)d\lambda + DN_{dark}(ULV) \qquad (14.)$$

Now we can define the average relative spectral response of the ULV over the wavelength interval from λ_1 to λ_2 as

$$< RelSpecResp_{ULV} >= \frac{\int_{\lambda 1}^{\lambda 2} RelSpecResp_{ULV}(\lambda)d\lambda}{\lambda_2 - \lambda_1}\ . \qquad (15.)$$

Substituting (15) into (14) and solving for the mean relative spectral response gives

$$< RelSpecResp_{ULV} >= \frac{DN_{bright}(ULV) - DN_{dark}(ULV)}{\overline{IT}(\lambda_2 - \lambda_1)Resp_{ULV}}. \qquad (16.)$$

Taking the mean value of *IT* from eqn. (13) gives

$$< RelSpecResp_{ULV} >=$$

$$\frac{DN_{bright}(ULV) - DN_{dark}(ULV)}{C(i)} \left(\frac{Resp_{std\,\det}}{Resp_{ULV}} \right) \left\langle RelSpecResp_{std\,\det} \right\rangle, \qquad (17.)$$

where

$$< RelSpecResp_{std\,\det} >= \frac{\int_{l1}^{l2} RelSpecResp_{std\,\det}(l)\,dl}{l_2 - l_1}. \qquad (18.)$$

Again noting that the ratio of the absolute responsivities of the standard detector and the ULV is a constant independent of wavelength gives the average relative spectral response of the ULV over interval between λ_1 and λ_2 as

$$< RelSpecResp_{ULV} >=$$

$$\frac{DN_{bright}(ULV) - DN_{dark}(ULV)}{C(i)} \left\langle RelSpecResp_{std\,\det} \right\rangle. \qquad (19.)$$

Here the mean values of the relative spectral response using each of the series of filters needs to be normalized to unity at the maximum relative spectral response. Note that eqn. (19) is very similar to eqn. (6) except that in the derivation of eqn. (19) we have defined the effective wavelength limits of the measurement.

B. Noise in the ULV system and error propagation

Even with the use of 10 nm wide filters, the signals in the ULV and DLV systems at the short wavelength end of the response in the integrating sphere are weak. In order to improve the signal to noise ratio, 231 readings were collected with the lamp on through each of the 18 filters at each of the 5 temperatures for both the ULV and DLV measurements. Between every other filter, we blocked the light from the lamp by a shutter before entering the integrating sphere, and 100 dark readings were taken for both the ULV and DLV systems. It is useful to determine the noise in the individual bright and dark readings for the ULV and DLV systems, and the uncertainties in the averages of the sets of bright and dark readings.

Due to the lower fixed gain of the ULV system and the 12-bit digitization of the signals, quantization error is a dominant source of error in the ULV system. We have examined the 90 sets of 231 bright measurements at each of the 5 temperatures and 18 filters to attempt to determine the size of relatively small intrinsic noise in the ULV system in the presence of the large quantization error. This was done by forming the

average value of each of the 90 sets of measurements, truncating each average value, and examining the distribution of the remaining fractional values in each of the 90 measurements. If the true fractional values are randomly distributed and the electrical noise is very small, the fractional values would have large peaks near 0.0 and 1.0, with very few average values between 0.1 and 0.9. If the electrical noise is larger, then the histogram of average fractional parts would be flatter, with the limit being a flat histogram when the electrical noise exceeds about 0.5 DN so that the measured values are moved beyond the quantization step size before entering the analog-to-digital (A/D) converter. Averaging the measurements in this case gives a good estimate of the true average value, and decreases the uncertainty in the measured value. If, on the other hand, the electrical noise is less than about 0.1 DN, then essentially the same values come out of the A/D recorder for each measurement, and the uncertainty in the true value of the measured function is not decreased by averaging but is determined by the size of the quantization step.

Figure 3 below shows the histogram of the average fractional values measured for the ULV bright observations at the 5 temperatures and 18 filters. Note that the histogram is not flat, as would be expected for electrical noise of 0.5 DN or greater, but instead has large peaks near 0.0 and 1.0. Note that a large peak is also present near 0.5 DN, however. Our attempts to reproduce this peak near 0.5 DN in the histograms for models with variable electrical noise relative to the size of the quantization step were completely unsuccessful.

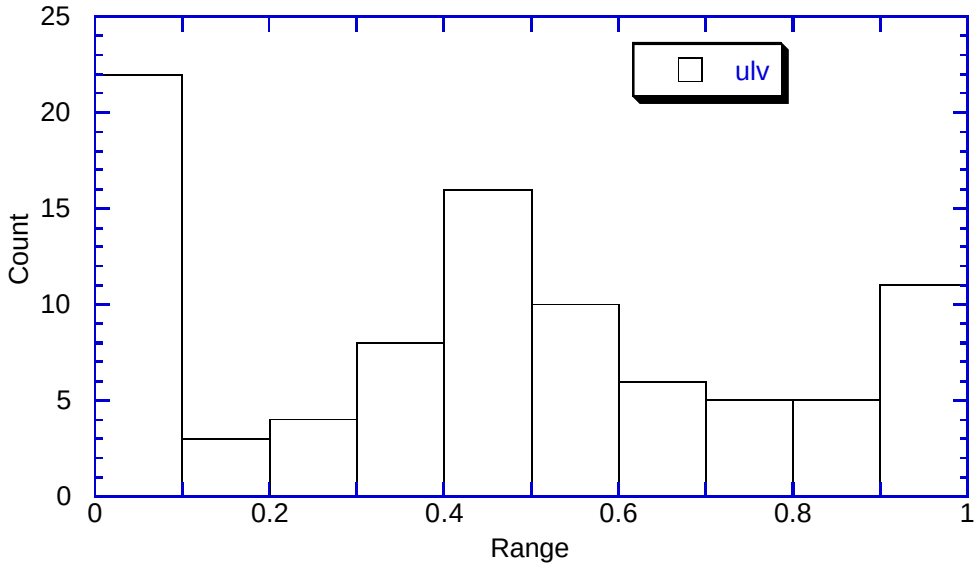

Fig.3. The histogram of the 90 sets of 231 measurements each collected through the 18 filters at the 5 temperatures during the ULV relative spectral response measurements. Note that a large peak near 0.5 DN is present in addition to the peaks expected near 0 and 1.0 DN.

A clue to the behavior of the ULV system may be seen in the behavior of the DLV system with its gain some factor 9 larger. With the larger gain, it can be seen that the ULV system produces histograms that are bimodal or trimodal depending on the mode of the instrument. That is, since the low level analog signals from the violet

photometers is amplified and digitized in the sensor head by the same A/D recorder used for reading the temperature sensors and all other housekeeping functions of the instrument, a small electrical cross talk from these other signals is picked up in the DLV signals depending on the mode of the measurements. These other peaks in the DLV system are displaced by 5 to 10 DN from the main peak in the DLV histogram. It is conjectured that the ULV system also suffers from some electrical cross talk in the sensor head depending on mode, but with its lower gain, the size of the shifts introduced in the ULV measurements might be about 0.5 DN. In this case the histogram above can be reproduced, and the size of the electrical noise as well as the size of the crosstalk shift can be determined.

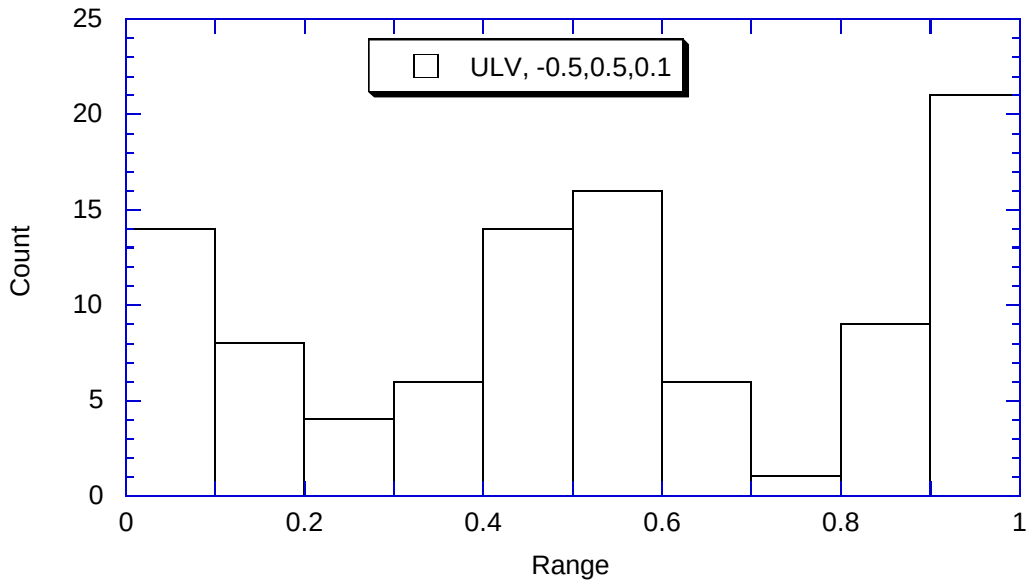

Fig. 4. A model histogram of the fractional parts of 90 sets of averages of 231 measurements is shown. The model introduces a shift of –0.5 dn 50% of the time due to electrical cross talk. A normally distributed electrical noise with a standard deviation of 0.1 DN is added. The data are then truncated in the A/D recorder. Note that a peak is introduced in the histogram near 0.5 DN in addition to the expected peaks near 0 and 1.0 DN. The histogram for this model is quite similar to the histogram observed in Fig. 3 for the ULV data collected in single measurement mode.

Figure 4 shows a model histogram for the fractional parts of 90 sets of averages of 231 samples when a fractional shift of –0.5 DN is introduced 50% of the time to simulate electrical cross talk. A normally distributed noise with a standard deviation of 0.1 DN is added to simulate electrical noise in the system before the data are truncated to simulate the A/D conversion. The histogram of the model in Fig. 4 is sufficiently similar to the observations in Fig. 3 to justify the use of such a model for reduction of ULV observations made in single measurement mode.

A second computer program was generated to determine the error in an infinitely large number of measurements in the presence of a variable crosstalk shift at a variable probability followed by electrical noise with a specified standard deviation followed by

truncation. The difference between the measured fractional value from the true signal as a function of the true fractional value of the signal is shown in Fig. 5.

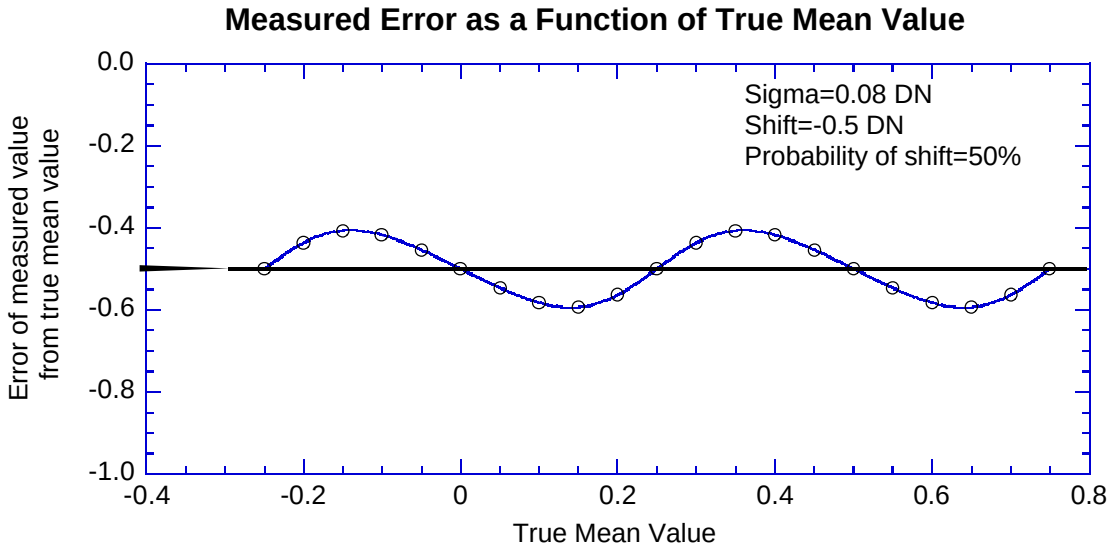

Fig. 5. Error in measured value after an infinite number of measurements as a function of the true fractional value of the measurements when the electrical noise has a standard deviation of 0.08 DN, and a crosstalk shift of –0.5 DN is added 50% of the time before truncation in the A/D converter. The maximum error (from the average truncation error of – 0.5 DN) is 0.1 DN. The rms truncation error is 0.064 DN.

The average error is –0.5 DN due to the truncation of the A/D converter. The error follows a curve around –0.5 DN with a maximum deviation of 0.1 DN. The rms deviation from the systematic error has a value of 0.064 DN. The maximum quantizatio error is less than 0.5 DN because of the shift of –0.5 DN introduced 50% of the time by the crosstalk. This corresponds to "dithering" the signal by 0.5 DN, and actually acts to reduce the maximum error due to quantization. We only suggest this behavior due to the presence of the observed peak in the histograms near 0.5 DN in Fig. 3 together with the clearly observed crosstalk in the DLV.

The actual error in measurements made in single measurement mode with the ULV results from the systematic quantization error shown in Fig. 5 combined in a square root-of-sum-of-squares way with the electrical noise reduced by 1/square root of the number of samples. Fig. 6 shows the behavior of the resulting total error when the maximum quantization error or the rms quantization error is combined with the electrical noise error. These errors are given by

$$s_{ULV} = \sqrt{\left(s^{2}_{quant} + s^{2}_{electrical} / N^{2} \right)}. \qquad (20.)$$

We take the maximum quantization error of 0.1 DN combined with an electrical noise with a standard deviation of 0.08 DN. Note that most of the benefit is realized by 10

samples. Increasing the number of samples above 10 or so produces very little additional reduction in the measurement error.

The error shown in Fig. 6 omits the systematic –0.5 DN shift produced by the truncation of the A/D converter. However, since the same shift is produced by the bright and dark measurements, the subtraction of the dark values from the bright measurements eliminates this effect. Thus we may take the error in the bright (or dark) ULV measurements from Fig. 6. For the reduction of the ULV data in this calibration report, we adopt an rms error of 0.1 DN so long as the number of observations exceeds 10 (which is does throughout our calibration measurements).

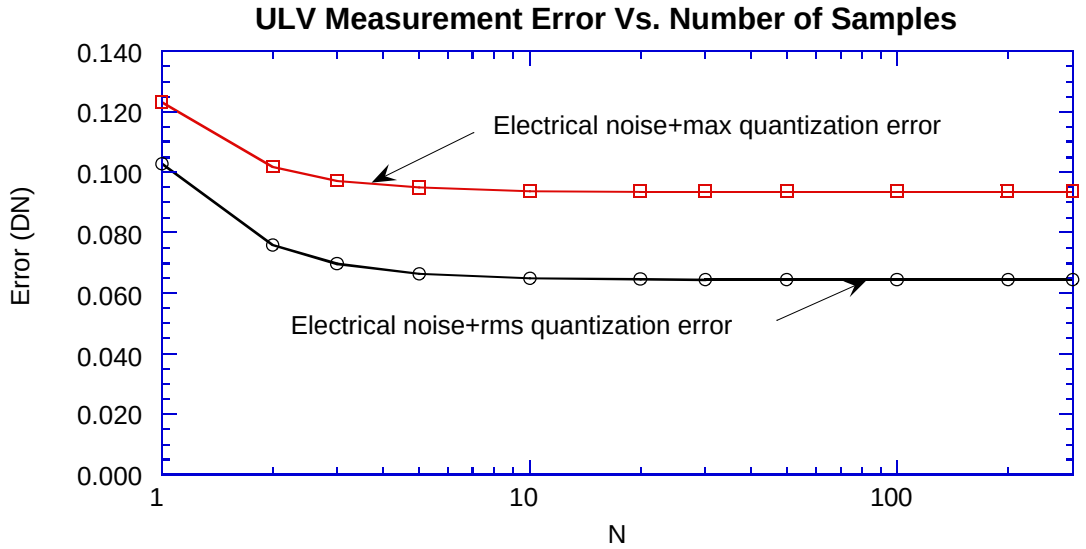

Fig. 6. Error for the ULV measurements is shown versus the number of samples. The curve with the squares is for the maximum quantization error, and the curve with the circles is for the rms quantization error combined with the electrical noise.

C. Noise in the DLV system and error propagation

The situation in the DLV is, if anything, even more complex than for the ULV. The distribution of the fractional values of the 90 sets of averages of 231 DLV bright measurements is shown in Fig. 7. Figure 7 does not show the concentration of values near 0.5 seen for the ULV in Fig. 3. There is also no very large concentration of values near 0 and 1.0 either, so the relatively flat shape of this histogram can be taken as evidence that the electrical noise in the DLV is 0.5 DN or larger, so there is hope that electrical noise can dither the signals up and down by a digital value and averaging the measured signal has some hope of beating down the noise.

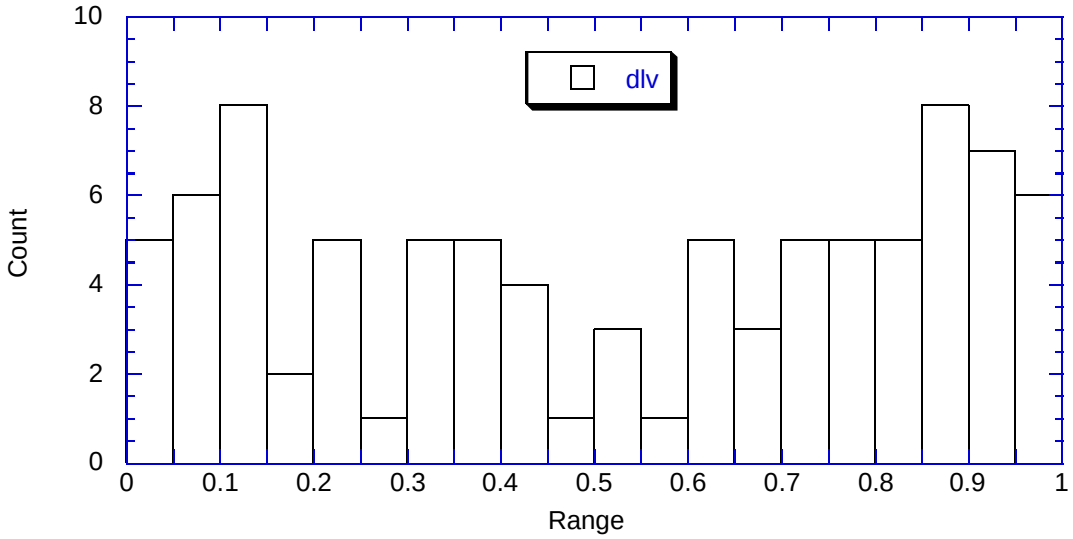

Fig. 7. Like Fig. 3 except for the fractional values of the 90 sets of averages of 231 measurements for the DLV in the relative spectral response data set. Unlike the situation for the ULV, the histogram is relatively flat, indicating that the electrical noise is some 0.5 DN or larger.

Figure 8 and 9 show the histograms of the 11 sets of 100 dark measurements each obtained during the relative spectral response measurements. Figure 8 shows the full histogram, indicating the presence of a strong peak centered on about 50 DN with a width of about 1 DN. However, as shown in the magnified view of Fig. 9, a significant population exists with shifts at about –10, -5, and +7 DN in the dark measurements made in single measurement mode. When the data are edited to remove these measurements, the standard deviation of the remaining data is about 0.64 DN in each of the 11 sets of dark measurements. If this were taken as the standard deviation of the electrical noise in the DLVS system, this value would be consistent with the relatively flat histogram in Fig. 7.

A similar situation exists for the bright measurements. When the bright data are edited to remove data more than 4 DN from the main peak, the standard deviation of the remaining measurement averages 0.642 DN, just as it does for the dark measurements. However, when the dark measurements are plotted as a function of time, the average measurements show drifts of some 0.33 DN from a smooth curve, even though averages of 100 measurements are included. Further, when the same filter was measured twice at 490 nm, the averages of the 231 measurements for each measurement differed by 0.77 DN, much more than should have been the case if the errors in the mean were decreasing as the reciprocal of the square root of the number of measurements. This is the case whether or not the measurements more than 4 DN from the main peak were eliminated from each of the two sets of measurements.

In short, it appears that another source of noise is present in the DLV data apart from the quantization noise, crosstalk, and a normally distributed electrical noise. The action of the other noise source appears to leave the uncertainty in the measurements at a level of about 0.3 to 0.8 DN regardless of how many measurements are averaged. For the reduction of the relative spectral response measurements made in single measurement

mode by the DLV, we will take the standard deviation of the measurements as 0.32 DN regardless of whether 100 or 231 measurements are averaged. We will also continue to observe the statistics of the ULV and the DLV during the descent measurements during the cruise checkouts to build up statistics on the noise in the ULV and DLV measurements in different portions of the descent.

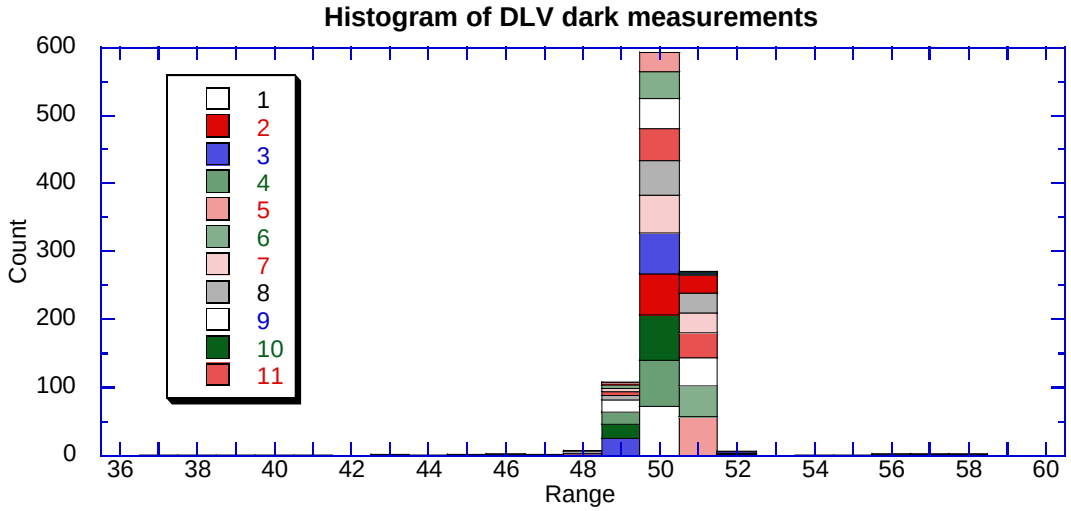

Fig. 8. Histograms of the 11 sets of 100 dark DLV measurements made in single measurement mode during the relative spectral response measurements are shown. The data show a very strong peak near 50 DN with a width of about 1 DN.

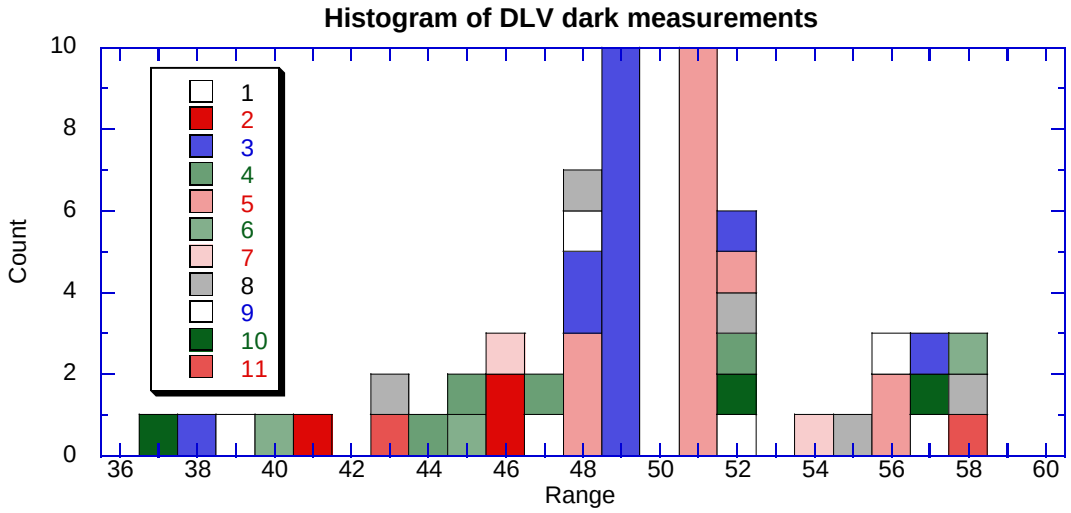

Fig. 9. A magnified view of the histogram of the dark DLV measurements shown in Fig. 8 is shown here. Note the presence of significant peaks some –10, -5, and +7 DN from the main peak. These other peaks are due to electrical cross talk in the sensor head in single measurement mode.

D. Reduction of Relative Spectral Response Measurements

The measurements needed to determine the relative spectral response of the ULV and DLV systems as a function of temperature were obtained between July 26 and August 1, 1996. Table 1 below shows the dates and the average temperatures of the violet system at which the violet data were obtained on these days.

Table 1.
Dates and Temperatures of measurements of ULV/DLV Relative Spectral Response

Date of Measurement	Temperature of Violet System
July 26, 1996	295.77 K
July 29, 1996	200.91 K
July 30, 1996	271.84 K
July 30, 1996	211.70 K
August 1, 1996	229.84 K

On each day, the DISR sensor head was mounted in the dry box with its head inserted into the 20-inch-diameter integrating sphere. Light from the high intensity lamp passed through a 10 nm wide filter, past a shutter, and entered the integrating sphere. The standard calibrated silicon detector with stops to limit its field of view looked into the integrating sphere to measure the intensity of the wall of the integrating sphere. A series of 231 ULV and DLV measurements were made in single measurement mode of the light in the integrating sphere for each filter. After every other filter, the shutter was closed, and a series of 100 dark readings were made with the ULV and DLV systems. The output from the standard calibrated silicon detector was read before and after each measurement of the bright signal with the DISR violet photometer. Periodic readings of the standard calibrated silicon detector were made with the shutter closed and the integrating sphere dark to verify that the dark signal from the standard detector was negligible. We reduced the data by averaging the readings of the silicon standard detector made before and after the ULV and DLV readings for each filter. The summaries of readings made at each temperature are shown in the following tables.

Table 2.
Readings at Temperature of 200.91 K

Table 3.
Readings at Temperature of 211.70 K

Table 4.
Readings at Temperature of 229.84 K

Shutter	Time	Detector	Reading	sigma	Filter
bright	7:26:26	Std. Si.	1.117E-09		330
bright	7:27:05	DLV	52.75	0.632	330
bright	7:27:45	ULV	44.68	0.466	330
bright	7:27:59	Std. Si.	1.117E-09		330
dark	7:28:59	DLV	**50.50**	0.932	
dark	7:29:15	ULV	**44.52**	0.502	
bright	7:30:42	Std. Si.	1.176E-09		340
bright	7:31:21	DLV	52.10	0.639	340

bright	7:32:02	ULV	44.57	0.497	340
bright	7:32:15	Std. Si.	1.177E-09		340
bright	7:36:30	Std. Si.	2.081E-09		350
bright	7:37:09	DLV	68.39	0.608	350
bright	7:37:49	ULV	46.49	0.501	350
bright	7:38:03	Std. Si.	2.030E-09		350
dark	7:39:03	DLV	**50.28**	0.500	
dark	7:39:19	ULV	**44.54**	0.501	
bright	7:40:23	Std. Si.	1.898E-09		360
bright	7:41:02	DLV	78.80	0.595	360
bright	7:41:43	ULV	47.89	0.317	360
bright	7:41:56	Std. Si.	1.895E-09		360
bright	7:43:32	Std. Si.	2.807E-09		370
bright	7:44:12	DLV	93.65	0.691	370
bright	7:44:52	ULV	49.01	0.093	370
bright	7:45:06	Std. Si.	2.783E-09		370
dark	7:46:05	DLV	**49.72**	0.600	
dark	7:46:22	ULV	**44.51**	0.502	
bright	7:47:22	Std. Si.	4.254E-09		380
bright	7:48:02	DLV	118.53	0.598	380
bright	7:48:42	ULV	52.51	0.501	380
bright	7:48:56	Std. Si.	4.262E-09		380
bright	7:49:51	Std. Si.	5.511E-09		390
bright	7:50:30	DLV	134.55	0.881	390
bright	7:51:10	ULV	54.50	0.501	390
bright	7:51:24	Std. Si.	5.436E-09		390
dark	7:52:23	DLV	**49.76**	0.765	
dark	7:52:40	ULV	**44.51**	0.503	
bright	7:53:42	Std. Si.	5.534E-09		400
bright	7:54:21	DLV	136.18	0.607	400
bright	7:55:01	ULV	54.52	0.501	400
bright	7:55:15	Std. Si.	5.511E-09		400
bright	7:56:09	Std. Si.	7.494E-09		410
bright	7:56:48	DLV	162.73	0.612	410
bright	7:57:29	ULV	57.80	0.473	410
bright	7:57:42	Std. Si.	7.441E-09		410
dark	7:58:42	DLV	**50.58**	0.703	
dark	7:58:58	ULV	**44.46**	0.501	
bright	8:00:01	Std. Si.	1.062E-08		420
bright	8:00:40	DLV	206.03	0.510	420
bright	8:01:21	ULV	63.00	0.000	420
bright	8:01:35	Std. Si.	1.058E-08		420
bright	8:02:38	Std. Si.	1.471E-08		430
bright	8:03:17	DLV	270.18	0.742	430
bright	8:03:57	ULV	70.98	0.146	430
bright	8:04:11	Std. Si.	1.469E-08		430
dark	8:05:11	DLV	**50.46**	0.585	
dark	8:05:27	ULV	**44.47**	0.502	
bright	8:06:34	Std. Si.	1.506E-08		440
bright	8:07:13	DLV	273.74	0.840	440
bright	8:07:54	ULV	71.01	0.113	440
bright	8:08:07	Std. Si.	1.503E-08		440
bright	8:09:04	Std. Si.	1.862E-08		450

bright	8:09:43	DLV	302.01	0.821	450
bright	8:10:23	ULV	74.48	0.501	450
bright	8:10:37	Std. Si.	1.853E-08		450
dark	8:11:37	DLV	**50.27**	0.557	
dark	8:11:53	ULV	**44.49**	0.503	
bright	8:13:01	Std. Si.	1.986E-08		460
bright	8:13:41	DLV	306.30	0.650	460
bright	8:14:21	ULV	75.00	0.000	460
bright	8:14:34	Std. Si.	1.979E-08		460
bright	8:16:35	Std. Si.	2.698E-08		470
bright	8:17:14	DLV	311.00	0.568	470
bright	8:17:54	ULV	75.65	0.480	470
bright	8:18:07	Std. Si.	2.687E-08		470
dark	8:19:07	DLV	**50.30**	0.827	
dark	8:19:23	ULV	**44.42**	0.497	
bright	8:20:22	Std. Si.	4.695E-08		480
bright	8:21:01	DLV	107.04	0.514	480
bright	8:21:41	ULV	50.96	0.204	480
bright	8:21:54	Std. Si.	4.690E-08		480
bright	8:23:05	Std. Si.	5.226E-08		490
bright	8:23:44	DLV	59.78	0.715	490
bright	8:24:24	ULV	45.00	0.000	490
bright	8:24:38	Std. Si.	5.205E-08		490
dark	8:25:38	DLV	**49.78**	0.492	
dark	8:25:54	ULV	**44.46**	0.501	
bright	8:26:57	Std. Si.	5.215E-08		490
bright	8:27:36	DLV	59.01	0.510	490
bright	8:28:17	ULV	45.00	0.093	490
bright	8:28:30	Std. Si.	5.204E-08		490
dark	8:29:30	DLV	**49.80**	0.502	
dark	8:29:46	ULV	**44.53**	0.502	
bright	8:31:01	DLV	52.97	0.470	500
bright	8:31:02	Std. Si.	3.082E-08		500
bright	8:32:22	ULV	44.68	0.466	500
bright	8:32:35	Std. Si.	3.078E-08		500
dark	8:33:35	DLV	**50.34**	0.603	
dark	8:33:51	ULV	**44.48**	0.502	

Table 5.
Readings at 271.70 K

Table 6.
Readings at 295.77 K

Table 7 contains the responsivities of the silicon standard detector as a function of wavelength, as well as the spectrum of the light produced by the high intensity lamp in the integrating sphere when no filter is in the beam.

Table 7.

Responsivity of Silicon Standard Detector and Output of High Intensity Lamp

Wavelength (nm)	Responsivity of Silicon Standard Detector (Amps/Watt)	Relative Intensity in Integrating Sphere without Filters (Watts/sq.m-micron-sr)
300	0.127678	0.0634
310	0.137164	0.1010
320	0.143431	0.1601
330	0.147088	0.2526
340	0.149407	0.3786
350	0.149625	0.5377
360	0.146579	0.7314
370	0.147123	0.9623
380	0.158114	1.2214
390	0.171829	1.5146
400	0.182839	1.8473
410	0.192231	2.2201
420	0.200455	2.6134
430	0.208931	3.0989
440	0.215561	3.6196
450	0.223346	4.1639
460	0.230554	4.7288
470	0.237315	5.2401
480	0.243759	5.7910
490	0.250016	6.3147
500	0.256268	6.8314
510	0.262391	7.3199

The transmissions of the 18 nominally 10-nm wide filters used in the measurements are given in Tables 8. The filter transmission normalized to unity at the peak are shown in Fig. 10.

Table 8a.
Transmissions of 10-nm wide filters

Wave-length (nm)	330 nm filter	Wave-length (nm)	340 nm filter	Wave-length (nm)	350 nm filter	Wave-length (nm)	360 nm filter
317.0	0.0050	325.5	0.0008	334.0	0.0028	346.5	0.0015
317.5	0.0063	326.0	0.0010	334.5	0.0035	347.0	0.0017
318.0	0.0078	326.5	0.0014	335.0	0.0044	347.5	0.0021
318.5	0.0099	327.0	0.0018	335.5	0.0056	348.0	0.0025
319.0	0.0127	327.5	0.0024	336.0	0.0072	348.5	0.0030
319.5	0.0166	328.0	0.0032	336.5	0.0092	349.0	0.0037
320.0	0.0215	328.5	0.0042	337.0	0.0120	349.5	0.0046
320.5	0.0283	329.0	0.0056	337.5	0.0159	350.0	0.0058
321.0	0.0377	329.5	0.0076	338.0	0.0213	350.5	0.0073
321.5	0.0502	330.0	0.0102	338.5	0.0284	351.0	0.0093
322.0	0.0655	330.5	0.0140	339.0	0.0385	351.5	0.0123
322.5	0.0856	331.0	0.0200	339.5	0.0526	352.0	0.0165
323.0	0.1087	331.5	0.0293	340.0	0.0717	352.5	0.0227
323.5	0.1330	332.0	0.0425	340.5	0.0963	353.0	0.0316
324.0	0.1544	332.5	0.0640	341.0	0.1259	353.5	0.0447

324.5	0.1744	333.0	0.0957	341.5	0.1621	354.0	0.0616
325.0	0.1886	333.5	0.1385	342.0	0.2011	354.5	0.0862
325.5	0.2003	334.0	0.1880	342.5	0.2402	355.0	0.1180
326.0	0.2084	334.5	0.2397	343.0	0.2762	355.5	0.1529
326.5	0.2149	335.0	0.2799	343.5	0.3055	356.0	0.1861
327.0	0.2201	335.5	0.3033	344.0	0.3315	356.5	0.2112
327.5	0.2249	336.0	0.3140	344.5	0.3529	357.0	0.2286
328.0	0.2288	336.5	0.3178	345.0	0.3709	357.5	0.2388
328.5	0.2324	337.0	0.3198	345.5	0.3861	358.0	0.2450
329.0	0.2356	337.5	0.3218	346.0	0.3978	358.5	0.2500
329.5	0.2379	338.0	0.3243	346.5	0.4074	359.0	0.2552
330.0	0.2395	338.5	0.3258	347.0	0.4129	359.5	0.2605
330.5	0.2410	339.0	0.3257	347.5	0.4140	360.0	0.2655
331.0	0.2422	339.5	0.3229	348.0	0.4101	360.5	0.2691
331.5	0.2436	340.0	0.3187	348.5	0.4029	361.0	0.2708
332.0	0.2453	340.5	0.3131	349.0	0.3914	361.5	0.2705
332.5	0.2474	341.0	0.3073	349.5	0.3772	362.0	0.2691
333.0	0.2496	341.5	0.3015	350.0	0.3609	362.5	0.2680
333.5	0.2512	342.0	0.2953	350.5	0.3424	363.0	0.2682
334.0	0.2508	342.5	0.2848	351.0	0.3234	363.5	0.2707
334.5	0.2469	343.0	0.2657	351.5	0.3006	364.0	0.2752
335.0	0.2373	343.5	0.2365	352.0	0.2748	364.5	0.2782
335.5	0.2211	344.0	0.1944	352.5	0.2460	365.0	0.2742
336.0	0.1981	344.5	0.1483	353.0	0.2154	365.5	0.2560
336.5	0.1722	345.0	0.1064	353.5	0.1840	366.0	0.2233
337.0	0.1434	345.5	0.0738	354.0	0.1552	366.5	0.1784
337.5	0.1164	346.0	0.0520	354.5	0.1270	367.0	0.1322
338.0	0.0923	346.5	0.0359	355.0	0.1018	367.5	0.0932
338.5	0.0737	347.0	0.0252	355.5	0.0809	368.0	0.0635
339.0	0.0583	347.5	0.0179	356.0	0.0635	368.5	0.0432
339.5	0.0460	348.0	0.0130	356.5	0.0501	369.0	0.0305
340.0	0.0365	348.5	0.0099	357.0	0.0392	369.5	0.0216
340.5	0.0291	349.0	0.0075	357.5	0.0304	370.0	0.0155
341.0	0.0237	349.5	0.0057	358.0	0.0234	370.5	0.0114
341.5	0.0193	350.0	0.0045	358.5	0.0180	371.0	0.0086
342.0	0.0159	350.5	0.0035	359.0	0.0137	371.5	0.0066
342.5	0.0132	351.0	0.0029	359.5	0.0106	372.0	0.0051
343.0	0.0111	351.5	0.0023	360.0	0.0081	372.5	0.0040
343.5	0.0095	352.0	0.0019	360.5	0.0062	373.0	0.0033
344.0	0.0081	352.5	0.0015	361.0	0.0048	373.5	0.0026
344.5	0.0070	353.0	0.0013	361.5	0.0037	374.0	0.0021
345.0	0.0061	353.5	0.0010	362.0	0.0029	374.5	0.0017
345.5	0.0054	354.0	0.0009	362.5	0.0023	375.0	0.0014
317.0	0.0050	325.5	0.0008	334.0	0.0028	346.5	0.0015

Table 8b.
Transmissions of 10-nm wide filters

Wave-length (nm)	370 nm filter	Wave-length (nm)	380 nm filter	Wave-length (nm)	390 nm filter	Wave-length (nm)	400nm filter
354.0	0.0014	369.0	0.0025	373.0	0.0027	389.0	0.0033

354.5	0.0016	369.5	0.0034	373.5	0.0032	389.5	0.0042
355.0	0.0018	370.0	0.0046	374.0	0.0038	390.0	0.0055
355.5	0.0021	370.5	0.0063	374.5	0.0046	390.5	0.0073
356.0	0.0024	371.0	0.0090	375.0	0.0057	391.0	0.0098
356.5	0.0028	371.5	0.0129	375.5	0.0071	391.5	0.0138
357.0	0.0032	372.0	0.0188	376.0	0.0088	392.0	0.0199
357.5	0.0038	372.5	0.0277	376.5	0.0110	392.5	0.0294
358.0	0.0045	373.0	0.0406	377.0	0.0141	393.0	0.0439
358.5	0.0054	373.5	0.0605	377.5	0.0183	393.5	0.0667
359.0	0.0066	374.0	0.0889	378.0	0.0240	394.0	0.1013
359.5	0.0078	374.5	0.1267	378.5	0.0320	394.5	0.1494
360.0	0.0096	375.0	0.1705	379.0	0.0427	395.0	0.2061
360.5	0.0117	375.5	0.2156	379.5	0.0580	395.5	0.2640
361.0	0.0144	376.0	0.2545	380.0	0.0789	396.0	0.3121
361.5	0.0175	376.5	0.2830	380.5	0.1073	396.5	0.3450
362.0	0.0211	377.0	0.3039	381.0	0.1412	397.0	0.3634
362.5	0.0249	377.5	0.3183	381.5	0.1836	397.5	0.3720
363.0	0.0291	378.0	0.3282	382.0	0.2309	398.0	0.3753
363.5	0.0335	378.5	0.3361	382.5	0.2751	398.5	0.3753
364.0	0.0379	379.0	0.3418	383.0	0.3111	399.0	0.3727
364.5	0.0420	379.5	0.3453	383.5	0.3344	399.5	0.3685
365.0	0.0457	380.0	0.3470	384.0	0.3468	400.0	0.3627
365.5	0.0492	380.5	0.3471	384.5	0.3508	400.5	0.3577
366.0	0.0522	381.0	0.3464	385.0	0.3493	401.0	0.3547
366.5	0.0551	381.5	0.3452	385.5	0.3463	401.5	0.3547
367.0	0.0575	382.0	0.3452	386.0	0.3427	402.0	0.3576
367.5	0.0603	382.5	0.3459	386.5	0.3398	402.5	0.3614
368.0	0.0632	383.0	0.3468	387.0	0.3376	403.0	0.3611
368.5	0.0662	383.5	0.3448	387.5	0.3360	403.5	0.3482
369.0	0.0693	384.0	0.3358	388.0	0.3343	404.0	0.3164
369.5	0.0727	384.5	0.3127	388.5	0.3324	404.5	0.2660
370.0	0.0763	385.0	0.2721	389.0	0.3301	405.0	0.2065
370.5	0.0803	385.5	0.2234	389.5	0.3269	405.5	0.1506
371.0	0.0844	386.0	0.1690	390.0	0.3225	406.0	0.1066
371.5	0.0888	386.5	0.1218	390.5	0.3169	406.5	0.0744
372.0	0.0935	387.0	0.0855	391.0	0.3102	407.0	0.0537
372.5	0.0984	387.5	0.0595	391.5	0.3008	407.5	0.0390
373.0	0.1032	388.0	0.0416	392.0	0.2887	408.0	0.0290
373.5	0.1085	388.5	0.0295	392.5	0.2730	408.5	0.0220
374.0	0.1139	389.0	0.0212	393.0	0.2532	409.0	0.0171
374.5	0.1193	389.5	0.0156	393.5	0.2296	409.5	0.0137
375.0	0.1246	390.0	0.0117	394.0	0.2021	410.0	0.0112
375.5	0.1299	390.5	0.0088	394.5	0.1726	410.5	0.0093
376.0	0.1345	391.0	0.0069	395.0	0.1437	411.0	0.0079
376.5	0.1378	391.5	0.0054	395.5	0.1166	411.5	0.0067
377.0	0.1403	392.0	0.0042	396.0	0.0927	412.0	0.0059
377.5	0.1410	392.5	0.0034	396.5	0.0726	412.5	0.0052
378.0	0.1393	393.0	0.0027	397.0	0.0565	413.0	0.0046
378.5	0.1352			397.5	0.0444	413.5	0.0041
379.0	0.1288			398.0	0.0345	414.0	0.0036
379.5	0.1198			398.5	0.0268		
380.0	0.1094			399.0	0.0211		
380.5	0.0981			399.5	0.0166		

381.0	0.0876			400.0	0.0132		
381.5	0.0768			400.5	0.0106		
382.0	0.0668			401.0	0.0085		
382.5	0.0578			401.5	0.0069		
383.0	0.0500			402.0	0.0056		
383.5	0.0433			402.5	0.0046		
384.0	0.0377			403.0	0.0038		
384.5	0.0328			403.5	0.0031		
385.0	0.0287						
385.5	0.0255						
386.0	0.0226						
386.5	0.0201						
387.0	0.0179						
387.5	0.0161						
388.0	0.0145						
388.5	0.0131						
389.0	0.0119						
389.5	0.0109						
390.0	0.0099						
390.5	0.0091						
391.0	0.0084						
391.5	0.0077						
392.0	0.0071						
392.5	0.0066						
393.0	0.0061						
393.5	0.0056						
394.0	0.0052						
394.5	0.0048						
395.0	0.0044						

Table 8c.
Transmissions of 10-nm wide filters

Wave-length (nm)	410 nm filter	Wave-length (nm)	420 nm filter	Wave-length (nm)	430 nm filter	Wave-length (nm)	440 nm filter
398.0	0.0011	405.0	0.0019	417.0	0.0025	427.5	0.0017
398.5	0.0015	405.5	0.0026	417.5	0.0034	428.0	0.0021
399.0	0.0020	406.0	0.0035	418.0	0.0045	428.5	0.0025
399.5	0.0027	406.5	0.0045	418.5	0.0062	429.0	0.0031
400.0	0.0035	407.0	0.0056	419.0	0.0087	429.5	0.0039
400.5	0.0049	407.5	0.0071	419.5	0.0125	430.0	0.0050
401.0	0.0067	408.0	0.0090	420.0	0.0186	430.5	0.0066
401.5	0.0095	408.5	0.0116	420.5	0.0283	431.0	0.0090
402.0	0.0137	409.0	0.0152	421.0	0.0444	431.5	0.0124
402.5	0.0202	409.5	0.0205	421.5	0.0708	432.0	0.0177
403.0	0.0302	410.0	0.0284	422.0	0.1144	432.5	0.0260
403.5	0.0458	410.5	0.0406	422.5	0.1803	433.0	0.0393

404.0	0.0703	411.0	0.0599	423.0	0.2689	433.5	0.0613
404.5	0.1072	411.5	0.0904	423.5	0.3638	434.0	0.1002
405.0	0.1598	412.0	0.1374	424.0	0.4406	434.5	0.1591
405.5	0.2264	412.5	0.2020	424.5	0.4867	435.0	0.2422
406.0	0.2972	413.0	0.2800	425.0	0.5072	435.5	0.3375
406.5	0.3590	413.5	0.3558	425.5	0.5149	436.0	0.4248
407.0	0.3999	414.0	0.4141	426.0	0.5176	436.5	0.4801
407.5	0.4260	414.5	0.4481	426.5	0.5186	437.0	0.5012
408.0	0.4401	415.0	0.4657	427.0	0.5184	437.5	0.5042
408.5	0.4469	415.5	0.4759	427.5	0.5164	438.0	0.5015
409.0	0.4497	416.0	0.4836	428.0	0.5120	438.5	0.4985
409.5	0.4495	416.5	0.4912	428.5	0.5072	439.0	0.4958
410.0	0.4467	417.0	0.4963	429.0	0.5021	439.5	0.4929
410.5	0.4426	417.5	0.4980	429.5	0.4991	440.0	0.4892
411.0	0.4382	418.0	0.4937	430.0	0.4994	440.5	0.4854
411.5	0.4347	418.5	0.4864	430.5	0.5031	441.0	0.4836
412.0	0.4317	419.0	0.4772	431.0	0.5084	441.5	0.4859
412.5	0.4260	419.5	0.4688	431.5	0.5112	442.0	0.4923
413.0	0.4107	420.0	0.4613	432.0	0.5043	442.5	0.4980
413.5	0.3770	420.5	0.4538	432.5	0.4787	443.0	0.4915
414.0	0.3199	421.0	0.4401	433.0	0.4299	443.5	0.4574
414.5	0.2483	421.5	0.4108	433.5	0.3613	444.0	0.3878
415.0	0.1768	422.0	0.3592	434.0	0.2794	444.5	0.2967
415.5	0.1192	422.5	0.2901	434.5	0.2076	445.0	0.2088
416.0	0.0787	423.0	0.2153	435.0	0.1495	445.5	0.1398
416.5	0.0519	423.5	0.1511	435.5	0.1067	446.0	0.0927
417.0	0.0347	424.0	0.1025	436.0	0.0755	446.5	0.0617
417.5	0.0237	424.5	0.0691	436.5	0.0534	447.0	0.0419
418.0	0.0165	425.0	0.0471	437.0	0.0385	447.5	0.0291
418.5	0.0117	425.5	0.0327	437.5	0.0281	448.0	0.0209
419.0	0.0085	426.0	0.0232	438.0	0.0208	448.5	0.0153
419.5	0.0063	426.5	0.0168	438.5	0.0156	449.0	0.0114
420.0	0.0047	427.0	0.0124	439.0	0.0118	449.5	0.0086
420.5	0.0036	427.5	0.0094	439.5	0.0091	450.0	0.0067
421.0	0.0027	428.0	0.0072	440.0	0.0070	450.5	0.0053
421.5	0.0021	428.5	0.0056	440.5	0.0055	451.0	0.0042
422.0	0.0016	429.0	0.0044	441.0	0.0043	451.5	0.0034
422.5	0.0013	429.5	0.0036	441.5	0.0034	452.0	0.0027
423.0	0.0010	430.0	0.0029	442.0	0.0027	452.5	0.0022

Table 8d.
Transmissions of 10-nm wide filters

Wave-length (nm)	450 nm filter	Wave-length (nm)	460 nm filter	Wave-length (nm)	470 nm filter	Wave-length (nm)	480 nm filter
438.5	0.0034	448.0	0.0003	457.0	0.0021	470.0	0.0023
439.0	0.0045	448.5	0.0004	457.5	0.0027	470.5	0.0033
439.5	0.0059	449.0	0.0006	458.0	0.0037	471.0	0.0048
440.0	0.0077	449.5	0.0009	458.5	0.0049	471.5	0.0070
440.5	0.0101	450.0	0.0012	459.0	0.0068	472.0	0.0105
441.0	0.0134	450.5	0.0018	459.5	0.0093	472.5	0.0159
441.5	0.0180	451.0	0.0026	460.0	0.0130	473.0	0.0252

442.0	0.0245	451.5	0.0040	460.5	0.0186	473.5	0.0399
442.5	0.0338	452.0	0.0065	461.0	0.0273	474.0	0.0638
443.0	0.0482	452.5	0.0108	461.5	0.0408	474.5	0.1024
443.5	0.0689	453.0	0.0185	462.0	0.0624	475.0	0.1609
444.0	0.0995	453.5	0.0328	462.5	0.0976	475.5	0.2434
444.5	0.1429	454.0	0.0587	463.0	0.1572	476.0	0.3491
445.0	0.2015	454.5	0.1062	463.5	0.2419	476.5	0.4477
445.5	0.2733	455.0	0.1746	464.0	0.3516	477.0	0.5245
446.0	0.3491	455.5	0.2606	464.5	0.4676	477.5	0.5765
446.5	0.4141	456.0	0.3521	465.0	0.5602	478.0	0.6084
447.0	0.4576	456.5	0.4345	465.5	0.6148	478.5	0.6285
447.5	0.4797	457.0	0.4957	466.0	0.6382	479.0	0.6392
448.0	0.4873	457.5	0.5338	466.5	0.6468	479.5	0.6429
448.5	0.4889	458.0	0.5500	467.0	0.6503	480.0	0.6407
449.0	0.4894	458.5	0.5517	467.5	0.6533	480.5	0.6335
449.5	0.4911	459.0	0.5476	468.0	0.6553	481.0	0.6238
450.0	0.4941	459.5	0.5451	468.5	0.6557	481.5	0.6168
450.5	0.4980	460.0	0.5454	469.0	0.6526	482.0	0.6138
451.0	0.5017	460.5	0.5454	469.5	0.6468	482.5	0.6158
451.5	0.5041	461.0	0.5392	470.0	0.6377	483.0	0.6170
452.0	0.5053	461.5	0.5228	470.5	0.6241	483.5	0.6033
452.5	0.5050	462.0	0.4977	471.0	0.6027	484.0	0.5576
453.0	0.5026	462.5	0.4714	471.5	0.5671	484.5	0.4671
453.5	0.4965	463.0	0.4532	472.0	0.5109	485.0	0.3564
454.0	0.4837	463.5	0.4534	472.5	0.4350	485.5	0.2493
454.5	0.4561	464.0	0.4697	473.0	0.3418	486.0	0.1623
455.0	0.4117	464.5	0.4789	473.5	0.2554	486.5	0.1057
455.5	0.3500	465.0	0.4288	474.0	0.1843	487.0	0.0694
456.0	0.2775	465.5	0.3060	474.5	0.1305	487.5	0.0462
456.5	0.2063	466.0	0.1785	475.0	0.0926	488.0	0.0315
457.0	0.1466	466.5	0.0906	475.5	0.0658	488.5	0.0216
457.5	0.1007	467.0	0.0485	476.0	0.0469	489.0	0.0155
458.0	0.0682	467.5	0.0276	476.5	0.0346	489.5	0.0114
458.5	0.0465	468.0	0.0167	477.0	0.0261	490.0	0.0085
459.0	0.0313	468.5	0.0108	477.5	0.0200	490.5	0.0064
459.5	0.0218	469.0	0.0073	478.0	0.0157	491.0	0.0049
460.0	0.0154	469.5	0.0052	478.5	0.0123	491.5	0.0038
460.5	0.0112	470.0	0.0038	479.0	0.0099	492.0	0.0029
461.0	0.0082	470.5	0.0029	479.5	0.0081	492.5	0.0023
461.5	0.0061	471.0	0.0022	480.0	0.0067	493.0	0.0018
462.0	0.0046	471.5	0.0018	480.5	0.0055	493.5	0.0014
462.5	0.0035	472.0	0.0014	481.0	0.0046	494.0	0.0011
463.0	0.0026	472.5	0.0011	481.5	0.0039	494.5	0.0009
463.5	0.0020	473.0	0.0009	482.0	0.0033	495.0	0.0007

Table 8e.
Transmissions of 10-nm wide filters

Wave-length (nm)	490 nm filter	Wave-length (nm)	500 nm filter
477.0	0.0021	487.0	0.0015

477.5	0.0028	487.5	0.0018
478.0	0.0038	488.0	0.0024
478.5	0.0054	488.5	0.0031
479.0	0.0076	489.0	0.0040
479.5	0.0111	489.5	0.0053
480.0	0.0168	490.0	0.0071
480.5	0.0261	490.5	0.0099
481.0	0.0431	491.0	0.0140
481.5	0.0713	491.5	0.0201
482.0	0.1200	492.0	0.0296
482.5	0.1965	492.5	0.0458
483.0	0.3043	493.0	0.0705
483.5	0.4263	493.5	0.1110
484.0	0.5147	494.0	0.1716
484.5	0.5586	494.5	0.2619
485.0	0.5777	495.0	0.3625
485.5	0.5835	495.5	0.4603
486.0	0.5863	496.0	0.5328
486.5	0.5882	496.5	0.5767
487.0	0.5880	497.0	0.5964
487.5	0.5835	497.5	0.6047
488.0	0.5751	498.0	0.6079
488.5	0.5639	498.5	0.6087
489.0	0.5548	499.0	0.6075
489.5	0.5507	499.5	0.6048
490.0	0.5537	500.0	0.5993
490.5	0.5645	500.5	0.5881
491.0	0.5750	501.0	0.5680
491.5	0.5687	501.5	0.5301
492.0	0.5249	502.0	0.4704
492.5	0.4296	502.5	0.3859
493.0	0.3168	503.0	0.2985
493.5	0.2126	503.5	0.2176
494.0	0.1385	504.0	0.1494
494.5	0.0873	504.5	0.1033
495.0	0.0576	505.0	0.0717
495.5	0.0387	505.5	0.0500
496.0	0.0269	506.0	0.0350
496.5	0.0188	506.5	0.0254
497.0	0.0137	507.0	0.0188
497.5	0.0103	507.5	0.0139
498.0	0.0078	508.0	0.0106
498.5	0.0059	508.5	0.0083
499.0	0.0046	509.0	0.0065
499.5	0.0037	509.5	0.0051
500.0	0.0029	510.0	0.0041
500.5	0.0023	510.5	0.0033
501.0	0.0019	511.0	0.0026
501.5	0.0016	511.5	0.0022
502.0	0.0013	512.0	0.0018

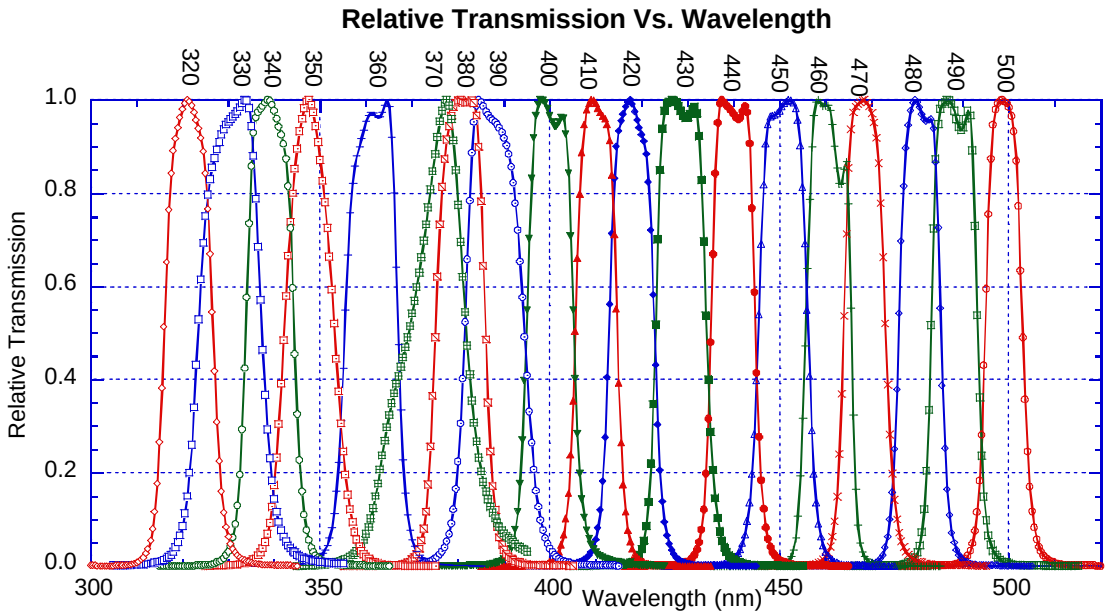

Fig. 10. The relative transmission of the 18 filters used to measure the relative spectral response of the ULV and DLV systems are shown.

Using the filter transmissions in Table 8, we can evaluate l1 and l2 according to eqn. (8) and (9) above. The average of the responsivity of the silicon standard reference detector can also be evaluated over each filter weighted with the relative shape of the intensity of the unfiltered lamp, from Table 7. With these values, we can evaluate the relative spectral response of the ULV and DLV systems at each of the five temperatures of the measurements. The results are contained in Tables 9 and 10 for the ULV and DLV respectively. The relative spectral response measurements are shown for the ULV and DLV at all 5 temperatures in Figs. 11 and 12. The vertical bars indicate the uncertainty in the relative spectral measurements, and the horizontal bars indicate the wavelength region over which the measurement gives the average relative spectral response.

Table 9a.
Relative Spectral Response of ULV at 200.91 K

<λ> (nm)	λ_1 (nm)	λ_2 (nm)	DN Bright	DN Dark	B-D	Mean Std. Det. Resp.	Std. Det. (nano-Amps)	Raw Rel. Resp.	Norm. Rel. Resp.	σ
		s =	*0.10*	*0.10*	*0.14*		*0.044*			
331.8	322.6	341.0	44.77	44.50	0.27	0.1474	1.416	0.0281	0.073	0.049
339.6	333.1	346.0	44.71	44.50	0.21	0.1492	1.427	0.0220	0.057	0.047
348.4	340.9	355.8	44.91	44.50	0.41	0.1494	2.483	0.0247	0.064	0.028
361.6	354.6	368.7	48.42	44.50	3.92	0.1466	2.270	0.2532	0.659	0.029
376.1	364.7	387.5	50.42	44.50	5.92	0.1544	3.338	0.2738	0.713	0.020
380.9	374.3	387.5	53.30	44.50	8.80	0.1595	4.937	0.2843	0.741	0.014
388.4	380.1	396.7	55.97	44.50	11.47	0.1695	6.265	0.3102	0.808	0.014
400.4	393.8	407.0	55.09	44.50	10.59	0.1832	6.240	0.3108	0.810	0.013
410.3	404.6	415.9	60.40	44.50	15.90	0.1924	8.853	0.3455	0.900	0.011
418.0	411.9	424.2	65.65	44.50	21.15	0.1989	12.120	0.3470	0.904	0.007

428.9	422.3	435.5	75.36	44.50	30.86	0.2079	17.230	0.3723	0.970	0.005
440.1	434.2	446.0	75.01	44.50	30.51	0.2158	17.150	0.3839	1.000	0.006
450.9	444.5	457.4	78.51	44.50	34.01	0.2240	21.420	0.3556	0.926	0.006
460.6	455.0	466.2	79.00	44.50	34.50	0.2310	22.300	0.3573	0.931	0.005
468.7	462.8	474.6	77.45	44.50	32.95	0.2365	28.850	0.2701	0.704	0.004
480.7	475.1	486.2	51.28	44.50	6.78	0.2442	53.960	0.0307	0.080	0.002
488.2	482.2	494.1	45.00	44.50	0.50	0.2489	56.860	0.0022	0.006	0.002
499.0	493.6	504.4	44.79	44.50	0.29	0.2556	33.960	0.0022	0.006	0.003

Table 9b.
Relative Spectral Response of ULV at 211.70 K

<λ> (nm)	λ_1 (nm)	λ_2 (nm)	DN Bright	DN Dark	B-D	Mean Std. Det. Resp.	Std. Det. (nano-Amps)	Raw Rel. Resp.	Norm. Rel. Resp.	σ
		s =	*0.10*	*0.10*	*0.14*		*0.044*			
331.8	322.6	341.0	44.62	44.50	0.12	0.1474	1.289	0.0137	0.0333	0.049
339.6	333.1	346.0	44.61	44.50	0.11	0.1492	1.340	0.0122	0.0297	0.047
348.4	340.9	355.8	46.92	44.50	2.42	0.1494	2.362	0.1531	0.3718	0.028
361.6	354.6	368.7	48.36	44.50	3.86	0.1466	2.162	0.2617	0.6355	0.029
376.1	364.7	387.5	50.45	44.50	5.95	0.1544	3.068	0.2994	0.7269	0.020
380.9	374.3	387.5	53.59	44.50	9.09	0.1595	4.738	0.3060	0.7431	0.014
388.4	380.1	396.7	56.30	44.50	11.80	0.1695	6.063	0.3298	0.8008	0.014
400.4	393.8	407.0	56.41	44.50	11.91	0.1832	6.026	0.3620	0.8790	0.013
410.3	404.6	415.9	60.45	44.50	15.95	0.1924	8.277	0.3707	0.9001	0.011
418.0	411.9	424.2	66.16	44.50	21.66	0.1989	11.410	0.3775	0.9166	0.007
428.9	422.3	435.5	75.31	44.50	30.81	0.2079	16.150	0.3966	0.9629	0.005
440.1	434.2	446.0	75.00	44.50	30.50	0.2158	15.980	0.4118	1.0000	0.006
450.9	444.5	457.4	78.50	44.50	34.00	0.2240	20.100	0.3789	0.9200	0.006
460.6	455.0	466.2	78.88	44.50	34.38	0.2310	20.700	0.3836	0.9314	0.005
468.7	462.8	474.6	79.46	44.50	34.96	0.2365	28.200	0.2931	0.7118	0.004
480.7	475.1	486.2	52.36	44.50	7.86	0.2442	53.820	0.0357	0.0866	0.002
488.2	482.2	494.1	45.00	44.50	0.50	0.2489	58.690	0.0021	0.0051	0.002
499.0	493.6	504.4	44.60	44.50	0.10	0.2556	33.530	0.0008	0.0019	0.003

Table 9c.
Relative Spectral Response of ULV at 229.84 K

<λ> (nm)	λ_1 (nm)	λ_2 (nm)	DN Bright	DN Dark	B-D	Mean Std. Det. Resp.	Std. Det. (nano-Amps)	Raw Rel. Resp.	Norm. Rel. Resp.	σ
		s =	*0.10*	*0.10*	*0.14*		*0.044*			
331.8	322.6	341.0	44.68	44.49	0.19	0.1474	1.117	0.0251	0.0659	0.049
339.6	333.1	346.0	44.57	44.49	0.08	0.1492	1.177	0.0101	0.0267	0.047
348.4	340.9	355.8	46.49	44.49	2.00	0.1494	2.056	0.1454	0.3822	0.028
361.6	354.6	368.7	47.89	44.49	3.40	0.1466	1.897	0.2627	0.6908	0.029
376.1	364.7	387.5	49.01	44.49	4.52	0.1544	2.795	0.2496	0.6563	0.020
380.9	374.3	387.5	52.51	44.49	8.02	0.1595	4.258	0.3004	0.7899	0.014
388.4	380.1	396.7	54.50	44.49	10.01	0.1695	5.474	0.3099	0.8147	0.014
400.4	393.8	407.0	54.52	44.49	10.03	0.1832	5.523	0.3326	0.8745	0.013
410.3	404.6	415.9	57.80	44.49	13.31	0.1924	7.468	0.3428	0.9014	0.011

418.0	411.9	424.2	63.00	44.49	18.51	0.1989	10.600	0.3472	0.9130	0.007
428.9	422.3	435.5	70.98	44.49	26.49	0.2079	14.700	0.3746	0.9849	0.005
440.1	434.2	446.0	71.01	44.49	26.52	0.2158	15.045	0.3804	1.0000	0.006
450.9	444.5	457.4	74.48	44.49	29.99	0.2240	18.575	0.3616	0.9508	0.006
460.6	455.0	466.2	75.00	44.49	30.51	0.2310	19.825	0.3554	0.9345	0.005
468.7	462.8	474.6	75.65	44.49	31.16	0.2365	26.925	0.2736	0.7195	0.004
480.7	475.1	486.2	50.96	44.49	6.47	0.2442	46.925	0.0337	0.0885	0.002
488.2	482.2	494.1	45.00	44.49	0.51	0.2489	52.155	0.0024	0.0064	0.002
499.0	493.6	504.4	44.68	44.49	0.19	0.2556	30.800	0.0016	0.0041	0.003

Table 9d.
Relative Spectral Response of ULV at 271.84 K

<λ> (nm)	λ_1 (nm)	λ_2 (nm)	DN Bright	DN Dark	B-D	Mean Std. Det. Resp.	Std. Det. (nano-Amps)	Raw Rel. Resp.	Norm. Rel. Resp.	σ
		s =	*0.10*	*0.10*	*0.14*		*0.044*			
331.8	322.6	341.0	45.03	45.00	0.03	0.1474	1.305	0.0034	0.0081	0.049
339.6	333.1	346.0	45.08	45.00	0.08	0.1492	1.355	0.0088	0.0210	0.047
348.4	340.9	355.8	48.07	45.00	3.07	0.1494	2.372	0.1934	0.4602	0.028
361.6	354.6	368.7	48.99	45.00	3.99	0.1466	2.196	0.2664	0.6338	0.029
376.1	364.7	387.5	51.31	45.00	6.31	0.1544	3.104	0.3138	0.7466	0.020
380.9	374.3	387.5	55.00	45.00	10.00	0.1595	4.848	0.3290	0.7829	0.014
388.4	380.1	396.7	57.00	45.00	12.00	0.1695	6.127	0.3319	0.7897	0.014
400.4	393.8	407.0	57.08	45.00	12.08	0.1832	6.125	0.3612	0.8595	0.013
410.3	404.6	415.9	61.45	45.00	16.45	0.1924	8.536	0.3707	0.8820	0.011
418.0	411.9	424.2	67.88	45.00	22.88	0.1989	11.660	0.3902	0.9284	0.007
428.9	422.3	435.5	77.00	45.00	32.00	0.2079	16.670	0.3990	0.9494	0.005
440.1	434.2	446.0	76.71	45.00	31.71	0.2158	16.280	0.4203	1.0000	0.006
450.9	444.5	457.4	80.36	45.00	35.36	0.2240	20.140	0.3933	0.9357	0.006
460.6	455.0	466.2	80.98	45.00	35.98	0.2310	21.420	0.3879	0.9230	0.005
468.7	462.8	474.6	82.52	45.00	37.52	0.2365	29.660	0.2991	0.7117	0.004
480.7	475.1	486.2	53.00	45.00	8.00	0.2442	56.350	0.0347	0.0825	0.002
488.2	482.2	494.1	46.45	45.00	1.45	0.2489	59.810	0.0060	0.0144	0.002
499.0	493.6	504.4	45.02	45.00	0.02	0.2556	32.600	0.0002	0.0004	0.003

Table 9e.
Relative Spectral Response of ULV at 295.77 K

<λ> (nm)	λ_1 (nm)	λ_2 (nm)	DN Bright	DN Dark	B-D	Mean Std. Det. Resp.	Std. Det. (nano-Amps)	Raw Rel. Resp.	Norm. Rel. Resp.	σ
		s =	*0.10*	*0.10*	*0.14*		*0.044*			
331.8	322.6	341.0	46.36	45.50	0.86	0.1474	1.423	0.0891	0.2180	0.049
339.6	333.1	346.0	46.20	45.50	0.70	0.1492	1.245	0.0839	0.2052	0.047
348.4	340.9	355.8	48.42	45.50	2.92	0.1494	2.389	0.1827	0.4469	0.028
361.6	354.6	368.7	49.41	45.50	3.91	0.1466	2.151	0.2665	0.6519	0.029
376.1	364.7	387.5	52.00	45.50	6.50	0.1544	3.156	0.3179	0.7777	0.020
380.9	374.3	387.5	55.00	45.50	9.50	0.1595	4.727	0.3206	0.7842	0.014
388.4	380.1	396.7	57.23	45.50	11.73	0.1695	6.033	0.3295	0.8060	0.014
400.4	393.8	407.0	57.82	45.50	12.32	0.1832	6.173	0.3655	0.8942	0.013

410.3	404.6	415.9	61.96	45.50	16.46	0.1924	8.604	0.3680	0.9003	0.011
418.0	411.9	424.2	68.03	45.50	22.53	0.1989	11.780	0.3803	0.9304	0.007
428.9	422.3	435.5	76.60	45.50	31.10	0.2079	16.310	0.3964	0.9697	0.005
440.1	434.2	446.0	76.53	45.50	31.03	0.2158	16.380	0.4088	1.0000	0.006
450.9	444.5	457.4	80.01	45.50	34.51	0.2240	20.320	0.3804	0.9306	0.006
460.6	455.0	466.2	80.53	45.50	35.03	0.2310	21.620	0.3742	0.9155	0.005
468.7	462.8	474.6	81.85	45.50	36.35	0.2365	29.560	0.2908	0.7113	0.004
480.7	475.1	486.2	53.15	45.50	7.65	0.2442	56.830	0.0329	0.0804	0.002
488.2	482.2	494.1	46.96	45.50	1.46	0.2489	60.550	0.0060	0.0147	0.002
499.0	493.6	504.4	46.27	45.50	0.77	0.2556	32.660	0.0060	0.0147	0.003

Table 10a.
Relative Spectral Response of DLV at 200.91 K

<λ> (nm)	λ_1 (nm)	λ_2 (nm)	DN Bright	DN Dark	B-D	Mean Std. Det. Resp.	Std. Det. (nano-Amps)	Raw Rel. Resp.	Norm. Rel. Resp.	σ
		s =	*0.32*	*0.32*	*0.45*		*0.044*			
331.8	322.6	341.0	53.48	50.73	2.8	0.1474	1.416	0.2863	0.088	0.019
339.6	333.1	346.0	52.44	50.73	1.7	0.1492	1.427	0.1788	0.055	0.018
348.4	340.9	355.8	71.94	50.73	21.2	0.1494	2.483	1.2766	0.394	0.013
361.6	354.6	368.7	83.53	50.73	32.8	0.1466	2.270	2.1182	0.654	0.019
376.1	364.7	387.5	101.07	50.73	50.3	0.1544	3.338	2.3279	0.719	0.013
380.9	374.3	387.5	129.86	50.73	79.1	0.1595	4.937	2.5566	0.790	0.010
388.4	380.1	396.7	149.12	50.73	98.4	0.1695	6.265	2.6613	0.822	0.008
400.4	393.8	407.0	146.61	50.73	95.9	0.1832	6.240	2.8142	0.869	0.008
410.3	404.6	415.9	184.64	50.73	133.9	0.1924	8.853	2.9096	0.899	0.006
418.0	411.9	424.2	229.87	50.73	179.1	0.1989	12.120	2.9391	0.908	0.005
428.9	422.3	435.5	310.18	50.73	259.5	0.2079	17.230	3.1301	0.967	0.004
440.1	434.2	446.0	308.01	50.73	257.3	0.2158	17.150	3.2370	1.000	0.004
450.9	444.5	457.4	339.65	50.73	288.9	0.2240	21.420	3.0212	0.933	0.003
460.6	455.0	466.2	345.12	50.73	294.4	0.2310	22.300	3.0489	0.942	0.003
468.7	462.8	474.6	333.25	50.73	282.5	0.2365	28.850	2.3156	0.715	0.002
480.7	475.1	486.2	112.96	50.73	62.2	0.2442	53.960	0.2816	0.087	0.001
488.2	482.2	494.1	60.98	50.73	10.3	0.2489	56.860	0.0449	0.014	0.001
499.0	493.6	504.4	53.08	50.73	2.4	0.2556	33.960	0.0177	0.005	0.001

Table 10b.
Relative Spectral Response of DLV at 211.70 K

<λ> (nm)	λ_1 (nm)	λ_2 (nm)	DN Bright	DN Dark	B-D	Mean Std. Det. Resp.	Std. Det. (nano-Amps)	Raw Rel. Resp.	Norm. Rel. Resp.	σ
		s =	*0.32*	*0.32*	*0.45*		*0.044*			
331.8	322.6	341.0	52.88	50.43	2.5	0.1474	1.289	0.2802	0.081	0.019
339.6	333.1	346.0	52.95	50.43	2.5	0.1492	1.340	0.2806	0.082	0.018
348.4	340.9	355.8	72.10	50.43	21.7	0.1494	2.362	1.3711	0.399	0.013
361.6	354.6	368.7	83.02	50.43	32.6	0.1466	2.162	2.2098	0.642	0.019
376.1	364.7	387.5	100.92	50.43	50.5	0.1544	3.068	2.5403	0.738	0.013
380.9	374.3	387.5	131.12	50.43	80.7	0.1595	4.738	2.7165	0.790	0.010
388.4	380.1	396.7	150.33	50.43	99.9	0.1695	6.063	2.7921	0.812	0.008

400.4	393.8	407.0	150.11	50.43	99.7	0.1832	6.026	3.0296	0.881	0.008
410.3	404.6	415.9	183.64	50.43	133.2	0.1924	8.277	3.0959	0.900	0.006
418.0	411.9	424.2	229.3	50.43	178.9	0.1989	11.410	3.1173	0.906	0.005
428.9	422.3	435.5	306.85	50.43	256.4	0.2079	16.150	3.3004	0.959	0.004
440.1	434.2	446.0	305.23	50.43	254.8	0.2158	15.980	3.4405	1.000	0.004
450.9	444.5	457.4	336.24	50.43	285.8	0.2240	20.100	3.1849	0.926	0.003
460.6	455.0	466.2	339.36	50.43	288.9	0.2310	20.700	3.2236	0.937	0.003
468.7	462.8	474.6	345.81	50.43	295.4	0.2365	28.200	2.4768	0.720	0.002
480.7	475.1	486.2	118.97	50.43	68.5	0.2442	53.820	0.3110	0.090	0.001
488.2	482.2	494.1	60.87	50.43	10.4	0.2489	58.690	0.0443	0.013	0.001
499.0	493.6	504.4	53.88	50.43	3.5	0.2556	33.530	0.0263	0.008	0.001

Table 10c.
Relative Spectral Response of DLV at 229.84 K

$<\lambda>$ (nm)	λ_1 (nm)	λ_2 (nm)	DN Bright	DN Dark	B-D	Mean Std. Det. Resp.	Std. Det. (nano-Amps)	Raw Rel. Resp.	Norm. Rel. Resp.	σ
		s =	*0.32*	*0.32*	*0.45*		*0.044*			
331.8	322.6	341.0	52.75	50.17	2.6	0.1474	1.117	0.3405	0.106	0.019
339.6	333.1	346.0	52.10	50.17	1.9	0.1492	1.177	0.2447	0.076	0.018
348.4	340.9	355.8	68.39	50.17	18.2	0.1494	2.056	1.3244	0.413	0.013
361.6	354.6	368.7	78.80	50.17	28.6	0.1466	1.897	2.2125	0.690	0.019
376.1	364.7	387.5	93.65	50.17	43.5	0.1544	2.795	2.4012	0.749	0.013
380.9	374.3	387.5	118.53	50.17	68.4	0.1595	4.258	2.5608	0.799	0.010
388.4	380.1	396.7	134.55	50.17	84.4	0.1695	5.474	2.6121	0.815	0.008
400.4	393.8	407.0	136.18	50.17	86.0	0.1832	5.523	2.8522	0.890	0.008
410.3	404.6	415.9	162.73	50.17	112.6	0.1924	7.468	2.8993	0.904	0.006
418.0	411.9	424.2	206.03	50.17	155.9	0.1989	10.600	2.9239	0.912	0.005
428.9	422.3	435.5	270.18	50.17	220.0	0.2079	14.700	3.1111	0.970	0.004
440.1	434.2	446.0	273.74	50.17	223.6	0.2158	15.045	3.2065	1.000	0.004
450.9	444.5	457.4	302.01	50.17	251.8	0.2240	18.575	3.0368	0.947	0.003
460.6	455.0	466.2	306.30	50.17	256.1	0.2310	19.825	2.9838	0.931	0.003
468.7	462.8	474.6	311.00	50.17	260.8	0.2365	26.925	2.2906	0.714	0.002
480.7	475.1	486.2	107.04	50.17	56.9	0.2442	46.925	0.2959	0.092	0.001
488.2	482.2	494.1	59.78	50.17	9.6	0.2489	52.155	0.0459	0.014	0.001
488.2	482.2	494.1	59.01	50.17	8.8	0.2489	52.155	0.0422	0.013	0.001
499.0	493.6	504.4	52.97	50.17	2.8	0.2556	30.800	0.0232	0.007	0.001

Table 10d.
Relative Spectral Response of DLV at 271.84 K

$<\lambda>$ (nm)	λ_1 (nm)	λ_2 (nm)	DN Bright	DN Dark	B-D	Mean Std. Det. Resp.	Std. Det. (nano-Amps)	Raw Rel. Resp.	Norm. Rel. Resp.	σ
		s =	*0.32*	*0.32*	*0.45*		*0.044*			
331.8	322.6	341.0	53.04	50.41	2.6	0.1474	1.305	0.2971	0.085	0.019
339.6	333.1	346.0	52.73	50.41	2.3	0.1492	1.355	0.2555	0.073	0.018
348.4	340.9	355.8	72.71	50.41	22.3	0.1494	2.372	1.4050	0.402	0.013
361.6	354.6	368.7	86.12	50.41	35.7	0.1466	2.196	2.3839	0.682	0.019
376.1	364.7	387.5	103.97	50.41	53.6	0.1544	3.104	2.6635	0.762	0.013

380.9	374.3	387.5	135.81	50.41	85.4	0.1595	4.848	2.8098	0.804	0.010
388.4	380.1	396.7	155.08	50.41	104.7	0.1695	6.127	2.8949	0.829	0.008
400.4	393.8	407.0	154.45	50.41	104.0	0.1832	6.125	3.1110	0.890	0.008
410.3	404.6	415.9	189.76	50.41	139.4	0.1924	8.536	3.1403	0.899	0.006
418.0	411.9	424.2	238.31	50.41	187.9	0.1989	11.660	3.2045	0.917	0.005
428.9	422.3	435.5	319.43	50.41	269.0	0.2079	16.670	3.3546	0.960	0.004
440.1	434.2	446.0	314.02	50.41	263.6	0.2158	16.280	3.4939	1.000	0.004
450.9	444.5	457.4	343.81	50.41	293.4	0.2240	20.140	3.2630	0.934	0.003
460.6	455.0	466.2	352.35	50.41	301.9	0.2310	21.420	3.2556	0.932	0.003
468.7	462.8	474.6	363.91	50.41	313.5	0.2365	29.660	2.4993	0.715	0.002
480.7	475.1	486.2	121.36	50.41	71.0	0.2442	56.350	0.3074	0.088	0.001
488.2	482.2	494.1	62.07	50.41	11.7	0.2489	59.810	0.0485	0.014	0.001
499.0	493.6	504.4	53.81	50.41	3.4	0.2556	32.600	0.0267	0.008	0.001

Table 10e.
Relative Spectral Response of DLV at 295.77 K

$\langle\lambda\rangle$ (nm)	λ_1 (nm)	λ_2 (nm)	DN Bright	DN Dark	B-D	Mean Std. Det. Resp.	Std. Det. (nano-Amps)	Raw Rel. Resp.	Norm. Rel. Resp.	σ
		s =	*0.32*	*0.32*	*0.45*		*0.044*			
331.8	322.6	341.0	53.73	51.44	2.3	0.1474	1.423	0.2373	0.0697	0.019
339.6	333.1	346.0	53.23	51.44	1.8	0.1492	1.245	0.2145	0.0630	0.018
348.4	340.9	355.8	72.76	51.44	21.3	0.1494	2.389	1.3337	0.3918	0.013
361.6	354.6	368.7	86.27	51.44	34.8	0.1466	2.151	2.3738	0.6973	0.019
376.1	364.7	387.5	105.39	51.44	54.0	0.1544	3.156	2.6387	0.7751	0.013
380.9	374.3	387.5	134.34	51.44	82.9	0.1595	4.727	2.7974	0.8218	0.010
388.4	380.1	396.7	153.90	51.44	102.5	0.1695	6.033	2.8779	0.8454	0.008
400.4	393.8	407.0	154.71	51.44	103.3	0.1832	6.173	3.0640	0.9001	0.008
410.3	404.6	415.9	188.84	51.44	137.4	0.1924	8.604	3.0719	0.9024	0.006
418.0	411.9	424.2	236.89	51.44	185.5	0.1989	11.78	3.1305	0.9196	0.005
428.9	422.3	435.5	311.14	51.44	259.7	0.2079	16.31	3.3099	0.9723	0.004
440.1	434.2	446.0	309.86	51.44	258.4	0.2158	16.38	3.4042	1.0000	0.004
450.9	444.5	457.4	339.58	51.44	288.1	0.2240	20.32	3.1761	0.9330	0.003
460.6	455.0	466.2	346.69	51.44	295.3	0.2310	21.62	3.1540	0.9265	0.003
468.7	462.8	474.6	356.78	51.44	305.3	0.2365	29.56	2.4425	0.7175	0.002
480.7	475.1	486.2	122.51	51.44	71.1	0.2442	56.83	0.3054	0.0897	0.001
488.2	482.2	494.1	62.94	51.44	11.5	0.2489	60.55	0.0473	0.0139	0.001
499.0	493.6	504.4	54.4	51.44	3.0	0.2556	32.66	0.0232	0.0068	0.001

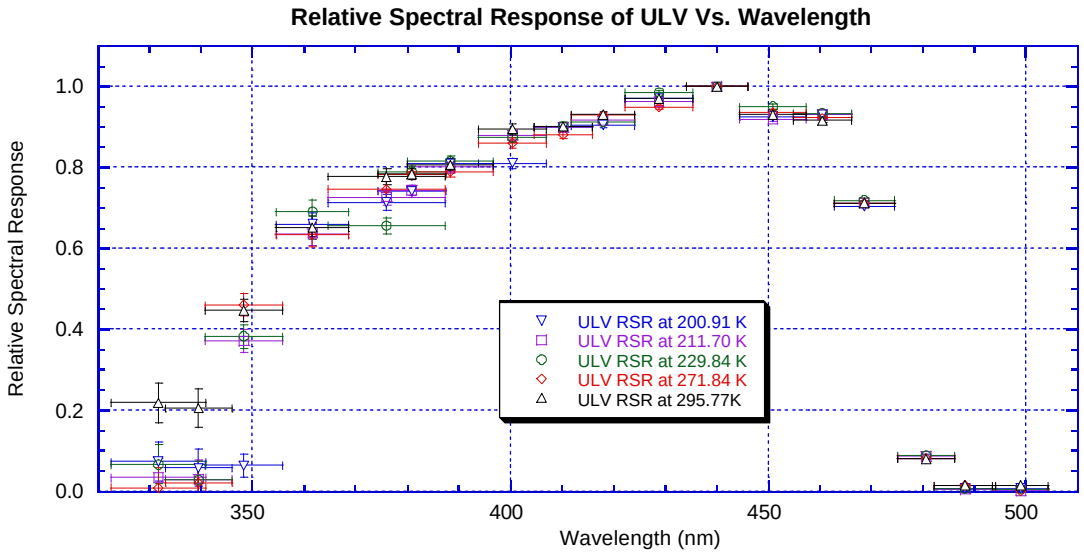

Fig. 11. The relative spectral response of the DLV system is shown as a function of wavelength at the five temperatures for which it was measured. The vertical bars indicate the uncertainty of each measurement, and the horizontal bars indicate the wavelength interval over which the measurement gives the average spectral response of the instrument.

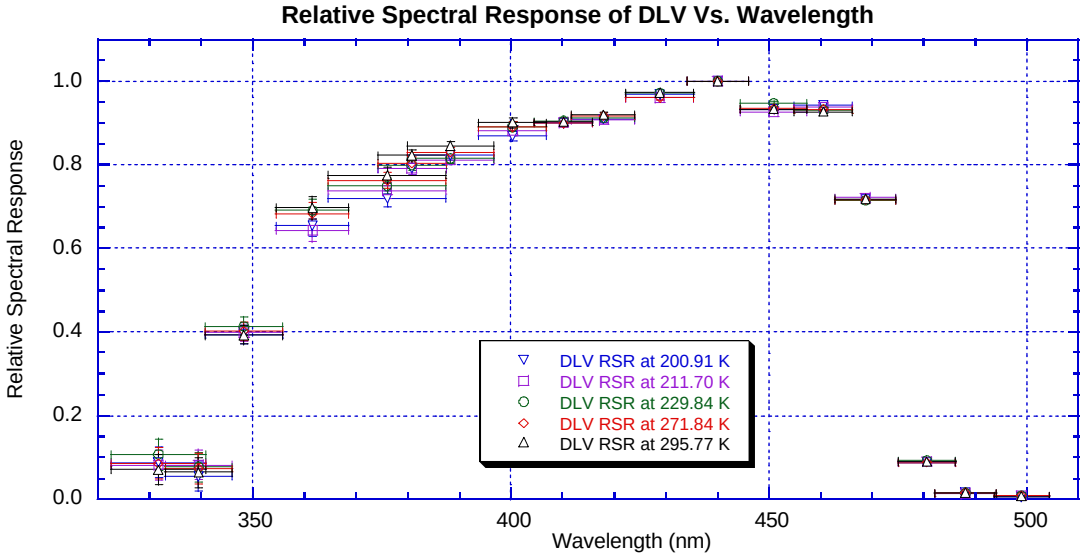

Fig. 12. Same as Fig. 11 but for the DLV system

The uncertainties in the measurements come primarily from the uncertainties in the ULV and DLV bright and dark readings. From the discussion above, we take the standard deviation of the bright readings and dark readings in the ULV to 0.1 DN, and the standard deviation of the bright and dark readings in the DLV to be 0.64 DN. The standard deviation in the readings of the silicon reference detector is estimated from the average of the standard deviations between the reference detector readings at the beginning and end of each filter. This gives the average standard deviation of the reference detector reading as about 0.044 nanoamps. The reading of the reference

detector with the shutter closed is some 5 to 6 orders of magnitude smaller than the readings with the shutter open, and is neglected here. The relative spectral response curves are normalized to unity in the band of peak response, and the errors in the normalized spectral response are propagated from the errors in the bright, dark, and silicon reference detector signals.

E. Model of Relative Spectral Response as a Function of Temperature

Once the relative spectral response has been evaluated as a function of wavelength at all the temperatures, it is useful to average the relative spectral response for all five temperatures. The mean relative spectral response of the DLV and ULV systems for the five measured temperatures are shown in Fig.13. Note that the shapes of the curves are very similar with significant differences only in the region from 360 to 410 nm. Since separate silicon detectors are used in the ULV and DLV sensors, some minor differences in the relative spectral response of these systems are to be expected.

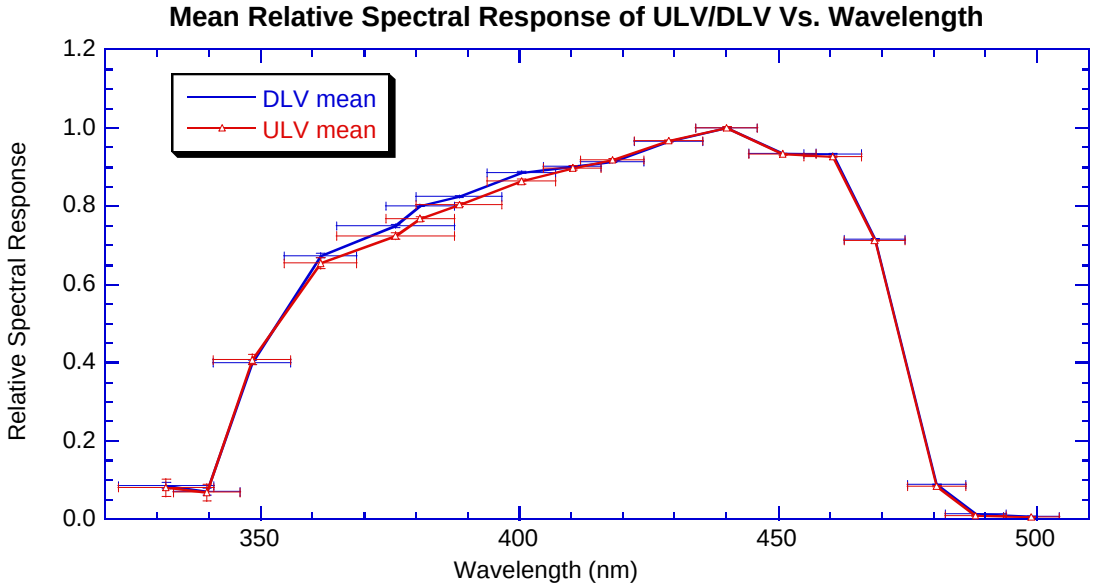

Fig. 13. The mean relative spectral response of the DLV and ULV systems are shown as functions of wavelength.

At each wavelength, the ratio of the relative spectral response at each temperature to the mean response can be determined as a function of wavelength. More precisely, we define a temperature coefficient, $C_T(\lambda)$ by the following relationship:

$$C_T(l) = \left(\frac{RelSpecResp(l,T)}{RelSpecResp(l,T_{mean})} - 1 \right) \left(\frac{1}{(T - T_{mean})} \right) \qquad (21.)$$

where T_{mean} is the mean temperature of the five temperatures at which the relative spectral response of the violet systems were measured, and the relative spectral response at the mean temperature is taken as the mean of the measurements at the five

temperatures. Thus, we have five estimates of the temperature coefficient at each wavelength of the measurements. The changes in the relative spectral response are relatively small with temperature, so we form a weighted average of the five estimates of the temperature coefficient at each wavelength. We weight the estimate at each temperature according to $1/\sigma^2$ where σ is the uncertainty in the temperature coefficient at each temperature. We estimate the uncertainty in the temperature coefficient at each temperature by propagating the errors in the relative spectral response measurements using equation (21). The table below gives the average value and uncertainty of the mean temperature coefficient at each of the 18 measured wavelengths for the DLV and ULV systems as well as the weighted average of the combination of the DLV and ULV measurements.

Table 11.
Estimates of Temperature Coefficients of Relative Spectral Response

Wavelength (nm)	$C_T(\lambda)$ for DLV	Sigma	$C_T(\lambda)$ for ULV	Sigma	Mean $C_T(\lambda)$	Sigma
331.8	-0.00198	0.00293	0.00718	0.00915	-0.00113	0.00284
339.6	-0.00011	0.00347	0.01078	0.01042	0.00097	0.00107
348.4	-0.00010	0.00045	0.00236	0.00093	0.00036	0.00034
361.6	0.00070	0.00038	-0.00019	0.00060	0.00045	0.00025
376.1	0.00069	0.00024	0.00100	0.00038	0.00078	0.00016
380.9	0.00039	0.00016	0.00059	0.00025	0.00045	0.00013
388.4	0.00034	0.00013	-0.00010	0.00024	0.00024	0.00011
400.4	0.00029	0.00013	0.00056	0.00020	0.00037	0.00010
410.3	0.00002	0.00010	-0.00009	0.00017	-0.00001	0.00007
418.0	0.00015	0.00007	0.00028	0.00010	0.00019	0.00005
428.9	0.00004	0.00005	-0.00009	0.00007	0.00000	0.00004
440.1	0.00000	0.00005	0.00000	0.00008	0.00000	0.00004
450.9	0.00001	0.00004	0.00007	0.00009	0.00002	0.00003
460.6	-0.00014	0.00004	-0.00018	0.00007	-0.00015	0.00003
468.7	0.00000	0.00003	0.00005	0.00008	0.00001	0.00003
480.7	0.00002	0.00011	-0.00037	0.00032	-0.00003	0.00012
488.2	0.00042	0.00068	0.01233	0.00303	0.00099	0.00069
499.0	0.00115	0.00229	0.00664	0.00839	0.00153	0.00236

Note in Table 11 that the uncertainties in the temperature coefficients are as large as the estimated coefficients at the first few and last few wavelengths where the measured relative spectral responses are small and uncertain. Figure 14 shows temperature coefficients with their error bars as a function of temperature. Note that from 360 to 470 nm the temperature coefficients are significantly less uncertain than at the ends of the spectral range, and that they vary roughly linearly with wavelength. We adopt the linear approximation as a way to further reduce the uncertainty in the rather small temperature coefficients. This gives

$$C_T(l) = 0.0028757 - 6.4513x10^{-6}\, l \ . \qquad (22.)$$

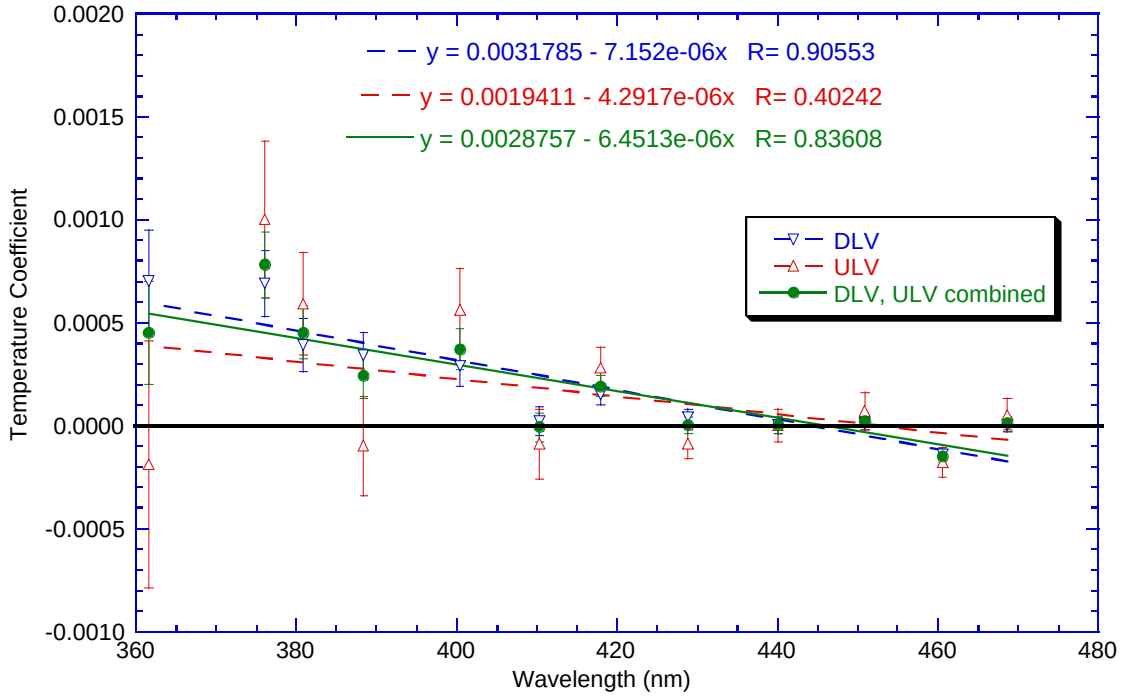

Fig. 14. The averaged temperature coefficients and their uncertainties are shown for the DLV, the ULV, and the combination of the DLV and ULV systems. We adopt the linear fit to the combination of the ULV and DLV systems as the best representation of the temperature dependence of the violet photometer system.

Now that the mean spectral response has been determined together with the temperature coefficients, it is possible to evaluate the relative model relative spectral response at the five temperatures at which measurements were made to compare the model to the measurements. The model relative spectral response values for the DLV and ULV systems at the five temperatures are shown in Figs. 15 and 16. The deviations of the model from the measurements are shown in Figs. 17 and 18. Note that the pattern of deviations is reasonably random in temperature and wavelength, and that the models fit the data to nearly the expected accuracy of the measurements. The rms deviation of the models to the DLV observations is 0.0072 and to the ULV observations is 0.028.

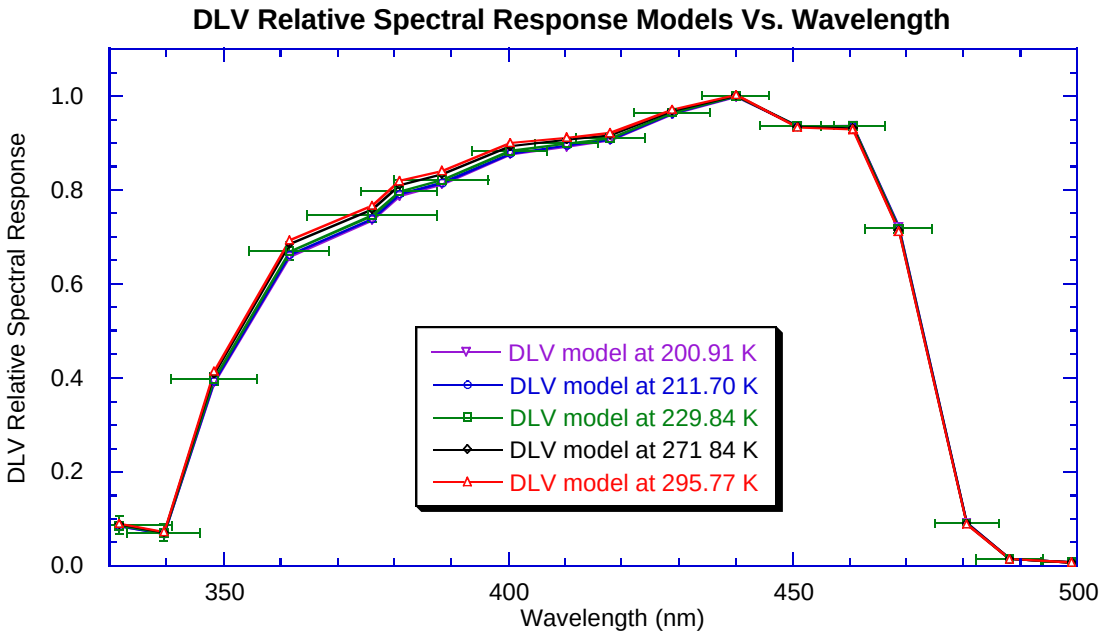

Fig. 15. The relative spectral response model of the DLV is shown at the five temperatures for which measurements were made. The horizontal bars indicate the spectral region over which the average response is known. The models have been connected by straight line segments in the center of each filter, although the actual spectral response has more structure than indicated by these straight lines.

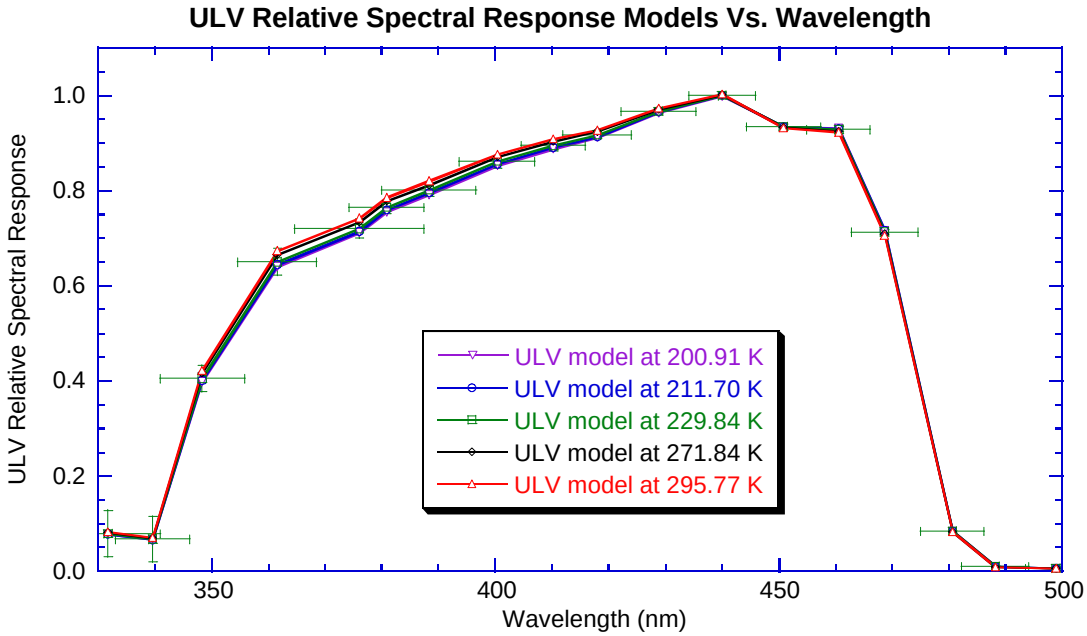

Fig. 16. Same as Fig. 15 but for the ULV.

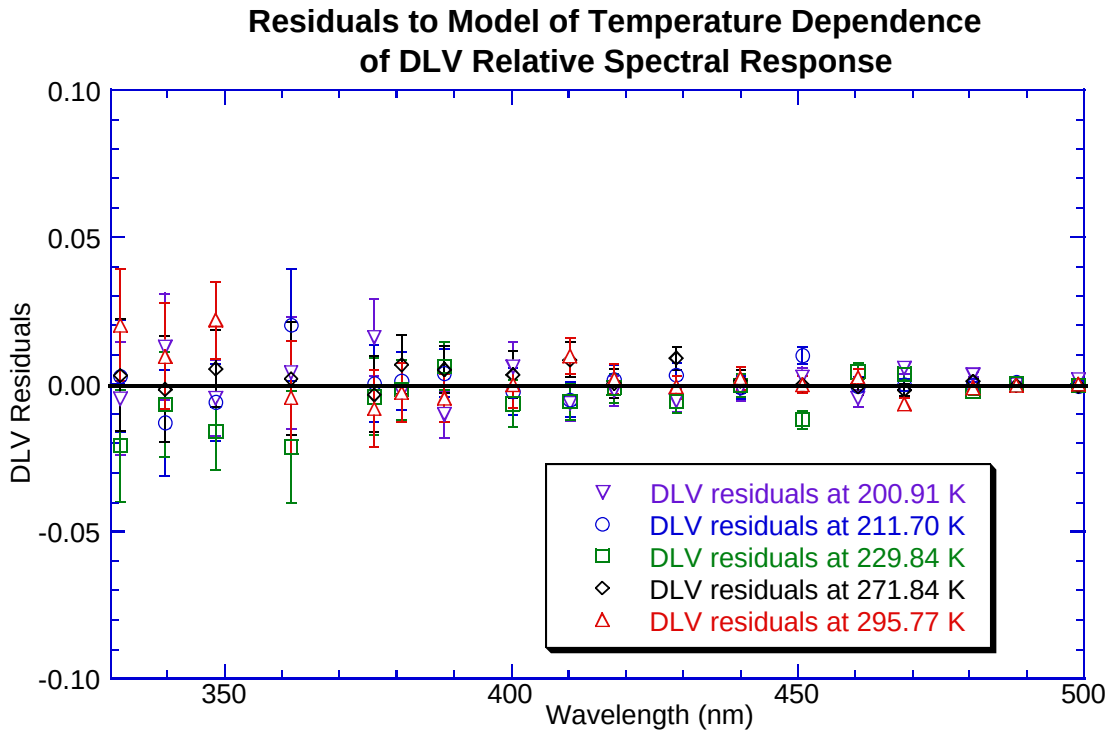

Fig. 17. The residuals of the spectral response model compared to the measured relative spectral response for the DLV is shown at the five measured temperatures, as labeled. The error bars are the error bars corresponding to the measurements only, and include no contribution for the determination of the temperature coefficients. The residuals are of the order of 1 percent over most of the spectral range, are not correlated with temperature, and are similar to the uncertainty in the measurements alone.

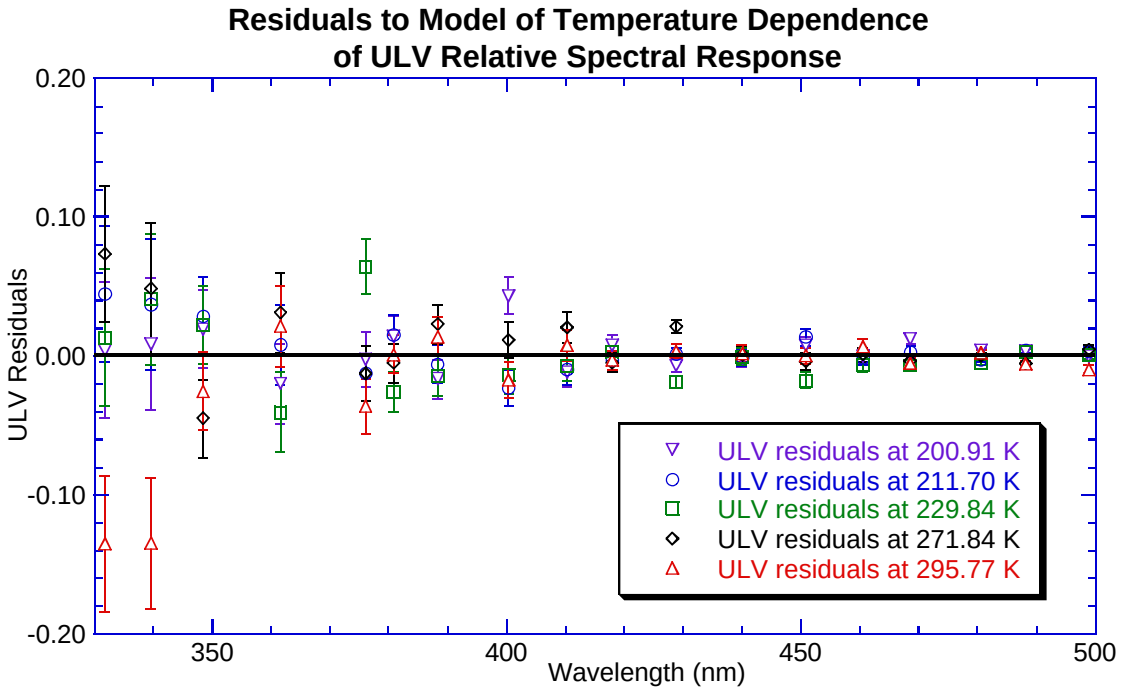

Fig. 18. The same as Fig. 17, but for the ULV system. Note that the scale is twice as large in view of the larger measurement errors of the ULV system. However, over most of the spectral range, the errors are of the order of 1 percent, not correlated with temperature, and are similar to the uncertainty in the measurements alone.

F. Measurement of Relative Spectral Response at High Spectral Resolution

Before the temperature coefficients derived above can be used to give the relative spectral response as a function of wavelength at an arbitrary temperature, the relative spectral response at modest spectral resolution consistent with the above measurements in the set of 18 filters must be determined. Two methods are available for this purpose. First, it is possible to simply pick trial values of the relative spectral response at some point in each filter, fit a spline curve through this set of points, and integrate the smooth curve for comparison with the observed mean values in each filter. If the trial curve gives a value higher or lower than the observed mean value, the set of trial points can be adjusted. After a few trials, it is possible to find a smooth curve that is consistent with the constraints. The disadvantages of this approach are obvious. The derived curve, while smooth, is certainly not unique, and any special bumps and wiggles in the actual spectral response curve may well not be retrieved by this method.

A second approach is to measure one of the spare instruments at higher spectral resolution at room temperature. One can assume that the temperature dependence of the spare instrument and the flight unit are similar. Indeed, the variation of the relative response with temperature as revealed by the filter measurements indicates that the changes in the relative response with temperature are small. The problem with measuring the spare unit is that undoubtedly variations between the instruments exist at some level, so we do not want to simply take the measurements of the spare unit as the relative

response of the flight unit. However, it is possible to apply a reasonably small and smooth modification to the measurements of the spare unit to make the mean values in the set of 18 filters agree with the measured mean values on the flight unit. If this curve resembles the smooth curve derived by the first method, then some confidence can be obtained in the methods.

Figure 19 shows the relative spectral response measured at a spectral resolution of 2 nm for the DLV of the field test unit (SN03) at 300 K scaled to 242 K using the temperature coefficients derived for the flight unit above. The mean values of the relative spectral response measured for the DLV of the flight unit are shown in the figure by the black horizontal bars. The green smooth curve is the fit to the mean values derived by simply using a smooth spline curve between trial points adjusted to give the observed mean values in each filter (except the one at 320 nm where the error bars are very large). The red curve is obtained by adjusting the measured curve of the field test unit until it fits the measured mean values of the flight unit. Note that the green curve and the red curves are very similar. The differences are in the upward curvature and the value at the short wavelength end, the slight overshoot at 350 nm in the red curve, and the presence of the shoulder in the red curve near 470 nm. None of these features could be resolved in the filter measurements, but seem very reasonable in view of the signatures observed in the field test unit.

The major difference between the red and blue curves corresponding to the flight model and the field test models, respectively, is the droop in response that occurs shortward of 400 nm. Note that this occurs shortward of the region where silicon is normally responsive, and the special ultraviolet coating for extended response provides the short wavelength response. It seems likely that the decreased response shortward of 400 nm in the flight detectors is due to variations in the efficiency of the coating used to extend the spectral response to these short wavelengths.

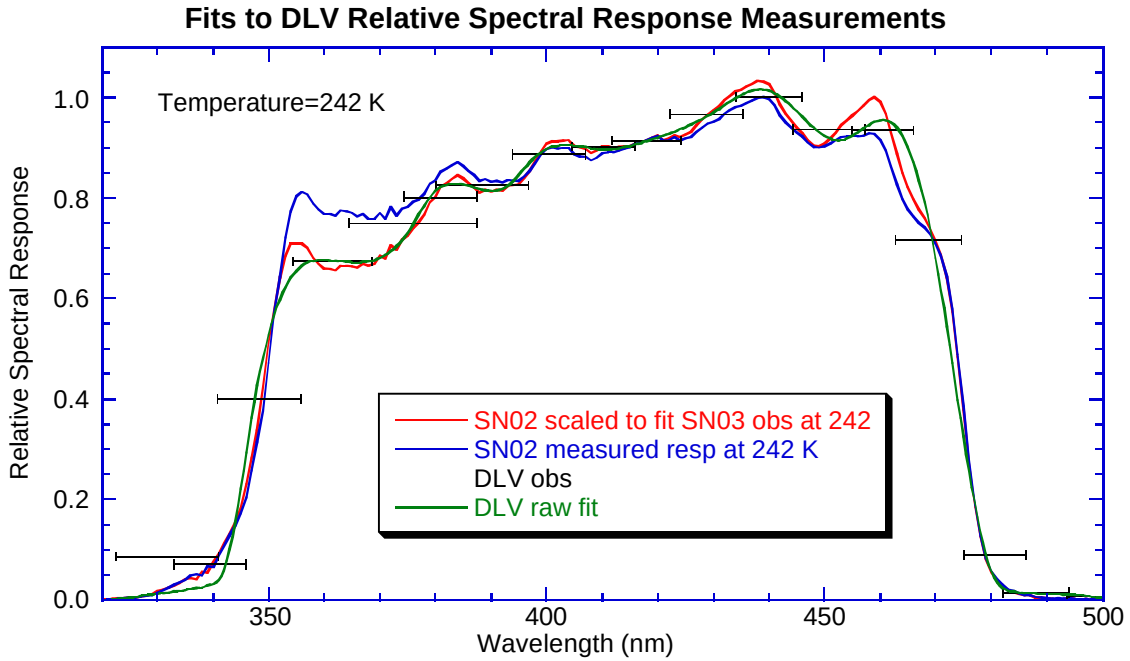

Fig. 19. Measured relative spectral response for DLV of SN02 scaled to 242 K (blue), measured mean DLV response for flight model at 242 K (horizontal black bars), smooth spline approximation to measured values (green curve), and the result of scaling the measurements of SN02 to fit the average values of the flight model (red curve) are shown. We adopt the red curve for the high spectral resolution version of the relative spectral resolution of the DLV of the flight model at 242 K except we normalize the curves to unity at the maximum value.

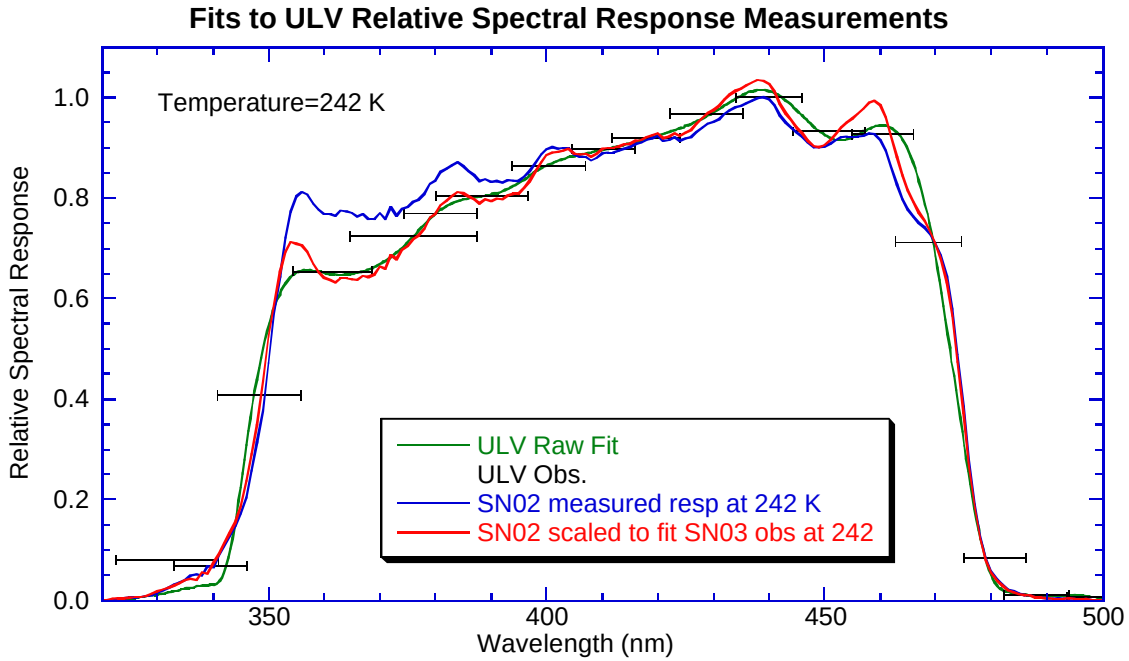

Fig. 20. Like Fig. 19 except for the ULV.

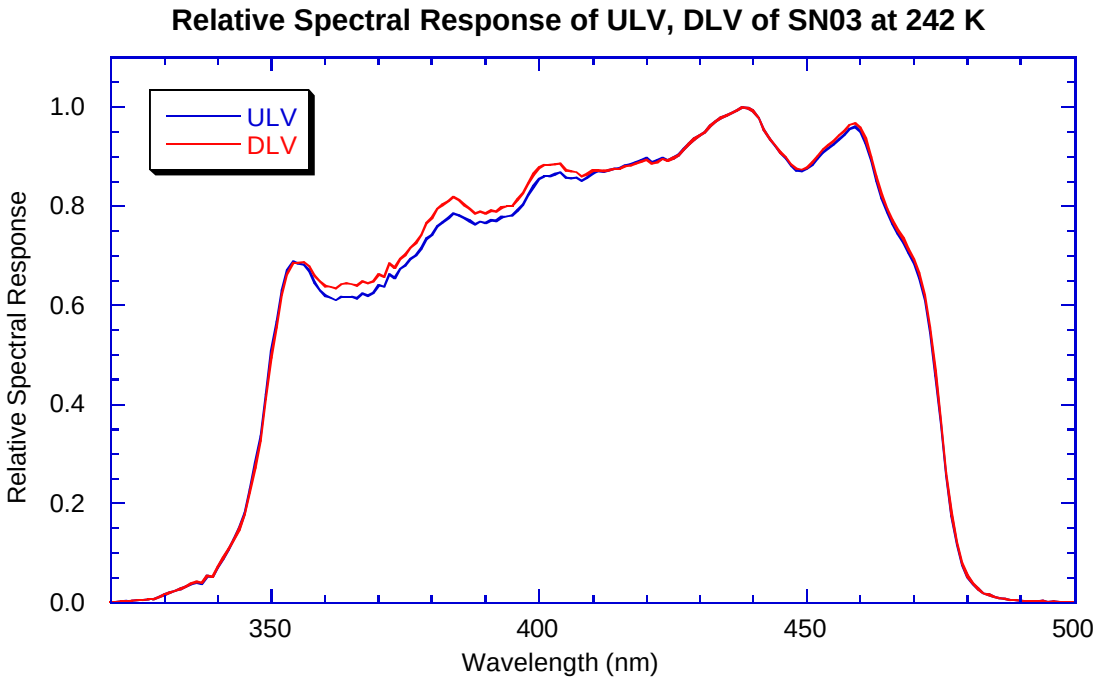

Fig. 21. Relative spectral response as a function of wavelength for the ULV and DLV systems on the flight model at a temperature of 242 K are shown, as labeled. The values plotted are given in Table 12 and are used with the temperature coefficients given by equation (22) to evaluate the relative spectral response of the ULV and DLV photometers on the flitght model based on the definition of the temperature coefficient given in equation (21).

The adopted form of the high resolution relative spectral response of the ULV and DLV systems at the base temperature of 242 K are shown in Fig. 21, and the values are tabulated in table 12. These values are used together with the definition of the temperature coefficients in equation (21) and the value of the coefficients given by equation (22) to evaluate the relative spectral response of the ULV and DLV systems at any wavelength and temperature. (Note that the numerical values of the relative spectral response at any temperature have to be separately normalized to unity at the peak response.)

Table 12.
Relative Spectral Response of DLV, ULV at 242 K

Wave-length (nm	DLV	ULV	Wave-length (nm	DLV	ULV	Wave-length (nm	DLV	ULV
319	0.0000	0.0000	380	0.7765	0.7429	441	0.9777	0.9775
320	0.0009	0.0009	381	0.7954	0.7600	442	0.9549	0.9545
321	0.0017	0.0019	382	0.8034	0.7678	443	0.9367	0.9360
322	0.0026	0.0027	383	0.8113	0.7766	444	0.9239	0.9228
323	0.0034	0.0036	384	0.8186	0.7856	445	0.9091	0.9076
324	0.0042	0.0045	385	0.8122	0.7820	446	0.8995	0.8976
325	0.0051	0.0053	386	0.8027	0.7755	447	0.8851	0.8827
326	0.0059	0.0061	387	0.7948	0.7705	448	0.8757	0.8729

327	0.0067	0.0069	388	0.7853	0.7635	449	0.8743	0.8709
328	0.0075	0.0077	389	0.7902	0.7701	450	0.8789	0.8750
329	0.0124	0.0126	390	0.7857	0.7668	451	0.8888	0.8843
330	0.0166	0.0168	391	0.7903	0.7717	452	0.9009	0.8958
331	0.0206	0.0207	392	0.7896	0.7712	453	0.9145	0.9089
332	0.0247	0.0246	393	0.7975	0.7787	454	0.9240	0.9178
333	0.0287	0.0284	394	0.7998	0.7805	455	0.9326	0.9258
334	0.0327	0.0321	395	0.8010	0.7810	456	0.9422	0.9350
335	0.0396	0.0386	396	0.8136	0.7926	457	0.9520	0.9445
336	0.0424	0.0412	397	0.8268	0.8049	458	0.9639	0.9560
337	0.0399	0.0386	398	0.8459	0.8230	459	0.9684	0.9602
338	0.0556	0.0538	399	0.8645	0.8410	460	0.9590	0.9509
339	0.0529	0.0514	400	0.8785	0.8549	461	0.9360	0.9281
340	0.0733	0.0716	401	0.8838	0.8607	462	0.9004	0.8929
341	0.0899	0.0887	402	0.8835	0.8617	463	0.8590	0.8519
342	0.1087	0.1084	403	0.8851	0.8649	464	0.8229	0.8162
343	0.1267	0.1276	404	0.8870	0.8686	465	0.7951	0.7887
344	0.1479	0.1502	405	0.8737	0.8577	466	0.7724	0.7660
345	0.1772	0.1810	406	0.8707	0.8570	467	0.7522	0.7458
346	0.2236	0.2292	407	0.8690	0.8576	468	0.7347	0.7279
347	0.2735	0.2809	408	0.8613	0.8523	469	0.7148	0.7076
348	0.3275	0.3364	409	0.8653	0.8586	470	0.6922	0.6843
349	0.4107	0.4215	410	0.8730	0.8682	471	0.6642	0.6555
350	0.4956	0.5074	411	0.8729	0.8698	472	0.6205	0.6112
351	0.5569	0.5682	412	0.8711	0.8695	473	0.5561	0.5468
352	0.6213	0.6311	413	0.8727	0.8723	474	0.4678	0.4591
353	0.6628	0.6698	414	0.8756	0.8763	475	0.3677	0.3602
354	0.6858	0.6891	415	0.8753	0.8766	476	0.2629	0.2571
355	0.6861	0.6852	416	0.8808	0.8828	477	0.1803	0.1761
356	0.6871	0.6818	417	0.8820	0.8845	478	0.1218	0.1189
357	0.6792	0.6697	418	0.8871	0.8897	479	0.0792	0.0774
358	0.6600	0.6468	419	0.8907	0.8934	480	0.0546	0.0533
359	0.6478	0.6311	420	0.8951	0.8977	481	0.0388	0.0379
360	0.6394	0.6197	421	0.8863	0.8888	482	0.0288	0.0283
361	0.6380	0.6157	422	0.8890	0.8912	483	0.0199	0.0195
362	0.6349	0.6108	423	0.8958	0.8977	484	0.0159	0.0157
363	0.6436	0.6181	424	0.8913	0.8929	485	0.0123	0.0122
364	0.6441	0.6180	425	0.8968	0.8980	486	0.0101	0.0100
365	0.6430	0.6171	426	0.9025	0.9033	487	0.0086	0.0086
366	0.6406	0.6153	427	0.9150	0.9155	488	0.0057	0.0057
367	0.6483	0.6236	428	0.9270	0.9272	489	0.0055	0.0055
368	0.6442	0.6207	429	0.9359	0.9359	490	0.0043	0.0043
369	0.6483	0.6257	430	0.9425	0.9422	491	0.0028	0.0028
370	0.6632	0.6414	431	0.9502	0.9499	492	0.0032	0.0032
371	0.6583	0.6376	432	0.9633	0.9629	493	0.0024	0.0024
372	0.6840	0.6634	433	0.9713	0.9710	494	0.0038	0.0039
373	0.6748	0.6550	434	0.9794	0.9791	495	0.0020	0.0020
374	0.6939	0.6735	435	0.9833	0.9831	496	0.0027	0.0027
375	0.7020	0.6809	436	0.9892	0.9892	497	0.0020	0.0020
376	0.7172	0.6944	437	0.9943	0.9943	498	0.0017	0.0017
377	0.7260	0.7010	438	1.0000	1.0000	499	0.0018	0.0018
378	0.7428	0.7149	439	0.9986	0.9987	500	0.0022	0.0022
379	0.7661	0.7349	440	0.9925	0.9924	501	0.0000	0.0000

The values of the relative spectral response given in Table 12 were obtained by scaling the measured relative spectral response of the field test unit (SN02) {after adjusting them using the temperature coefficients of SN03 to a temperature of 242 K} to fit the constraints of the average response in the set of 18 filters averaged over temperature. The ability of the shifted curves to fit the constraints of the filter measurements of the flight model can be judged from Table 13. This table gives the observed mean response and the actual mean response of the scaled SN02 observations as well as the residuals from the observed values for the DLV and the ULV. Note that except for the filters at the two shortest wavelengths, where the observations are most uncertain, the residuals are of the order of one or two tenths of a percent of the peak response, as good or better than the accuracy of the filter observations.

Table 13.
Residuals to Average Response in Filter Set for DLV, ULV Relative Spectral Response Models Based on Measurements of SN02

λ1	λ2	DLV Observed	DLV model	Model-Observed	ULV Observed	ULV model	Model-Observed
322.6	341.0	0.086	0.029	-0.057	0.080	0.029	-0.051
333.1	346.0	0.070	0.089	0.020	0.068	0.090	0.022
340.9	355.8	0.400	0.400	0.000	0.408	0.406	-0.002
354.6	368.7	0.673	0.674	0.001	0.654	0.656	0.001
364.7	387.5	0.749	0.749	0.000	0.724	0.723	-0.001
374.3	387.5	0.801	0.799	-0.002	0.768	0.770	0.002
380.1	396.7	0.824	0.826	0.001	0.804	0.801	-0.002
393.8	407.0	0.886	0.885	-0.001	0.863	0.866	0.003
404.6	415.9	0.901	0.900	-0.001	0.897	0.896	0.000
411.9	424.2	0.913	0.913	0.001	0.918	0.917	-0.002
422.3	435.5	0.966	0.965	-0.001	0.967	0.967	0.000
434.2	446.0	1.000	0.998	-0.002	1.000	1.000	0.000
444.5	457.4	0.935	0.936	0.001	0.933	0.933	0.000
455.0	466.2	0.934	0.932	-0.002	0.927	0.926	-0.001
462.8	474.6	0.716	0.718	0.001	0.712	0.712	0.000
475.1	486.2	0.089	0.090	0.001	0.084	0.089	0.005
482.2	494.1	0.014	0.009	-0.005	0.009	0.009	0.000
493.6	504.4	0.007	0.002	-0.005	0.005	0.002	-0.004

Once the relative spectral response of the ULV and DLV photometers has been generated at a particular temperature, it is useful to determine the short and long wavelength limits and the mean response of a effective rectangular filter that will have the same energy between the short and long wavelength limits as the actual instrument does for an intensity spectrum that is up to quadratic in wavelength. The method for determining these limits and mean response has been given earlier. The results are shown in Fig.22 for the short and long wavelength limits as a function of temperature for the ULV and DLV systems of the flight unit. We see that the ULV and DLV systems are well matched, with the limiting wavelengths agreeing to within 0.2 nm for the short or long wavelength limits determined by either the ULV or DLV systems over the range of operating temperatures. We adopt the mean results for the short and long wavelength systems, or

$$\lambda_1 = 354.10 - 0.00950\ T \qquad (23.)$$

$$\lambda_2 = 478.35 - 0.00726\ T \qquad (24.)$$

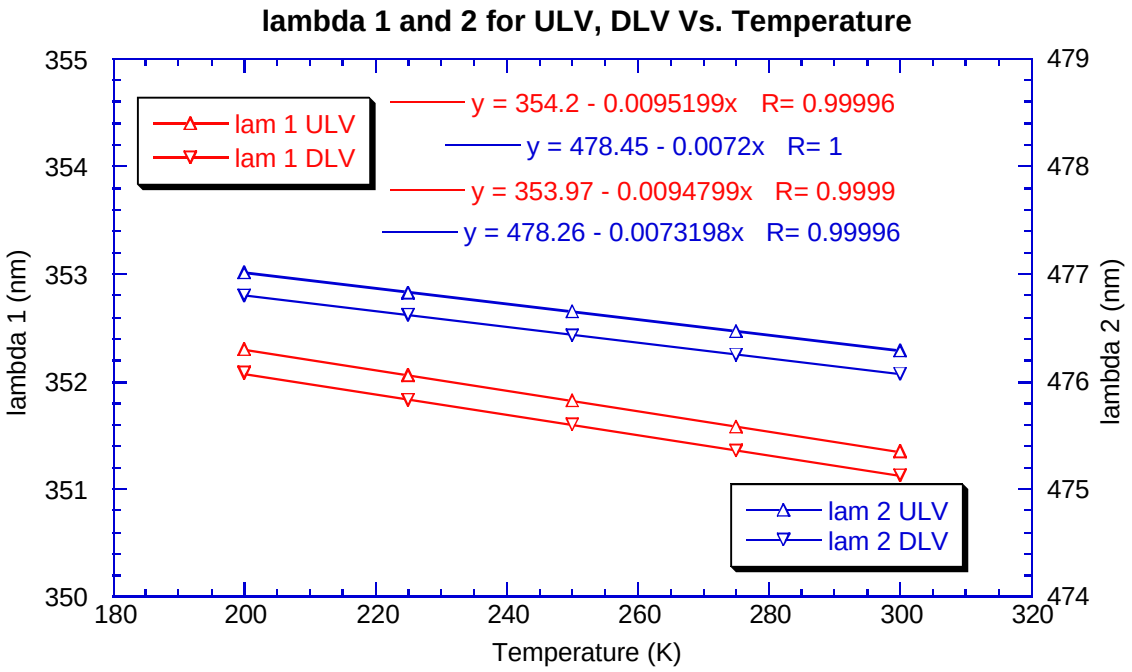

Fig. 22. The limiting wavelengths lampda 1 and lambda 2 for the equivalent square filter as a function of temperature for the ULV and DLV systems on the flight model, as labeled. Note that the ULV and DLV have the same limiting wavelengths to within 0.2 nm. We adopt the average of the ULV and DLV systems for equivalent wavelength range of the violet photometer as a function of temperature.

The average spectral responses of the equivalent rectangular filter for the ULV and DLV systems are shown as a function of temperature in Fig. 23. The linear fits to the observations are also shown. We adopt the mean response for the equivalent rectangular filters as

$$<R_{ULV}> = 0.8089 + 0.0001112\ T \qquad (25.)$$

$$<R_{DLV}> = 0.8182 + 0.000116\ T \qquad (26.)$$

for the ULV and DLV filters, respectively.

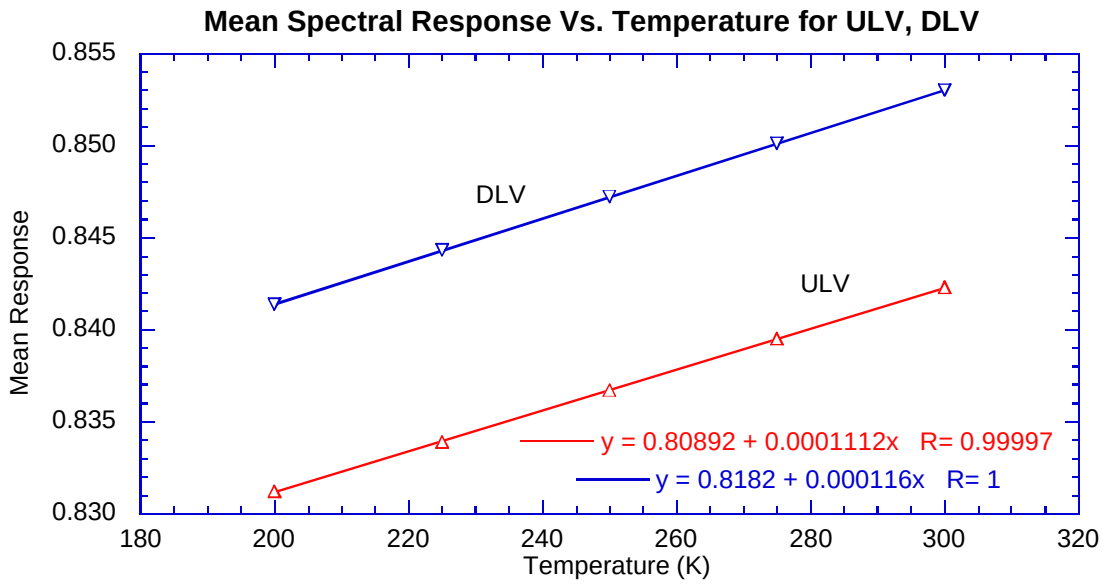

Fig. 23. The mean response of the equivalent square filter for the ULV and DLV systems as a function of temperature are shown.

IV. Relative Spatial Response

The relative spatial responses of the ULV and DLV systems were measured at room temperature. An 8-inch diameter spherical mirror was used to produce a collimated beam of light. The DISR sensor head was mounted on an altitude-azimuth mount with either the ULV or DLV window centered on the axes of rotation of the mount. We turned the mount under computer control and collected data from the violet photometers at a wide range of angles relative to the outward normal of the ULV and DLV diffusers. Dark readings were interspersed with the bright readings to permit removal of the electrical bias of the violet photometers. A reference detector was used to track any drifts in the brightness of the light from the collimator. The coordinates of the altitude-azimuth mount were converted to local azimuth and zenith angle in the sensor head coordinate system. The resulting measurements were interpolated to fill in the grid to one degree spacing in azimuth and zenith angle. A small amount of smoothing was done during the interpolation to remove artifacts caused by non-uniform stepping of the altitude-azimuth mount. The resulting relative spatial response of the ULV and DLV (each normalized to unity at the direction of peak response) are plotted in Figs. 24 and 25. An appendix to this report contains the measurements in a table available in electronic form in the version of this report contained on our web site.

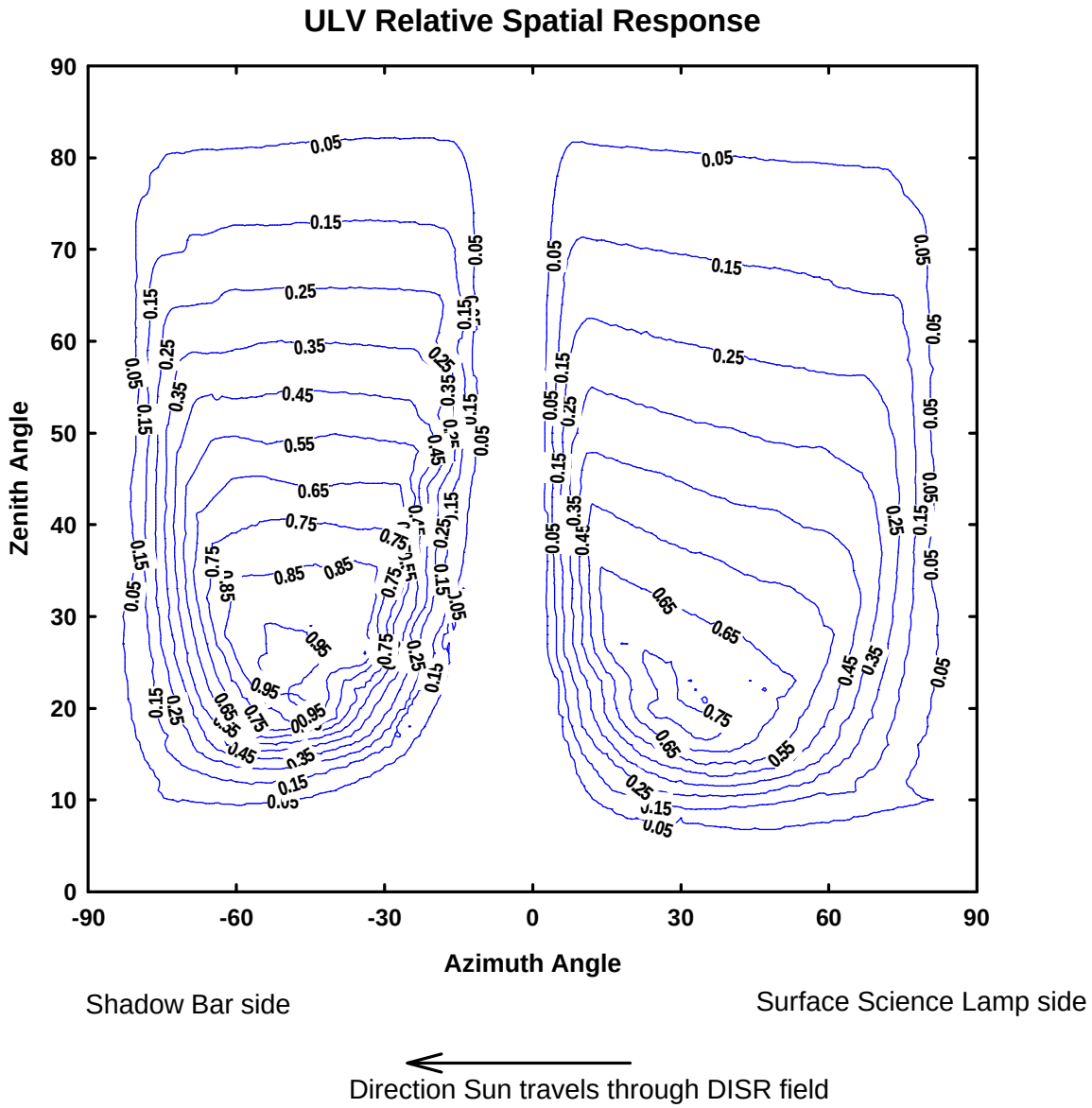

Fig. 24. Contour plot of the relative spatial response of the ULV photometer. Azimuth angle increases counter-clockwise when looking down on the instrument from above. The drop in contrast due to the shadow bar between about –10 to 0 degrees azimuth is apparent.

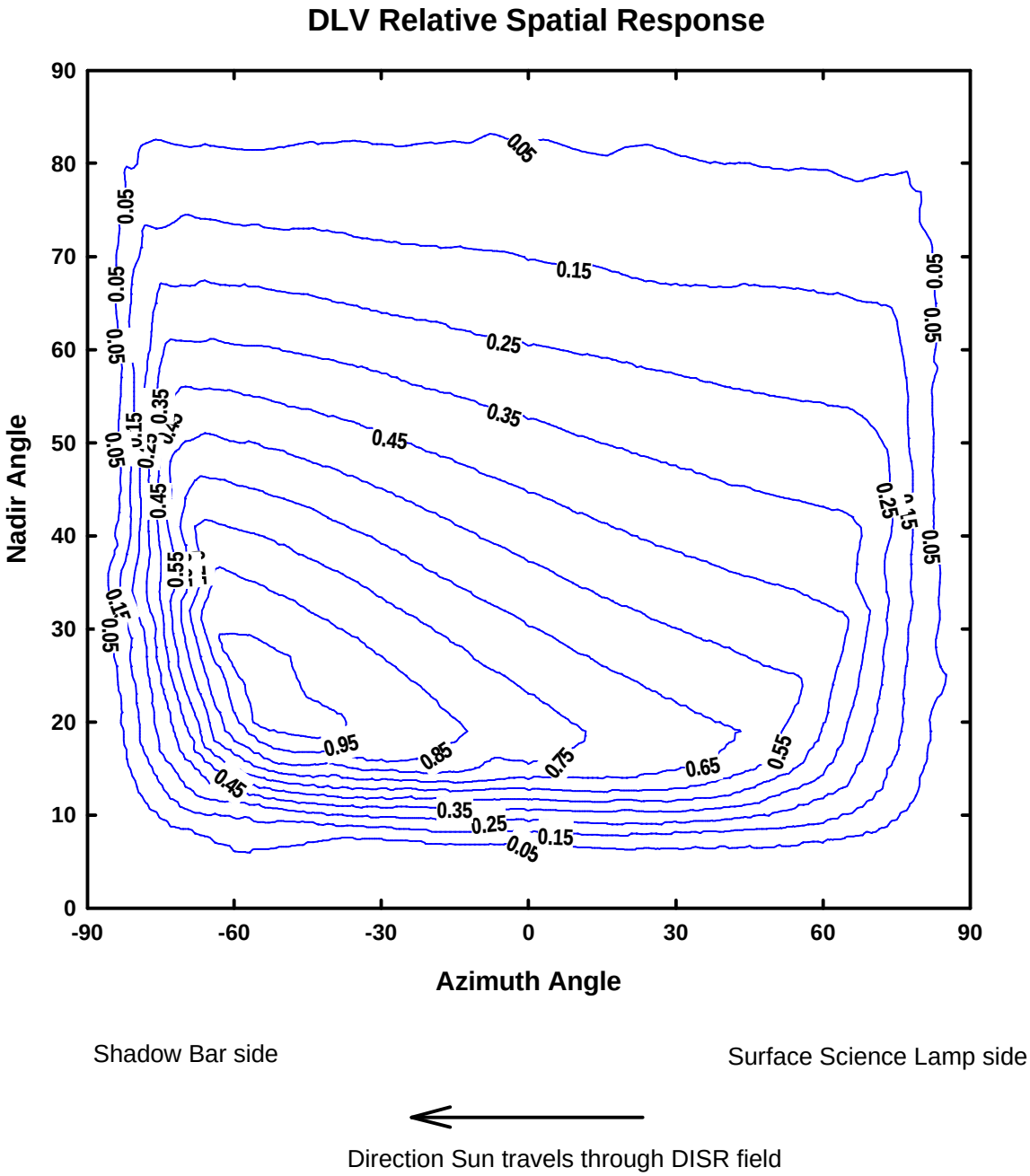

Fig. 25. Like Fig. 24 except for the DLV. Note the lack of shadow bar in the DLV field, and that the vertical axis is nadir angle rather than zenith angle.

It is of some interest to estimate the departure of the relative spatial response function achieved in the ULV and DLV systems with the cosine(zenith angle) response desired. One approach is to simply average the spatial response in azimuth angle, and plot the relative spatial response in zenith angle times the element of solid angle which is proportional to sine(zenith angle). Fig. 26 shows the actual result for the ULV in blue with the ideal response in red. The centroid of the actual ULV response is at a zenith angle of 44.05 degrees while the ideal centroid is at 45 degrees. Thus, the ULV response is centered at about the correct zenith angle and is a bit narrower in zenith angle than the

ideal response. The situation for the DLV is shown in Fig. 27, with the centroid of the DLV response times solid angle at 137.73 degrees compared to the ideal centroid of 135 degrees. Again, the centroid is within a few degrees of the ideal location and the field of view is a bit narrower than ideal. The violet system photometers give the average intensity of the diffuse radiation field centered very near the desired zenith angles with weighting functions that are qualitatively rather similar to the ideal weighting functions.

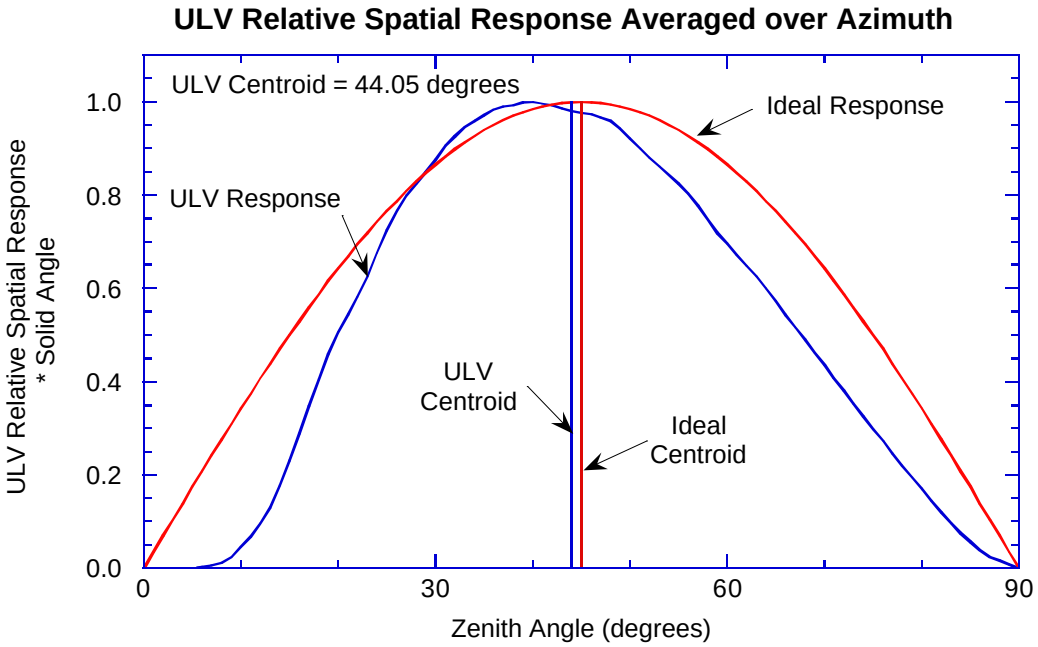

Fig. 26. The relative spatial response of the ULV field of view averaged over azimuth and multiplied by the element of solid angle in zenith [(sin(zenith angle)], is shown in blue as a function of zenith angle. The ideal value of this function is shown in red. The centroid of the ULV function is within 1 degree of the ideal zenith angle, and the response function is somewhat narrower in zenith than the ideal function.

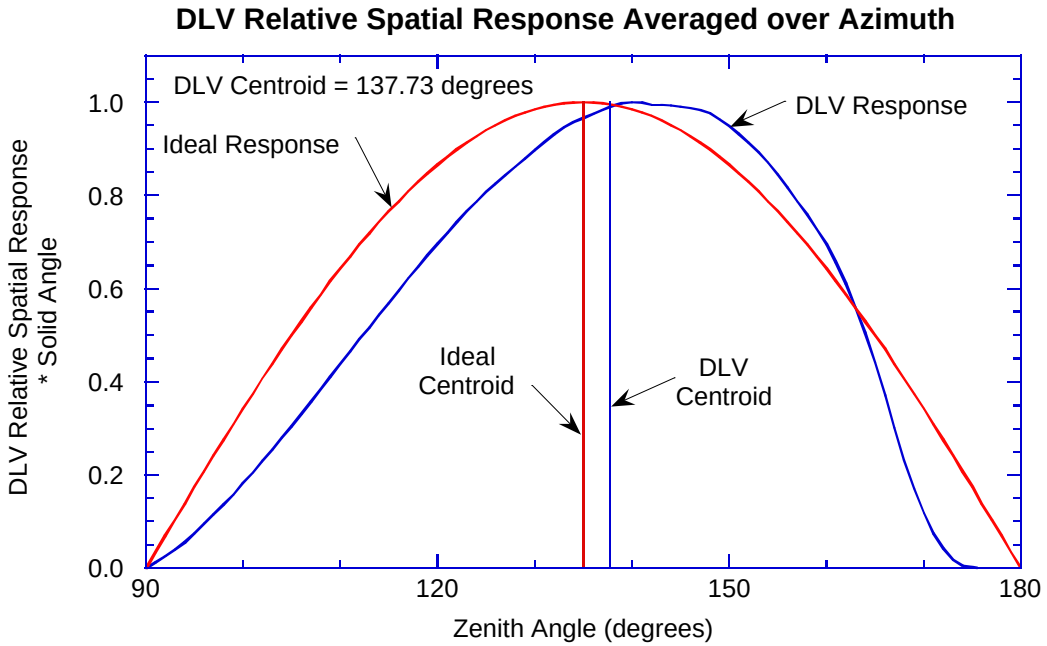

Fig. 27 Like Fig. 26 but for the DLV. The centroid of the DLV response times sin (zenith angle) is within 2.7 degrees of the ideal value of 135 degrees, and the relative response function is again somewhat narrower than the in the ideal case.

A more quantitative estimate of the errors that might be introduced by these departures from the ideal spatial response functions can be achieved be evaluating several integrals of the relative spatial response of the ULV and DLV systems. These include the integrals of 1/cos(zenith angle), 1, and cos(zenith angle) times the relative spatial response integrated over solid angle. The results of these integrals for the ULV and DLV systems are contained in Table 14. For an ideal diffuser with response proportional to cosine zenith angle, the ratios of these moments would be 1 to ½ to 1/3. The actual values of the integrals are also shown in Table 14. If these integrals are normalized to 0.5 for the integral with unit weighting function, the errors in the ratios from the ideal ratios are shown in the third column of the table.

Table 14.
Integrals over solid angle of Relative Spatial Response of ULV, DLV

Weighting Function	**ULV**	**Normalized**	**%Error**
1/cos (zenith angle)	1.1801	0.8804	-12.0
1	0.6702	0.5000	0.0
cos (zenith angle)	0.4554	0.3397	+1.9
	DLV	**Normalized**	**%Error**
1/cos (zenith angle)	1.4366	0.8787	-12.1
1	0.8175	0.5000	0.0
cos (zenith angle)	0.5683	0.3476	+4.3

The implications of these values are as follows. The error in estimating the diffuse flux from the measurements made using the non-ideal diffusers in the violet photometer systems depends on the shape of the radiation field. If the radiation field is isotropic, then it is possible to normalize the integrals of the relative spatial response (multiply the measurements by (0.5/0.6702 for the ULV) and obtain the exact diffuse flux. However, if the radiation field is not isotropic but is proportional to 1/cos(zenith angle), then the error made in the diffuse flux will be –12%. If the radiation field is instead proportional to cos(zenith angle), then the error will +1.9% for the diffuse flux measured by the ULV and +4.3% for the diffuse flux measured by the DLV. In practice, the shape of the radiation field can be expanded in a series of terms in cos(zenith angle) to various powers, and will not be purely described by a single component. The first three terms can be expected to be among the largest, however, and the errors in Table 14 give a useful estimate of the errors to be expected in the diffuse fluxes derived directly from the measurements. We plan to iterate the reduction of the measurements with models of the radiation field that will give the shape of the radiation field. By this means we expect to reduce the diffuse flux errors to much smaller values than the limits shown in Table 14.

V. Absolute Responsivity as a function of temperature

Once the relative spectral response and the relative spatial response of the violet photometers have been determined, the absolute peak responses of the ULV and DLV systems can be determined as functions of temperature. For this test, we illuminated the integrating sphere with a high-intensity lamp, and measured the response of the ULV and DLV systems to this illumination as a function of the temperature of the violet photometers. We monitored any drift in the brightness of the lamp with time during the many hours of the test by a silicon detector in the top of the integrating sphere filtered to cover the same bandpass as the ULV and DLV systems. We measured the spectrum of the light in the integrating sphere by observing the front wall of the sphere with a monochrometer followed by a standard silicon detector. The responsivity of the monochrometer-silicon detector system was calibrated by measuring the brightness of a standard lamp calibrated by the bureau of standards. In addition, in a separate measurement (B. Rizk and L. MacFarlane, 2000) we used a small photometer mounted inside the sphere to record the variations in brightness of the wall of the sphere in various directions. This information was available to tie the brightness of the portion of the wall of the sphere measured by the monochrometer-standard silicon detector to the average brightness of the wall of the sphere weighted by the relative spatial response of the ULV and DLV photometers.

With this general description of our approach, the net bright minus dark data numbers (DN) recorded by the ULV or DLV are given by

$$DN_{bright} - DN_{dark} = Resp_{peak} \iint I(l, J, j) Rel(l) Rel_{spatial}(J, j) dl \; d\Omega . \qquad (27.)$$

Now if the radiation field in the integrating sphere is given by the spectrum I(λ,90,90) at a point at the front of the sphere (directly opposite the center of hole in the sphere in which the DISR sensor head is mounted and designated as 90 degrees zenith angle and 90

degrees azimuth) times a relative brightness that is independent of wavelength and dependant only on direction, $I_{rel}(\theta,\phi)$, then eqn. (27) becomes

$$DN_{bright} - DN_{dark} = Resp_{peak} \int I(l,90,90) Rel(l) dl \int I_{rel}(J,j) Rel_{spatial}(J,j)\, d\Omega . \quad (28.)$$

Now the spectrum of the wall of the integrating sphere is known at the location viewed by the monochrometer-standard silicon detector system. This system views the region from 81 to 99 degrees zenith angle and 82 to 98 degrees azimuth angle in the sphere. The signal from the standard silicon detector behind the monochrometer is given by

$$I(amps) = Resp_{monochrometer/detector}(l) I(l,90,90) \frac{\int I_{rel}(J,j) d\Omega}{\int d\Omega} . \quad (29.)$$

Thus, the spectrum of the wall at the front of the sphere is given by

$$I(l,90,90) = \frac{I(amps) \int d\Omega}{Resp_{monochrometer/detector}(l) \int I_{rel}(J,j) d\Omega} \quad (30.)$$

where the integral over solid angle covers the range in zenith angle from 81 to 99 degrees and in azimuth angle from 82 to 98 degrees of the field of view of the monochrometer-standard detector system.

Now let us recast the last three equations slightly to clarify the small size of the corrections that result from including the measured departures of the shape of the radiation field from an isotropic field. Let us define the average ratio of the brightness over the ULV field of view to the brightness at the front of the integrating sphere by

$$I_{ULV/front} = \frac{\int I_{rel}(J,j) Rel_{ULVspatial}(J,j) d\Omega}{\int Rel_{ULVspatial}(J,j) d\Omega} , \quad (31.)$$

and the ratio of the brightness integrated over the field of view of the monochrometer to the brightness at the front of the integrating sphere as

$$I_{monochrometer/front} = \frac{\int I_{rel}(J,j) d\Omega}{\int d\Omega} . \quad (32.)$$

Now equation (28) becomes

$$DN_{bright} - DN_{dark} = Resp_{peak} I_{ULV/front} \int I(l,90,90) Rel(l) dl \int Rel_{spatial}(J,j)\, d\Omega , \quad (33.)$$

(and similarly for the DLV) and equation (30) becomes

$$I(\lambda,90,90) = \frac{I(amps)}{Resp_{monochrometer/detector}(\lambda) I_{monochrometer/front}}. \qquad (34.)$$

Now the intensity measured by the monochrometer is

$$I_{mono} = \frac{I(amps)}{Resp_{monochrometer/detector}}, \qquad (35.)$$

so equation (33) becomes

$$DN_{bright} - DN_{dark} =$$
$$Resp_{peak} \frac{I_{ULV/front}}{I_{monochrometer/front}} \int I_{mono}(\lambda) Rel(\lambda) d\lambda \int Rel_{spatial}(J,j)\, d\Omega. \qquad (36.)$$

This gives for the peak response of the violet photometers

$$Resp_{peak} = \frac{I_{ULV/front}}{I_{monochrometer/front}} \frac{(DN_{bright} - DN_{dark})}{\int I_{mono}(\lambda) Rel(\lambda) d\lambda \int Rel_{spatial}(J,j)\, d\Omega}. \qquad (37.)$$

When the absolute response analysis of the violet photometer systems was first done, the relative spatial response function had not yet been reduced. In these early reductions, the integral of the relative spatial response function over solid angle was taken as unity. For historical reasons, therefore, it is useful to define the measured responsivity as distinguished from the peak responsivity as

$$Resp_{measured} = Resp_{peak} \int Rel(J,j) d\Omega$$
$$= \frac{I_{ULV/front}}{I_{monochrometer/front}} \frac{(DN_{bright} - DN_{dark})}{\int I_{mono}(\lambda) Rel(\lambda) d\lambda}. \qquad (38.)$$

Figures 28 and 29 show the brightness in the integrating sphere relative to the front of the sphere over the fields of view of the DLV and ULV as they were mounted in the sphere. These relative brightness distributions have been multiplied by the relative spatial response of the violet photometers and by the solid angle of the monochrometer. The numerical values of the relevant integrals over solid angle are given in Table 15.

Table 15.
Integrals of relative brightness in integrating sphere with fields of view of ULV, DLV, and monochrometer

Function	ULV integral	DLV integral

Integral of average relative brightness * spatial response	0.65800 ster.	0.80428 ster.
Integral of relative spatial response	0.66962 ster.	0.81752 ster.
Average Iviolet/I(90,90)	0.982641	0.983801
Average Imono/I(90,90)	0.987988	0.987988
Average Iviolet/Imono.	0.994588	0.995762

We see that the average brightness over the ULV field of view weighted with the relative spatial response of the ULV and solid angle is 1.74% below the brightness at the front of the integrating sphere, and the corresponding value is 1.62% for the DLV. The brightness of the location of the monochrometer field of view is 1.2% darker than the front of the integrating sphere. Thus, the average brightness of the ULV is 0.541% lower than the monochrometer scan, and the average brightness of the DLV is 0.424% lower than the monochrometer scan.

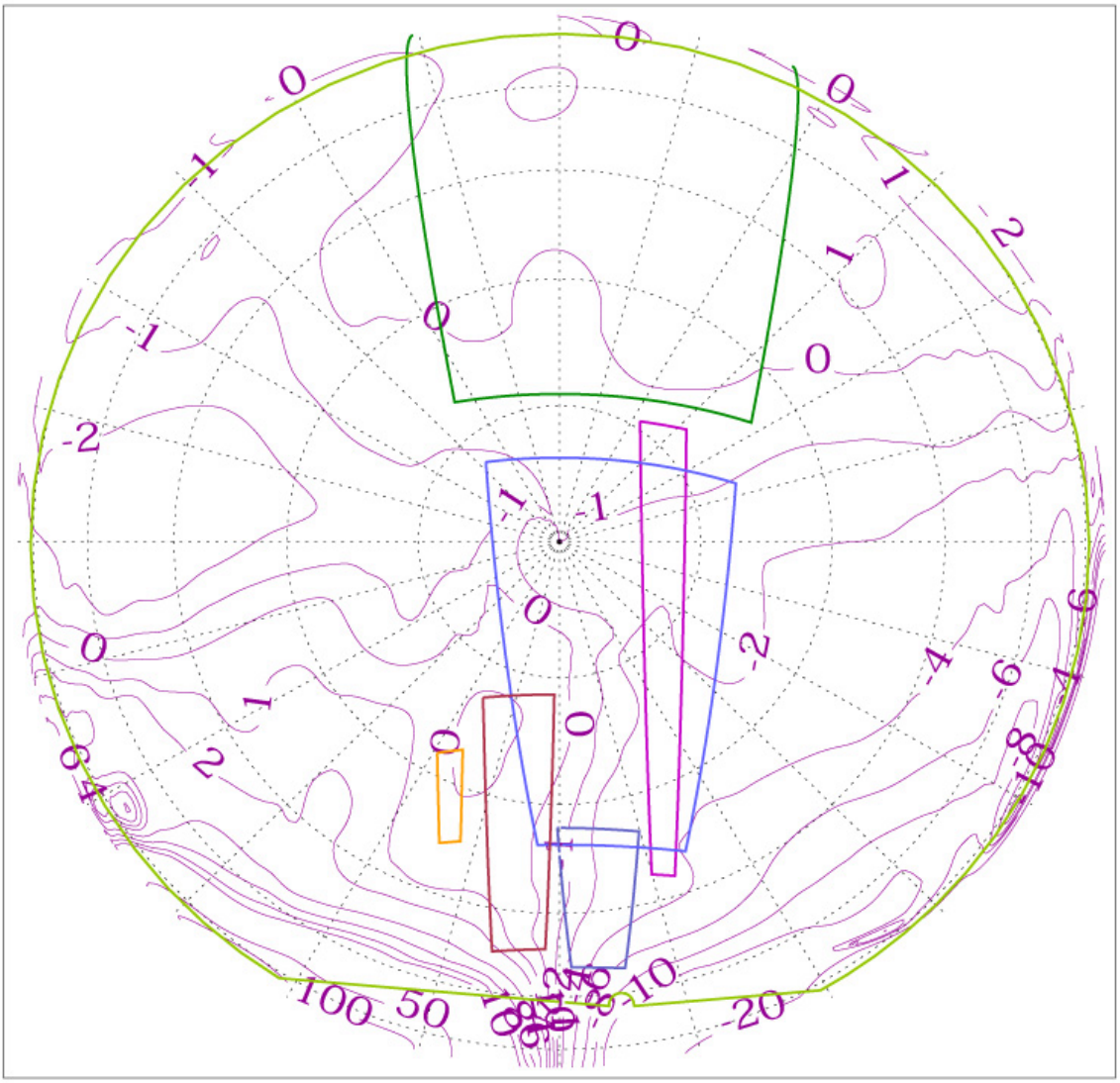

Fig. 28. The fields of view of the downward-looking DISR instruments superimposed on the countours of the relative brightness measured in the 20-inch diameter integrating sphere. The light green outline corresponds to the DLV, the dark green to the SLI, the light blue to the MRI, the dark blue to the HRI, the brown to the DLVS, and the yellow to the DLIS. The numbers indicate the percent difference from the brightness at the front of the sphere.

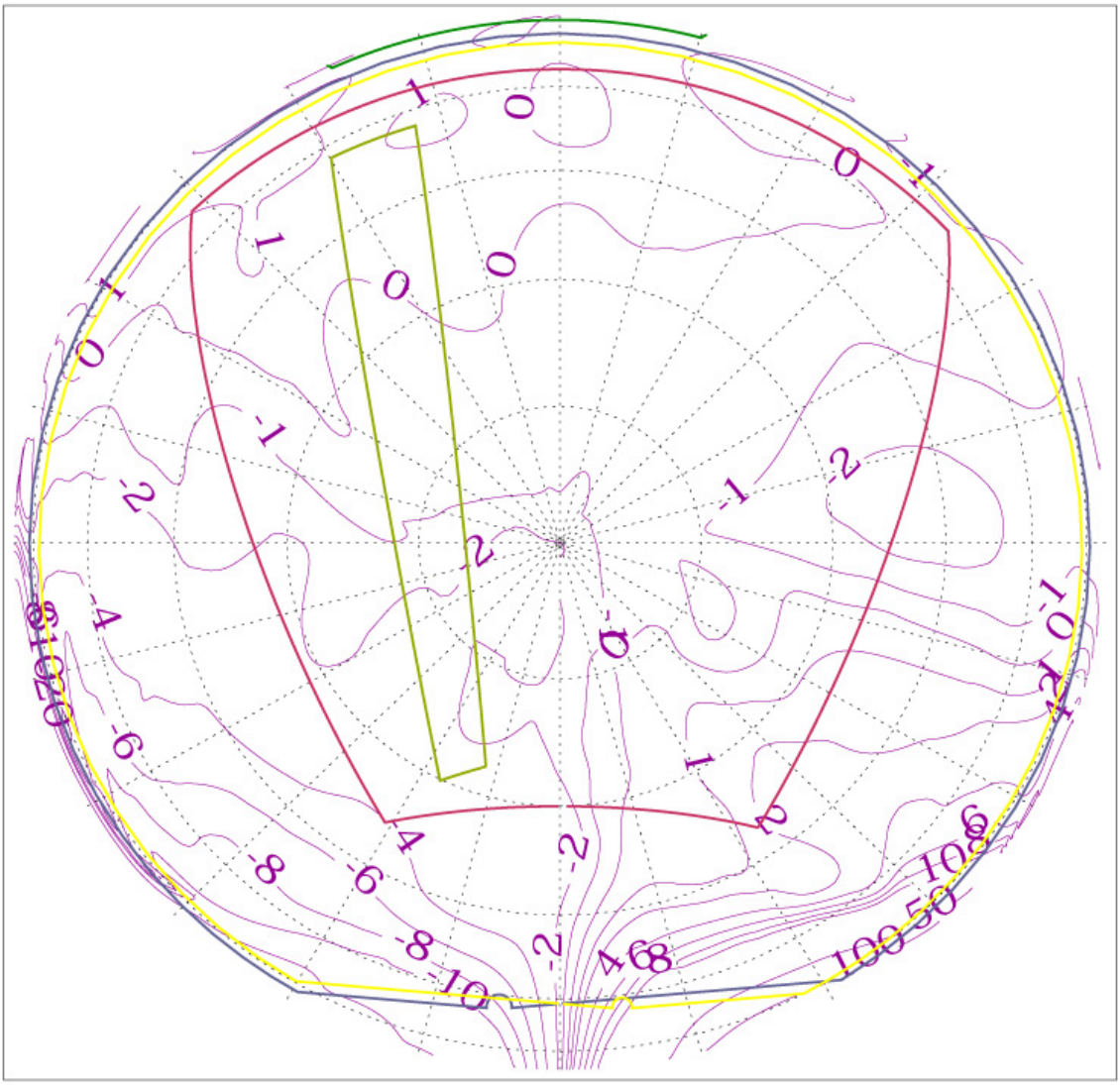

Fig. 29. Like Fig. 28 but for the upward-looking instruments. The Yellow is the field of view of the ULV, the light green is the Solar Aureole, and the brown is the Sun Sensor field of view. .

The measurements of the absolute response of the violet photometers were made on July 25, 1996 over a range of temperatures from 200 to 290 K. In addition, we made a brief set of measurements on August 16 at room temperature (295 K). We concentrate on the July 25 data first. On that day we cooled the sensor head such that the temperature of the violet photometers was below 200 K. We then used a shutter to alternately block or

open the path from the high intensity lamp into the integrating sphere. We took sets of 100 measurements of the DLV and the ULV with the shutter closed and open interspersed with measurements of the silicon detector mounted at the top of the inside of the integrating sphere. The filter was designed to match the spectral range of the violet photometer flight systems. Measurements by this detector could permit small adjustments in case the brightness of the lamp drifted with time. The sensor head was then permitted to warm gradually to room temperature over a period of many hours during which we alternated between ULV, DLV, and filtered silicon integrating sphere detector measurements with the shutter open and closed. Table 16 contains the averages of the sets of 100 ULV and DLV measurements as well as the measurements of the integrating sphere detector as functions of time and violet system temperature.

Table 16.
DLV Dark measurements during absolute response test on July 25, 1996

DLV Dark	Sigma	Time	Temp. (K)	Model Dark	Model-Obs
50.16	2.25	11:20:40	201.801	50.59	-0.43
50.99	1.60	11:31:16	200.410	50.56	0.43
50.22	1.37	11:41:51	199.416	50.53	-0.31
50.64	1.53	11:47:57	199.019	50.52	0.12
50.06	1.75	11:55:11	198.423	50.50	-0.44
50.61	1.35	12:02:26	198.026	50.49	0.12
50.01	1.56	12:08:13	197.926	50.48	-0.47
50.71	1.31	12:15:28	198.224	50.46	0.25
50.62	1.95	12:22:43	198.721	50.45	0.17
51.00	1.33	12:34:06	208.159	50.44	0.56
49.89	1.36	12:41:21	218.590	50.43	-0.54
50.57	1.42	12:48:36	223.557	50.42	0.15
50.51	1.73	12:53:28	227.332	50.41	0.10
50.72	1.65	13:00:42	231.306	50.41	0.31
50.56	0.99	13:07:57	235.479	50.40	0.16
50.46	1.49	13:16:34	239.254	50.40	0.06
49.93	1.32	13:23:49	241.340	50.40	-0.47
49.94	1.52	13:31:03	243.625	50.39	-0.45
50.53	1.67	13:37:24	245.513	50.39	0.14
50.70	0.83	13:44:40	248.096	50.39	0.31
50.75	1.65	13:51:54	250.182	50.40	0.35
50.94	0.85	14:01:35	251.573	50.40	0.54
50.51	1.31	14:12:12	251.970	50.41	0.10
50.93	1.44	14:22:48	251.871	50.41	0.52
50.28	1.93	14:30:00	251.672	50.42	-0.14
50.09	1.52	14:40:35	251.175	50.44	-0.35
50.53	1.37	14:51:11	251.672	50.45	0.08
50.58	1.62	14:58:28	252.765	50.46	0.12
50.57	0.72	15:05:42	254.156	50.48	0.09
50.57	1.56	15:12:56	255.944	50.49	0.08
50.60	1.54	15:18:13	258.229	50.50	0.10
50.02	1.43	15:25:27	261.209	50.52	-0.50
49.88	0.90	15:32:42	264.786	50.53	-0.65
50.76	1.81	15:41:49	269.057	50.56	0.20
50.53	1.75	15:49:03	270.647	50.58	-0.05
50.42	1.18	15:56:17	271.839	50.60	-0.18

50.68	2.24	16:01:07	273.429	50.61	0.07
50.61	1.70	16:04:18	274.124	50.62	-0.01
50.51	1.77	16:07:29	274.819	50.63	-0.12
50.78	1.71	16:15:46	276.310	50.66	0.12
50.58	0.67	16:26:23	277.800	50.69	-0.11
50.03	1.62	16:36:58	278.893	50.73	-0.70
51.64	0.77	18:10:45	290.913	51.18	0.46
50.59	1.92	18:18:00	291.410	51.22	-0.63
51.69	1.92	18:25:16	291.609	51.26	0.43
51.60	0.72	18:28:38	291.708	51.28	0.32
51.74	0.96	18:31:49	291.708	51.30	0.44
51.41	1.51	18:34:59	291.708	51.32	0.09
51.21	1.89	18:43:25	291.708	51.38	-0.17
51.45	0.99	18:54:01	292.006	51.44	0.01
51.18	1.70	19:04:37	292.105	51.52	-0.34

Table 17.
ULV Dark measurements during absolute response test on July 25, 1996

ULV Dark	Sigma	Time	Temp. (K)	Model Dark	Model-Obs
44.46	0.50	11:20:56	201.801	44.39	0.07
44.49	0.50	11:31:32	200.311	44.40	0.09
44.42	0.50	11:42:07	199.416	44.42	0.00
44.50	0.50	11:48:13	199.019	44.43	0.07
44.50	0.50	11:55:28	198.423	44.44	0.06
44.50	0.50	12:02:42	198.125	44.45	0.05
44.48	0.50	12:08:29	197.926	44.46	0.02
44.47	0.50	12:15:44	198.224	44.47	0.00
44.51	0.50	12:22:59	198.622	44.48	0.03
44.42	0.50	12:34:22	208.656	44.50	-0.08
44.47	0.50	12:41:37	218.888	44.52	-0.05
44.47	0.50	12:48:52	223.657	44.53	-0.06
44.49	0.50	12:53:44	227.332	44.54	-0.05
44.54	0.50	13:00:58	231.604	44.55	-0.01
44.54	0.50	13:07:57	235.479	44.56	-0.02
44.49	0.50	13:16:50	239.353	44.58	-0.09
44.44	0.50	13:24:05	241.539	44.59	-0.15
44.50	0.50	13:31:19	243.426	44.61	-0.11
44.56	0.50	13:37:41	245.612	44.62	-0.06
44.54	0.50	13:44:56	248.294	44.63	-0.09
44.60	0.49	13:52:11	250.182	44.65	-0.05
44.62	0.49	14:01:52	251.672	44.67	-0.05
44.77	0.42	14:12:29	251.970	44.69	0.08
44.69	0.46	14:23:05	251.871	44.71	-0.02
44.79	0.41	14:30:16	251.573	44.72	0.07
44.59	0.49	14:40:52	251.175	44.75	-0.16
44.70	0.46	14:51:27	251.672	44.77	-0.07
44.77	0.42	14:58:44	252.765	44.78	-0.01
44.89	0.31	15:05:42	254.156	44.80	0.09
44.96	0.20	15:13:13	256.242	44.82	0.14
44.96	0.20	15:18:29	258.229	44.83	0.13
44.99	0.10	15:25:44	261.408	44.85	0.14
45.00	0.00	15:32:59	264.984	44.86	0.14
45.00	0.00	15:42:05	269.355	44.88	0.12

45.00	0.00	15:49:19	270.746	44.90	0.10
45.00	0.00	15:56:33	271.839	44.92	0.08
45.01	0.10	16:01:23	273.429	44.93	0.08
44.55	0.00	16:04:34	274.223	44.94	-0.38
45.00	0.00	16:07:45	274.919	44.95	0.05
45.00	0.00	16:16:02	276.310	44.97	0.03
44.98	0.14	16:26:39	277.800	44.99	-0.01
45.00	0.00	16:37:14	278.893	45.02	-0.02
45.29	0.46	18:11:01	290.913	45.27	0.02
45.25	0.46	18:18:16	291.509	45.29	-0.04
45.31	0.49	18:25:32	291.609	45.32	-0.01
45.28	0.45	18:28:55	291.609	45.33	-0.05
45.33	0.47	18:32:05	291.708	45.34	-0.01
45.41	0.49	18:35:16	291.708	45.34	0.07
45.31	0.46	18:43:42	291.807	45.37	-0.06
45.40	0.49	18:54:17	292.006	45.40	0.00
45.41	0.50	19:04:53	292.105	45.43	-0.02

The variation of dark signals from the ULV and DLV systems with time are shown in Fig. 30. We fit the data by the quadratic functions shown. The small bimodality of the DLV data lead to a scatter of the DLV dark values of some 0.5 DN, but this is negligible compared to the more than 3000 DN measured with the sphere illuminated by the high intensity lamp.

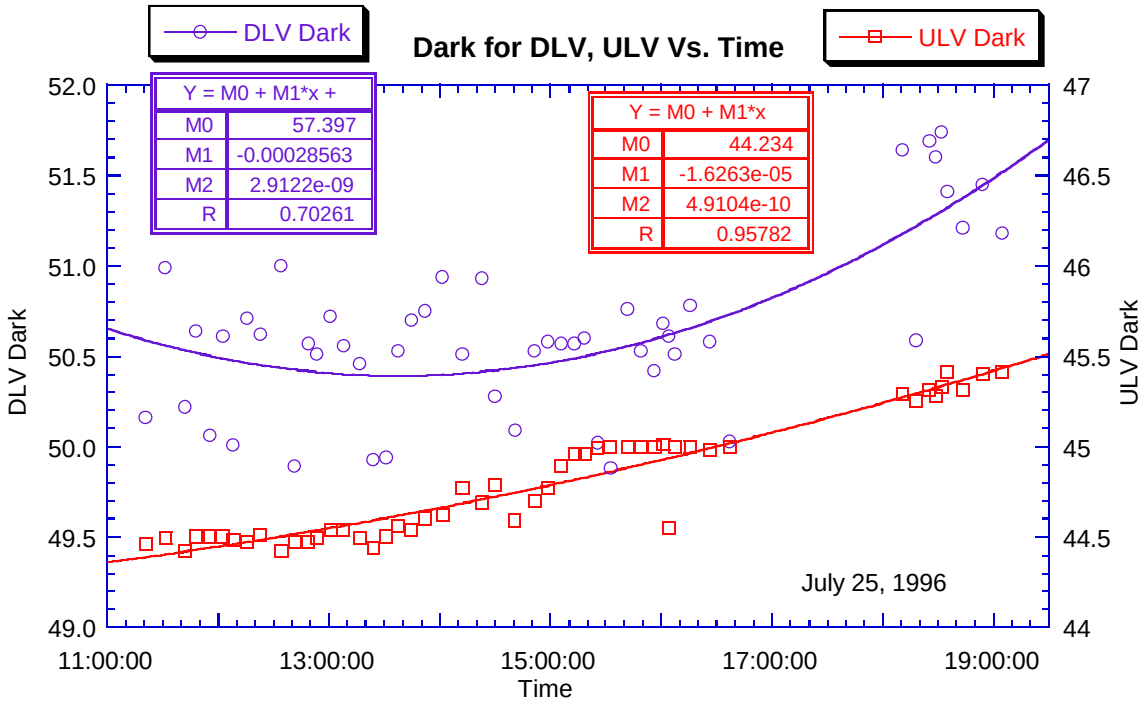

Fig. 30. The averages of 100 dark values of the DLV and ULV are shown as a function of time for the July 25, 1996 test. The smooth curves are parabolas fit to the data and were used to subtract the dark bias from the bright measurements shown below.

Fig. 31 shows the variation in the signal from the filtered silicon detector at the top of the integrating sphere that tracked the change in the brightness of the high intensity lamp. We see that the light level was quite stable, with the total excursion over the test measured as less than 2 percent.

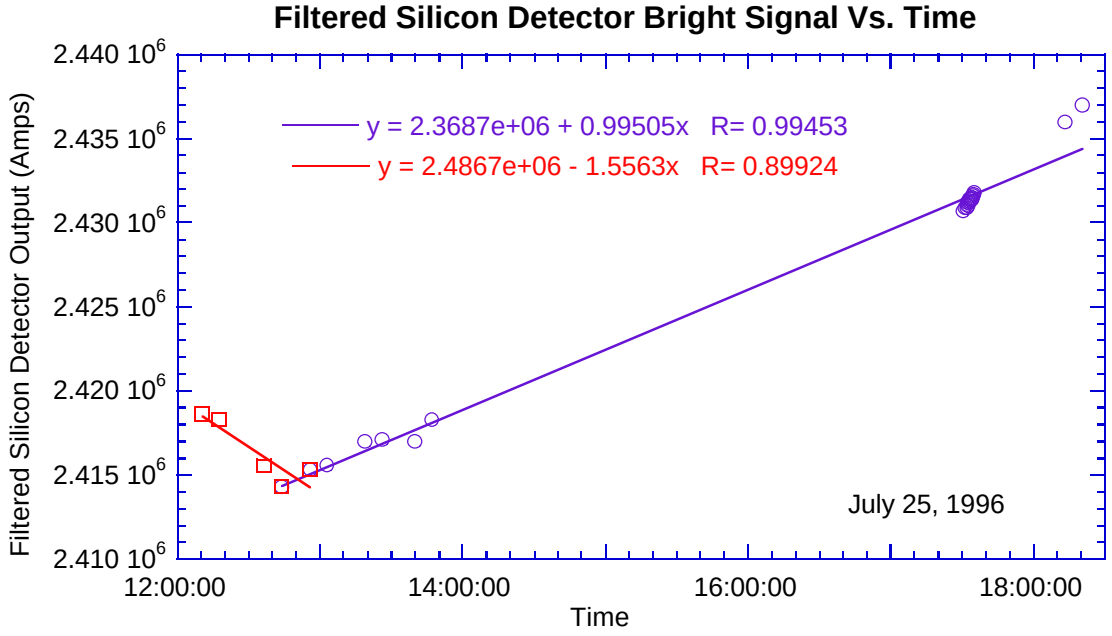

Fig. 31. Output of filtered silicon detector in the top of the integrating sphere as a function of time. The measurements are fit with the straight lines shown. The equations of the lines are given with the x value equal to the number of seconds since the start of the day.

Tables 18 and 19 show the determination of the intensity in the integrating sphere on July 25 and August 15 from the monochrometer measurements on these two dates. The plot of intensity in the integrating sphere in Fig. 32 was obtained by scaling the intensity on August 15 to the same relative reading of the filtered silicon detector in the top of the integrating sphere (2.367×10^6) as seen on July 25. The two curves of intensity are very similar, with only slight variations possibly due to a very small difference in the color temperature of the high intensity lamp between the two dates.

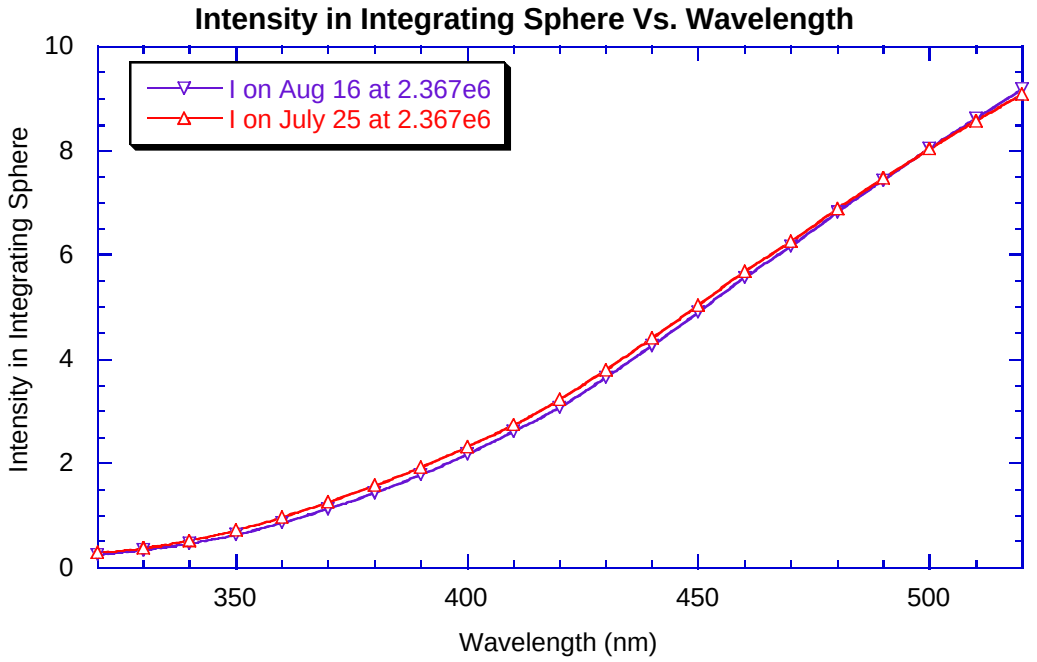

Fig. 32. Intensity in integrating sphere as measured on July 25 and August 16, 1996 as a function of wavelength. The measurements have been scaled to the same reading of the filtered silicon detector in the top of the integrating sphere (2.367×10^6). The measured values extend down to a wavelength of 350 nm, and have been extrapolated to shorter wavelengths. The difference in the two curves results from slightly different color temperatures of the high-intensity lamp on the two days.

Table 18

Measurement of Intensity in integrating sphere on July 25, 1996

Time	Si reading (Amps)	Wave-length (nm)	Resp of mono-det(Amps/watt/sq m.-micron-sr)	Intensity (Watts/sq.m-micron-sr)	filtered si – dark (relative units)	Scaled Intensity (Watts/sq.m-micron-sr)
17:30:20	1.132E-10	350	1.576E-10	0.71823	2.3661E+06	0.7184
17:31:18	1.325E-10	360	1.369E-10	0.96814	2.3663E+06	0.9683
17:31:53	1.854E-10	370	1.475E-10	1.25729	2.3663E+06	1.2575
17:32:06	2.621E-10	380	1.664E-10	1.57550	2.3665E+06	1.5756
17:32:18	3.423E-10	390	1.778E-10	1.92520	2.3666E+06	1.9253
17:32:31	4.202E-10	400	1.81E-10	2.32193	2.3664E+06	2.3222
17:32:43	5.166E-10	410	1.886E-10	2.73855	2.3666E+06	2.7386
17:32:55	6.422E-10	420	1.989E-10	3.22876	2.3667E+06	3.2287
17:33:08	7.771E-10	430	2.046E-10	3.79777	2.3667E+06	3.7978
17:33:20	9.131E-10	440	2.072E-10	4.40622	2.3668E+06	4.4060
17:33:33	1.044E-09	450	2.073E-10	5.03667	2.3668E+06	5.0365
17:33:45	1.161E-09	460	2.043E-10	5.68393	2.3668E+06	5.6836
17:33:58	1.243E-09	470	1.985E-10	6.26291	2.3668E+06	6.2625
17:34:10	1.339E-09	480	1.944E-10	6.88644	2.3669E+06	6.8859
17:34:23	1.487E-09	490	1.991E-10	7.47011	2.3669E+06	7.4694
17:34:35	1.639E-09	500	2.039E-10	8.03786	2.3670E+06	8.0368
17:34:48	1.754E-09	510	2.045E-10	8.57660	2.3671E+06	8.5750
17:35:00	1.820E-09	520	2.003E-10	9.08728	2.3672E+06	9.0855

Table 19
Measurement of Intensity in integrating sphere on August 15, 1996

Time	Si reading (Amps)	Wave-length (nm)	Resp of mono-det(Amps/watt/sq m.-micron-sr)	Intensity (Watts/sq.m-micron-sr)	filtered si – dark (relative units)	Scaled Intensity (Watts/sq.m-micron-sr)
11:07:09	8.474E-11	350	1.576E-10	0.5377	2.008E+06	0.6338
11:07:23	1.001E-10	360	1.369E-10	0.7314	2.008E+06	0.8621
11:07:42	1.419E-10	370	1.475E-10	0.9623	2.008E+06	1.1341
11:07:55	2.032E-10	380	1.664E-10	1.2214	2.008E+06	1.4395
11:08:07	2.693E-10	390	1.778E-10	1.5146	2.009E+06	1.7850
11:08:20	3.343E-10	400	1.81E-10	1.8473	2.009E+06	2.1769
11:08:32	4.188E-10	410	1.886E-10	2.2201	2.009E+06	2.6161
11:08:45	5.198E-10	420	1.989E-10	2.6134	2.009E+06	3.0791
11:08:57	6.341E-10	430	2.046E-10	3.0989	2.009E+06	3.6513
11:09:09	7.501E-10	440	2.072E-10	3.6196	2.009E+06	4.2649
11:09:22	8.631E-10	450	2.073E-10	4.1639	2.009E+06	4.9059
11:09:34	9.659E-10	460	2.043E-10	4.7288	2.009E+06	5.5712
11:09:47	1.040E-09	470	1.985E-10	5.2401	2.009E+06	6.1731
11:09:59	1.126E-09	480	1.944E-10	5.7910	2.009E+06	6.8219
11:10:12	1.257E-09	490	1.991E-10	6.3147	2.009E+06	7.4390
11:10:24	1.393E-09	500	2.039E-10	6.8314	2.009E+06	8.0474
11:10:37	1.497E-09	510	2.045E-10	7.3199	2.010E+06	8.6221
11:10:49	1.561E-09	520	2.003E-10	7.7941	2.010E+06	9.1805

Tables 20 and 21 show the reduction of the bright and dark measurements of the DLV and ULV from the data of July 25, 1996 covering a large range in temperature, and the derived values of Respmeas are shown as a function of temperature in Fig. 31 by the open symbols. We emphasize that the responsivities shown are $Resp_{meas}$ from equation (38), and need to be multiplied by the integral of the spatial response function over solid angle to give the peak responsivities of the DLV and ULV systems. The absolute response measurements on August 15 are compared with the July 25 measurements in Fig. 33 as well. The data from August 15 seem to have a drift with time, and do not seem quite as internally consistent for the ULV as the measurements from July 25 even though they give about the same average value. For the DLV, the measurements of August 15 lead to slightly higher responsivity than do the measurements of July 25 by about 2.5 or 3 percent. The sequence of measurements on July 25 shows consistency to about 0.25%, and these measurements are preferred over the DLV measurements of August 15 at warm temperature.

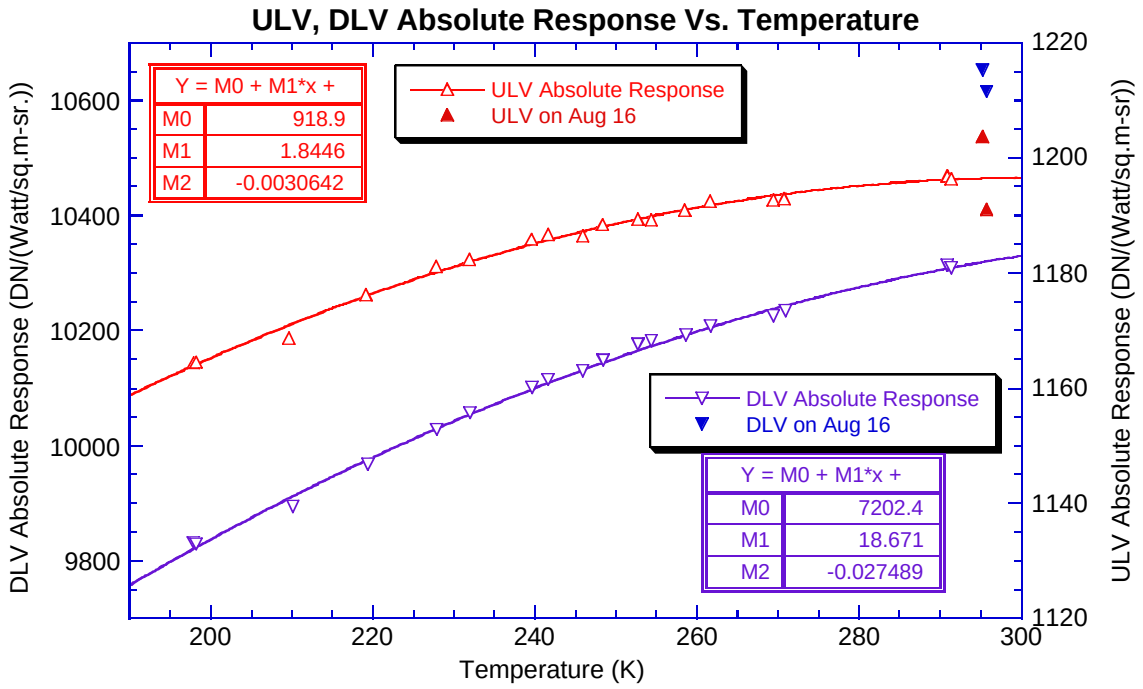

Fig. 33. The measured absolute response [$Resp_{meas}$ of equation (38)] of the DLV (left scale) and ULV are shown as a function of violet temperature. The data are fitted with quadratic functions of temperature having the coefficients shown. The open symbols are the data from July 25, 1996, and the filled symbols are the measurements of August 15, 1996.

Table 20.
Absolute Responsivity, $Resp_{meas}$ of DLV Vs. Temperature

Bright (DN)	σ (DN)	Dark (DN)	Time	Temp. (K)	Fil. Si. - dark (Rel. units)	B-D scaled	Inte-gral of I(λ) Rel(λ)	Abs. Resp.
3382.19	1.59	50.47	12:09:22	197.926	2353997	3349.69	0.3422	9830.4
3380.54	2.23	50.46	12:16:37	198.224	2353320	3349.00	0.3422	9828.3
3401.35	1.27	50.43	12:35:15	210.146	2351580	3372.45	0.3423	9893.4
3426.37	1.99	50.42	12:42:30	219.385	2350903	3398.62	0.3424	9967.1
3447.02	1.83	50.41	12:54:36	227.929	2350350	3420.23	0.3425	10027.7
3458.04	1.33	50.41	13:01:51	232.002	2350783	3430.70	0.3426	10057.1
3474.92	1.65	50.40	13:17:43	239.651	2351730	3446.31	0.3427	10100.4
3480.66	1.62	50.39	13:24:58	241.638	2352163	3451.46	0.3427	10114.8
3487.24	1.10	50.39	13:38:34	245.910	2352975	3456.89	0.3427	10129.3
3494.44	1.61	50.39	13:45:49	248.493	2353408	3463.49	0.3428	10147.8
3511.18	1.75	50.46	14:59:36	252.765	2357813	3473.75	0.3428	10176.5
3513.78	1.81	50.48	15:06:51	254.354	2358246	3475.71	0.3428	10181.7
3519.05	1.53	50.50	15:19:22	258.626	2358993	3479.87	0.3429	10192.5
3525.08	1.50	50.52	15:26:37	261.706	2359426	3485.27	0.3429	10207.3
3533.31	2.35	50.56	15:42:57	269.455	2360401	3492.04	0.3430	10224.6
3537.33	1.58	50.58	15:50:12	270.945	2360834	3495.41	0.3430	10234.0
3579.52	1.95	51.18	18:11:53	290.913	2369293	3524.47	0.3432	10312.5
3578.79	1.82	51.23	18:19:09	291.410	2369727	3523.05	0.3432	10308.2

Table 21.
Absolute Responsivity $Resp_{meas}$ of ULV Vs. Temperature

Bright (DN)	σ (DN)	Dark (DN)	Time	Temp. (K)	Fil. Si. - dark (Rel. units)	B-D scaled	Inte-gral of I(λ) Rel(λ)	Abs. Resp.
435.04	0.20	44.46	12:09:06	197.926	2354022	392.68	0.3391	1164.41
434.98	0.14	44.47	12:16:20	198.224	2353347	392.72	0.3391	1164.52
436.26	0.44	44.50	12:34:59	209.649	2351605	394.27	0.3392	1168.69
438.79	0.41	44.52	12:42:14	219.186	2350928	396.92	0.3393	1176.19
440.43	0.50	44.54	12:54:20	227.829	2350334	398.65	0.3394	1181.00
441.00	0.00	44.55	13:01:35	231.902	2350767	399.13	0.3394	1182.29
442.47	0.50	44.58	13:17:27	239.552	2351714	400.42	0.3395	1185.83
442.84	0.37	44.59	13:24:42	241.638	2352147	400.71	0.3395	1186.60
443.00	0.00	44.62	13:38:17	245.910	2352958	400.71	0.3396	1186.43
443.76	0.43	44.63	13:45:33	248.394	2353392	401.38	0.3396	1188.34
445.01	0.10	44.79	14:59:20	252.765	2357797	401.73	0.3397	1189.22
445.10	0.30	44.80	15:06:35	254.354	2358230	401.73	0.3397	1189.16
445.87	0.53	44.83	15:19:06	258.527	2358977	402.35	0.3397	1190.83
446.54	0.50	44.85	15:26:20	261.607	2359409	402.93	0.3397	1192.44
446.91	0.29	44.89	15:42:41	269.455	2360385	403.10	0.3398	1192.64
447.08	0.27	44.90	15:49:56	270.746	2360818	403.18	0.3398	1192.83
450.48	0.50	45.28	18:11:37	290.913	2369277	404.76	0.3401	1196.77
450.45	0.50	45.30	18:18:53	291.410	2369711	404.64	0.3401	1196.38

VI. Software and schedule of measurements

The ULV, DLV system collects five ULV samples and two DLV samples in each data cycle during descent except when in calibration cycles or in the Very Low Near Surface Mode, when data are collected as fast as the data rate permits regardless of azimuth angle. In other modes during descent, DLV data are collected near 0 and 180 degrees azimuth from the sun, and near 5 degrees (under the shadow bar), near 140 degrees and near 180 degrees azimuth from the sun (with no direct solar beam on the diffuser) and near 320 and 340 degrees azimuth from the sun with the direct solar beam on the diffuser. The ULV measurements at 5, 140, and 180 degrees azimuth need to be interpolated to the same altitude and fit with a function of azimuth (such as proportional to cosine (azimuth) to give the diffuse signal as a function of azimuth angle. The expected contribution of the diffuse beam can then be subtracted from the measurements that include the direct solar beam at 320 and 340 degrees to give the size of the direct solar beam. The two DLV measurements can be averaged to give an indication of the size of the upward diffuse solar flux, as described in section VIII below.

VII. Dark data values during descent

A. DLV

Figures 8 and 9 show the histogram of the dark data values produced by the DLV system in single measurement mode. The average value is about 50 DN at room

temperature, and does not vary much with temperature down to 200 K. In descent, however, DLV data are collected with the instrument operating in a variety of modes including non-imaging cycles, imaging cycles, High Near Surface (HNS) mode, Medium Near Surface (MNS) mode, Very Low Near Surface (VLNS) mode, and Surface mode. The actual dark values of the DLV must be known in each of these modes of operation to correct the data collected during Titan descent for the bias in the DLV system. Table 22 gives the dates of descent tests in which dark DLV and ULV data were collected in all the modes that will be used during Titan descent. Here we summarize the characteristics of the dark values of the DLV system in these tests, and compare them with the dark DLV measurements during a descent test made in the F4 inflight checkout.

Table 22.
List of Prelaunch Descent Tests

Test number	Date (1997)	Characteristics
L1	February 24	Integrated System Test 2
L2	March 7	Solar Vacuum Test 1b
L3	March 6	Solar Vacuum Test 1b, ATLO
L4	May 7	First X-Test
L5	June 4	Integrated System Test 3
L6	June 10	Integrated System Test 3
L7	June 18	Pre CF Test
L8	August 2	DISR Mated Test
L9	September 10	Probe reopened Test
L10	September 12	Probe reclosed Test
L11	September 19	Pad Contingency Checkout Test

The data from test L1 above show DLV values near 1000 DN, and it seems likely that some lamps were shining on the violet photometer sensors. Test 3 has DLV values near 3 DN, and was done at violet system temperatures near 200 K. Such values have not been seen before or since, and some unknown problem occurred in this cold test in the solar vacuum chamber. Test L5 has DLV data numbers near 150 DN, and again some light must have been incident on the violet photometers. Tests L4 and L6 through L11 showed dark DLV values as expected, and the histograms of the dark data collected in various instrument modes are shown in the following series of Figures.

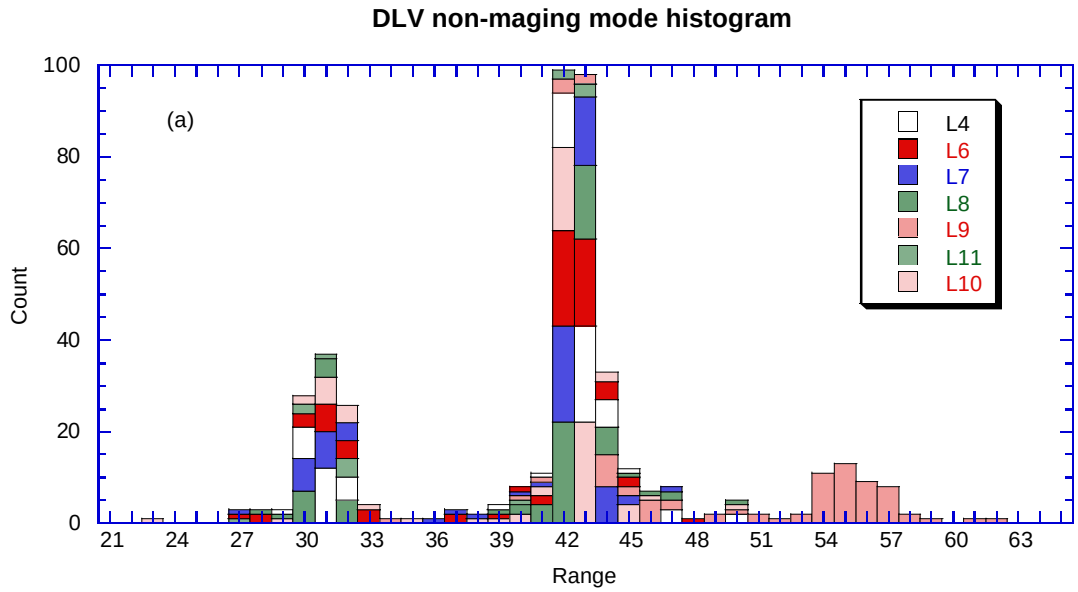

Fig. 34. Summed histogram of DLV dark values in 7 prelaunch descent sequences in non-imaging mode.

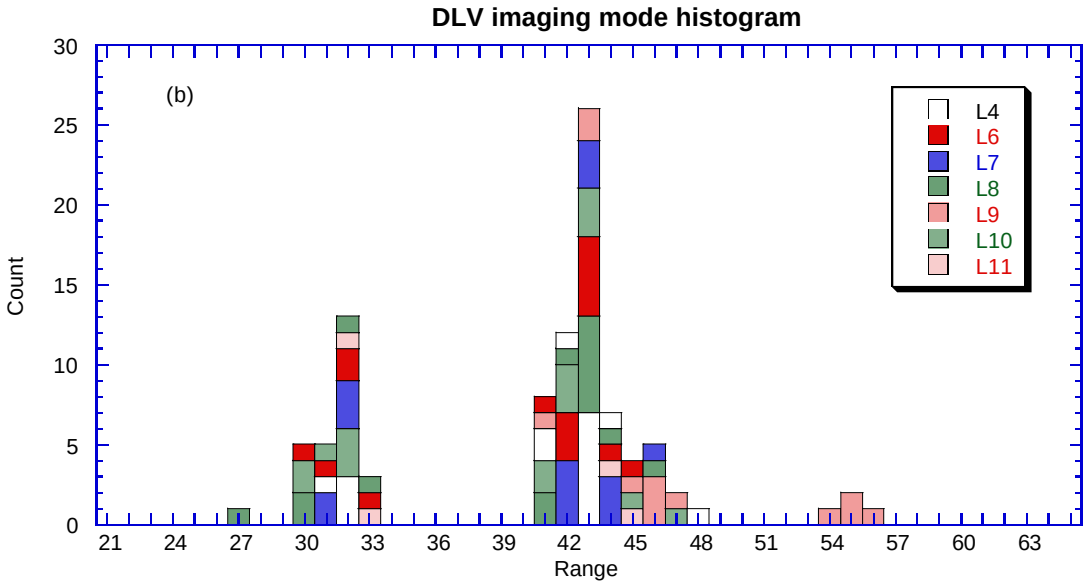

Fig. 35. Like Fig. 34 but for imaging mode.

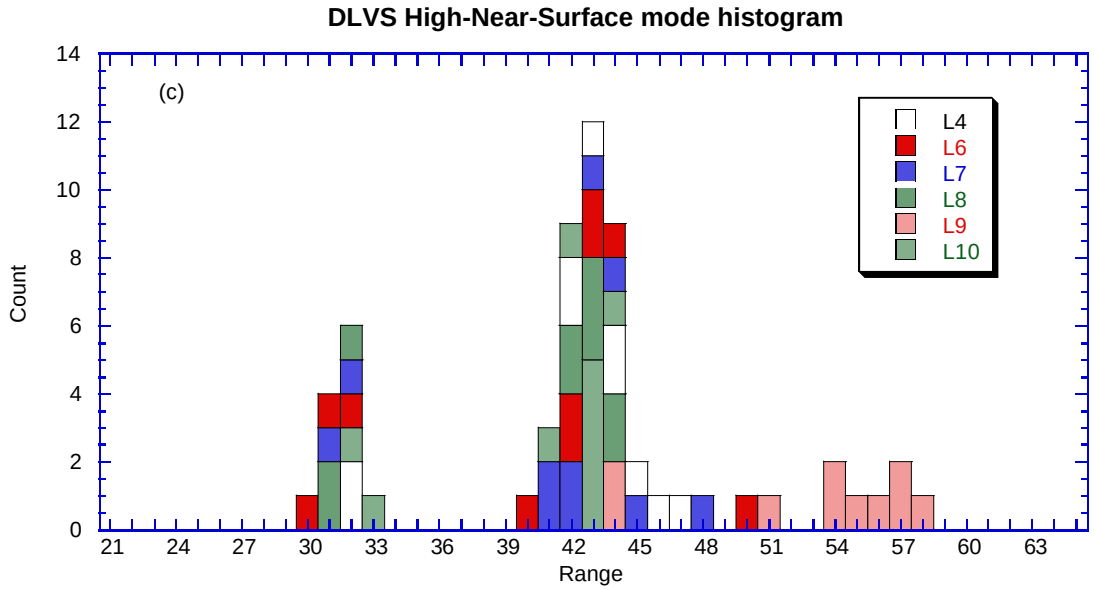

Fig. 36. Like Fig. 34 but for the High Near Surface mode of the DLV.

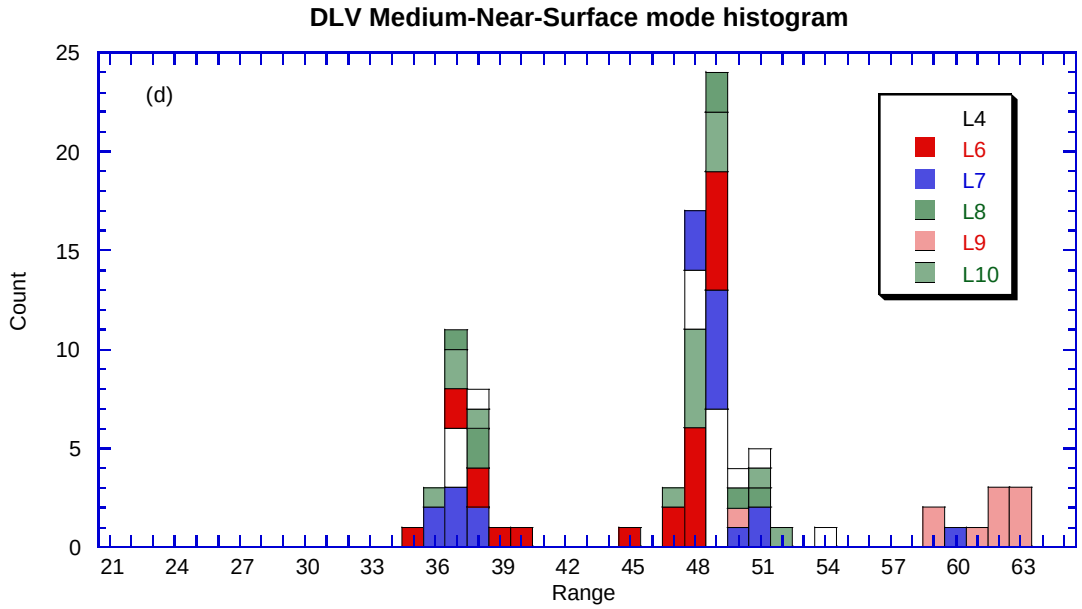

Fig. 36. Like Fig. 34 but for the Medium Near Surface mode of the DLV.

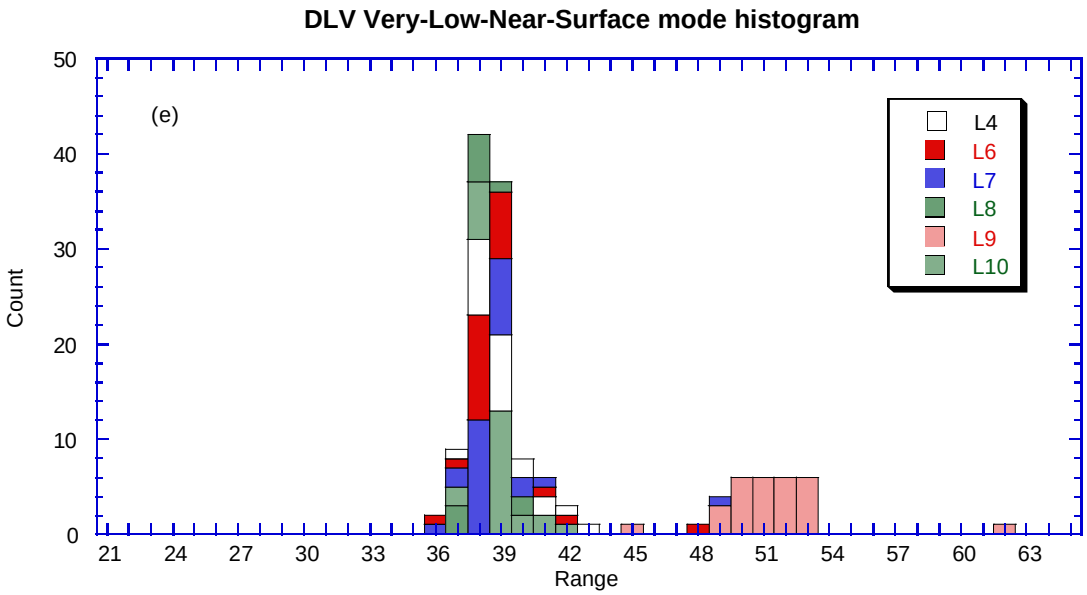

Fig. 38. Like Fig. 34 but for the Very Low Near Surface mode of the DLV.

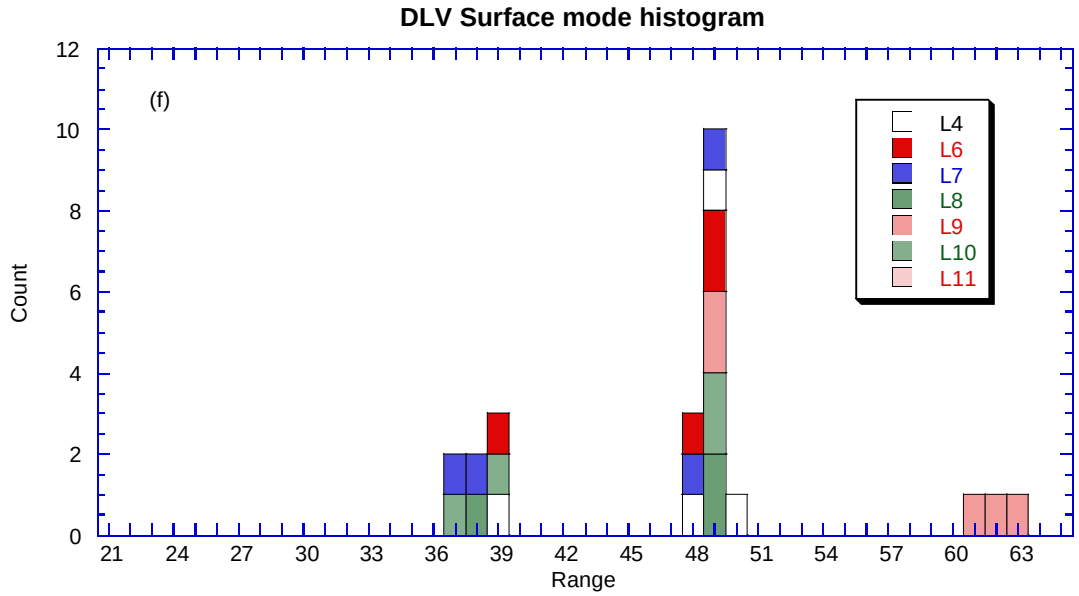

Fig. 39. Like Fig. 34 but for the surface mode of the DLV.

Note that the histograms for the non-imaging mode, imaging-mode, and High-Near-Surface modes (panels a, b, and c) are very similar. These three modes can be combined to a single histogram as shown in Fig. 40. Notice also that only on test L9 was there a significant peak near 55 DN. This test was done with the probe open in the humid air at Cape Kennedy shortly before launch. It is possible that this peak will be much less prominent in space and on Titan. (The histogram of the prelaunch tests with non-imaging mode, imaging mode, and HNS mode data with test L9 omitted is shown in Fig. 39.) Figure 40 shows the histogram of the DLV dark data numbers in non-imaging mode, imaging mode, and HNS mode during the descent test done during the F4 inflight

checkout. Notice that the locations of the peaks and relative heights of the peaks in the DLV darks are very similar to that shown in Fig. 40 for the prelaunch descent tests. In fact, the size of the peak near 55 DN is much less prominent in space than in the L2 test before launch, as might be expected.

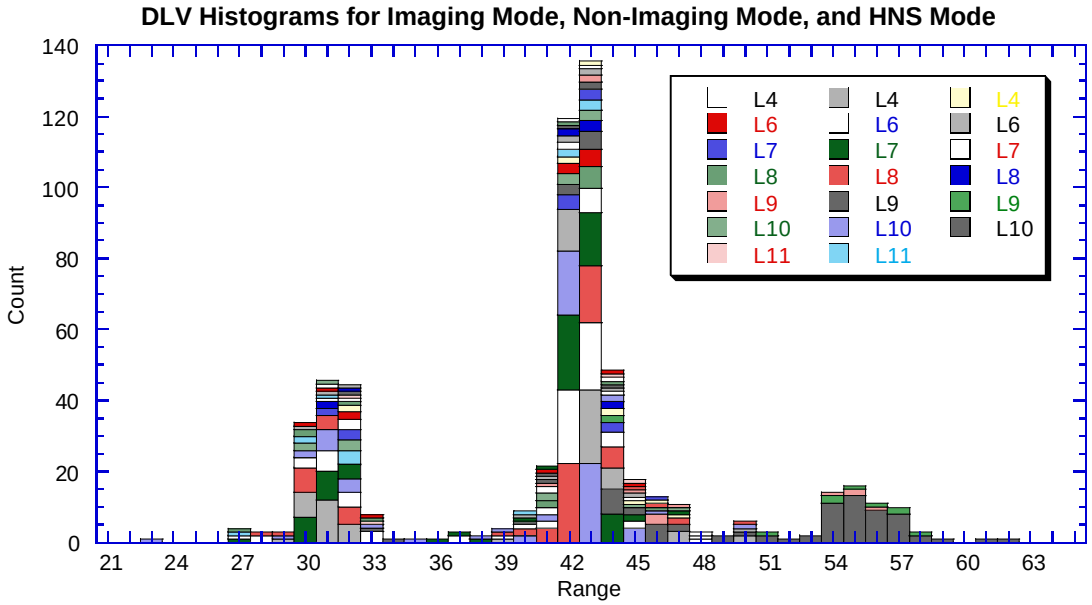

Fig. 40. The stacked histogram for tests L4 and L6 through L11 for non-imaging mode, imaging mode, and HNS mode is shown. Notice that the peak near 55 DN consists mostly of observations from the L9 test.

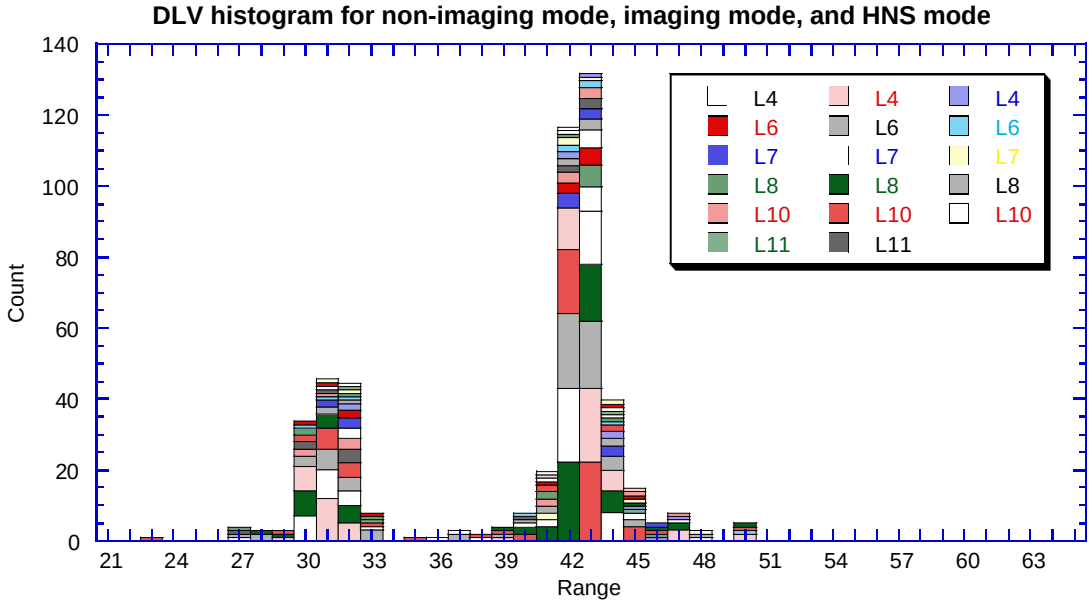

Fig. 41. Same as Fig. 40 but omitting the data from test L9.

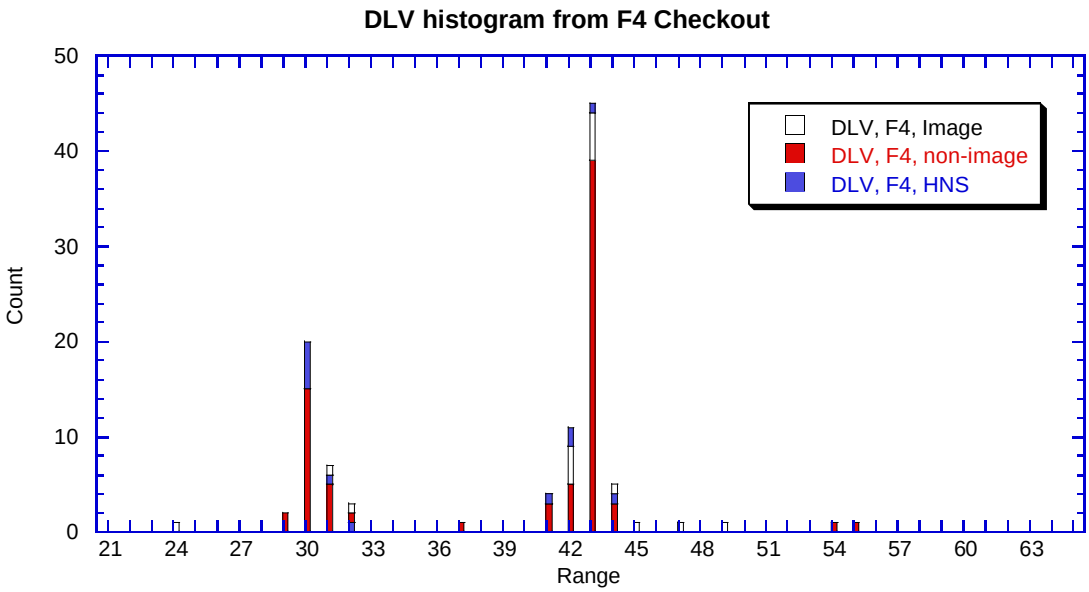

Fig. 42. The histogram for dark DLV observations in F4 inflight checkout for non-imaging mode, imaging mode, and HNS mode data is shown. Note the similarity to Fig.41 above for the prelaunch descent tests.

In the MNS mode, VLNS mode, and Surface modes, the locations of the peaks in the histograms in the prelaunch tests are shown in panels (d), (e), and (f). Notice that the locations of the peaks in these modes are shifted to higher data numbers by about 6 DN compared to the locations of the peaks in the non-imaging mode, imaging mode, and HNS modes. Notice that the histograms for the MNS and Surface modes are similar, while the VLNS mode histogram has essentially only the single peak near 38 DN. The data from the F4 inflight checkout are in rough agreement with this observation, but the amount of data available in these modes from a single descent test is rather limited. The data available from the F4 checkout seem to indicate that the shift between the histogram locations in the VLNS, MNS, and Surface modes from the locations of the peaks in the non-imaging, imaging, and HNS modes is about 7 or 8 DN rather than the 6 DN seen in the prelaunch descent tests. This will be tracked as more inflight checkout data is collected and our statistics improve. The size of this shift in the dark in these modes that occur only late in the descent may prove moot as the violet flux at deep levels of Titan's atmosphere seems likely to prove to be too small to measure in any case.

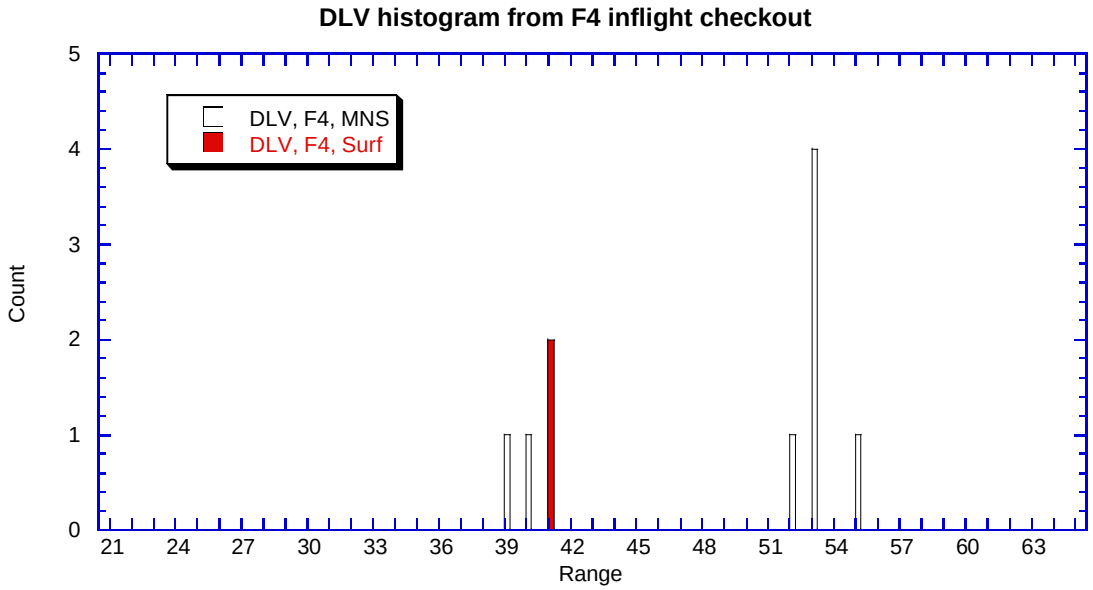

Fig. 43. Summed histogram of the DLV dark values in Medium Near Surface mode and the Surface mode from the F4 inflight checkout.

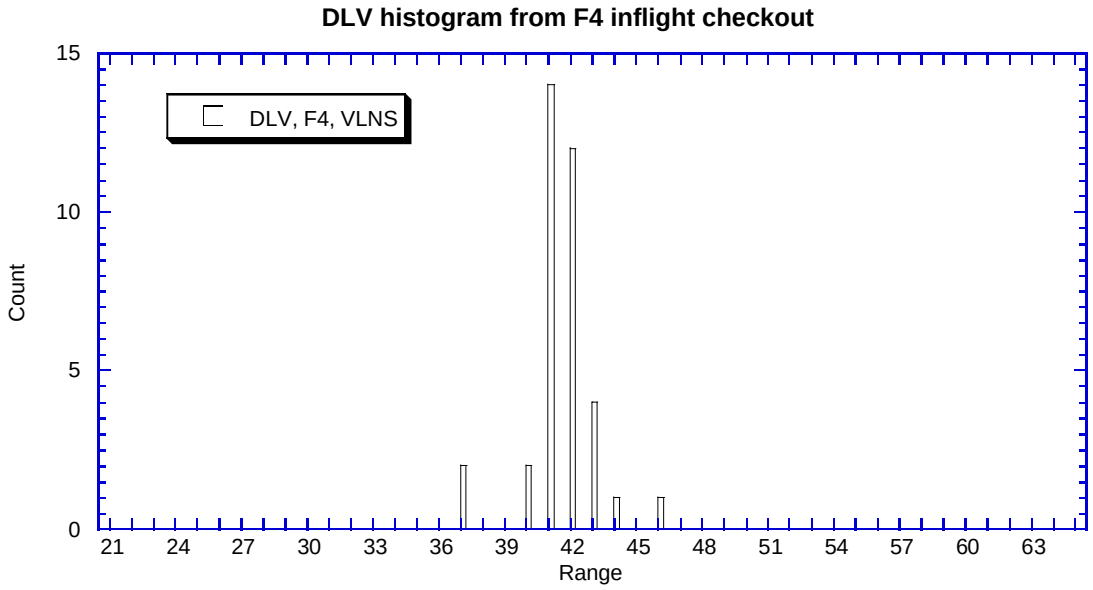

Fig. 44. Like Fig. 43 but for the Very Low Near Surface mode of the F4 inflight checkout.

B. ULV dark during Descent Mode

For all except the Medium Near Surface Mode, the dark in descent mode for the ULV system appears to be the same as measured in single measurement mode. The dark in single measurement mode as a function of temperature from the data of July 25, 1996, is shown in Fig. 45. We note the tendency for the ULV values to cluster near integer or half-integer values as discussed in the noise section above. A reasonable parabolic fit to

the relation of ULV dark as a function of temperature is given by DN= 49.806 – 0.05156 T + 0.00012429*T^2. The fit is good to about 0.2 DN in view of the clustering of the data near integer and half-integer values.

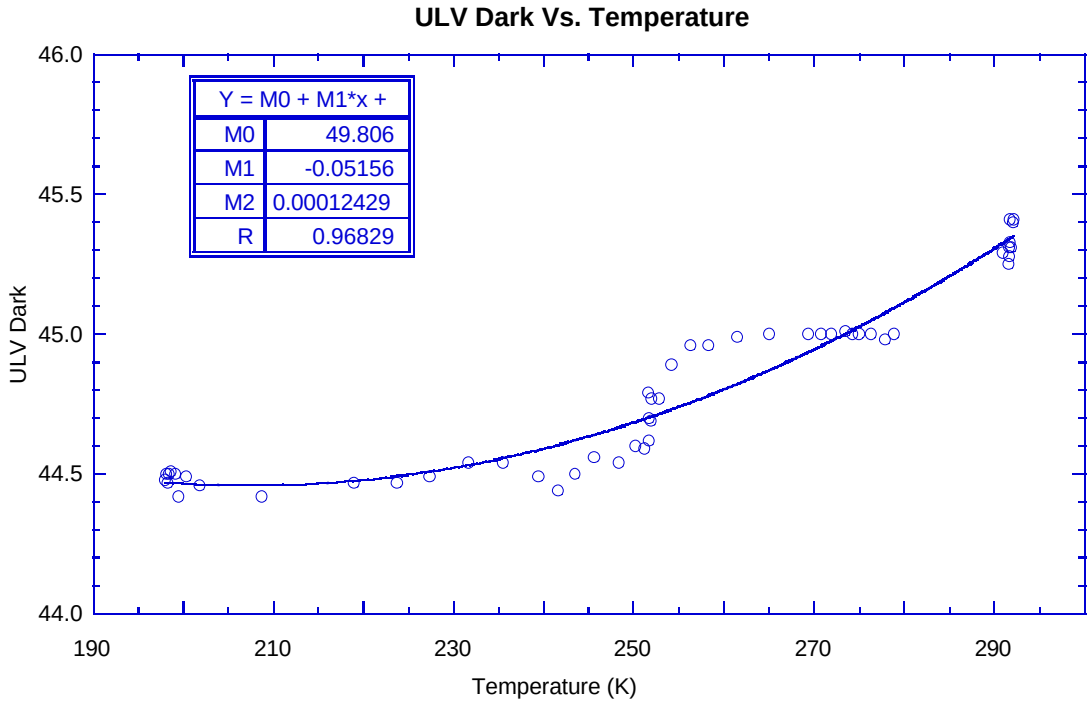

Fig. 45. The dark data from the ULV as a function of temperature from the absolute calibration test in single measurement mode on July 25, 1996. Note the tendency of the data to cluster around integer or half integer values, even though the averages of 100 separate measurements are plotted in each point.

Table 23 shows the averages of the ULV dark data in six prelaunch tests in several different modes. The mean and standard deviations of all the available readings in each descent test are shown. Note that the standard deviations of the dark values are significantly larger in Medium Near Surface mode than in any of the other modes (some 1.5 DN compared to 0.2 - 0.4 DN. This indicates the presence of a second peak in the dark values in the ULV in this mode. The histogram of the data in this mode in each of the tests is shown in Fig. 46. In Medium Near Surface Mode, however, the ULV dark data show a cluster of values near about 45 DN and a secondary peak near some 49 DN, as shown in Fig. 46 for five prelaunch tests.

Table 23.
Mean and standard deviation of ULV dark data in descent modes from prelaunch tests

Test	Normal Mode		High Near Surface.		Medium Near Surface.		Very Low Near Surface	
	Ave.	σ	Ave.	σ	Ave.	σ	Ave.	σ

L4	44.94	0.41	44.95	0.69	45.24	1.52	44.96	0.21
L6	44.93	0.35	44.84	0.47	45.50	1.60	44.93	0.27
L7	44.92	0.37	45.04	0.45	44.80	0.52	44.89	0.32
L8	44.94	0.43	45.04	0.54	45.29	1.80	44.91	0.30
L10	45.06	0.44	44.80	0.58	45.00	0.00	44.04	0.20
L11	45.22	0.59	-	-	-	-	-	-

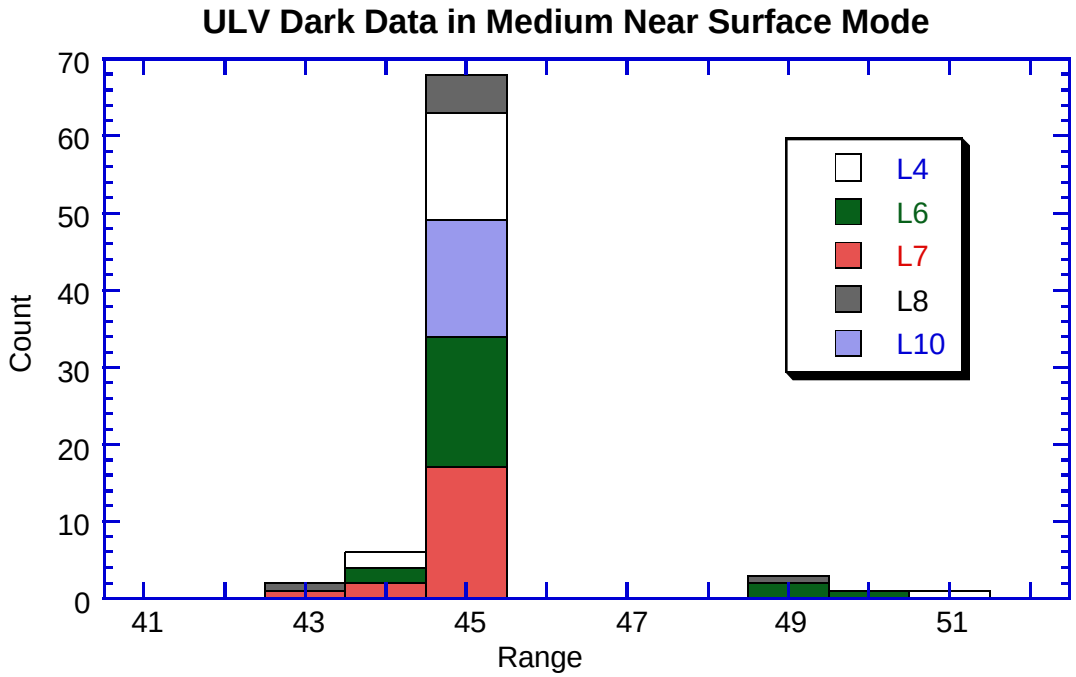

Fig. 46. The summed histogram of the dark data in the ULV in five prelaunch tests in the Medium Near Surface mode are shown. Note that in this mode the ULV histogram is bimodal with a small peak 4 to 5 DN greater than the main peak. A similar effect is expected for the ULV during Titan entry, but only in this portion of the descent mode.

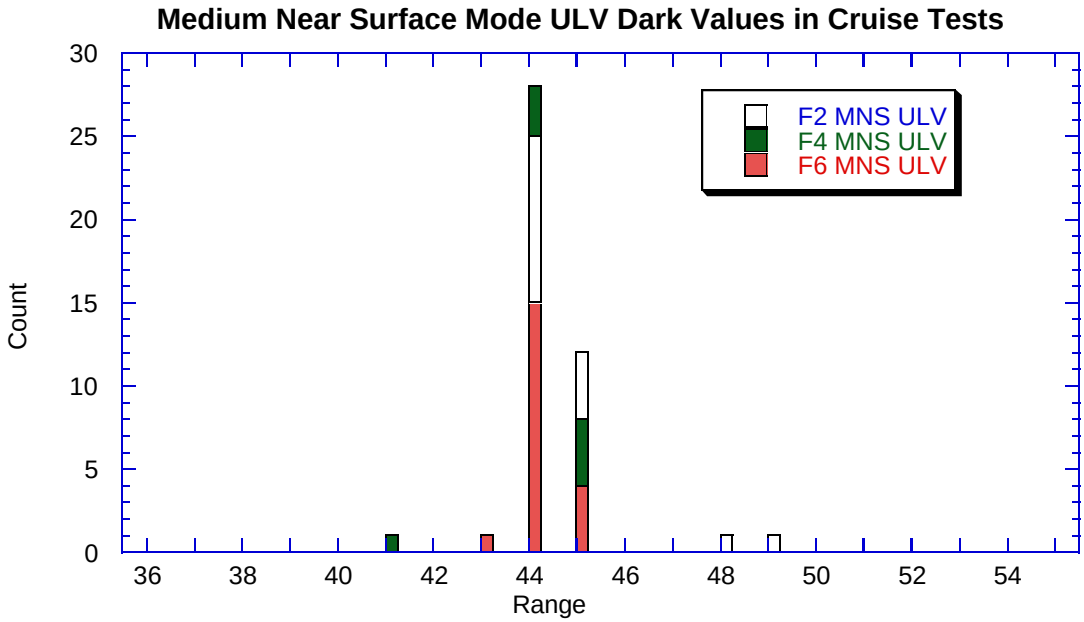

Fig. 47. Summed histogram of ULV dark values in Medium Near Surface Mode from F2, F4, and F6 descent tests during cruise. Note that in addition to the peak near 44 DN, a few values are seen at 48 and 49 DN, as in the prelaunch tests in this mode.

VIII. Notes on determination of fluxes from Titan entry data

The method of estimating the diffuse upward and downward fluxes from the ULV and DLV observations is derived here for the case of analysis of Titan observations.

The instrument output is given by

$$DN - DNdark = \mathrm{Resp}_{peak} \int \left[\int I(l, J, j)\,\mathrm{Rel}_{spec}(l)\,dl \right] \mathrm{Rel}_1(J, j)\,d\Omega \qquad (39.)$$

where DN is the data number observed, DNdark is the data number due to the electrical bias when the instrument is in the dark, Resp_{peak} is the peak absolute responsivity (at the maximum of the spectral and spatial relative response functions) of the instrument, Rel_1 is the relative spatial response function when the observations were collected, and I is the diffuse intensity from zenith angle J and azimuth angle j. The relative spectral response function and the relative spatial response functions are dimensionless, and normalized to unity at their peaks. The units of the peak responsivity are data numbers/(watt/sq. m).

The relative spectral response function, $\mathrm{Resp}_{spec}(\lambda)$, is given in Fig. 48.

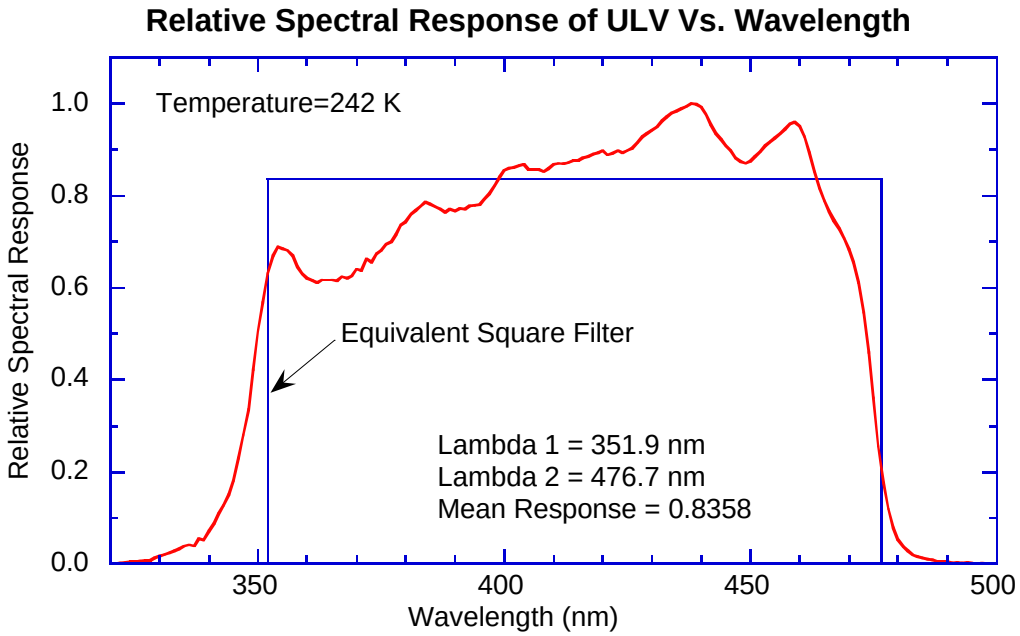

Figure 48. The relative spectral response of SH032 ULV channel at 242 K. Also shown are the boundaries of an equivalent rectangular filter that gives the same response for a variation of intensity with wavelength that can be described by a polynomial up to second order in wavelength.

The straight lines in Fig. 48 show the equivalent rectangular filter that gives the same integrated response as the actual filter for any spectrum I(λ) that can be described by a polynomial of degree 2 or less. While the solar spectrum is much more complex than a quadratic polynomial in this spectral region, most of the variations are due to Fraunhoffer solar lines that vary much more rapidly with wavelength than the relatively smooth relative response function of the violet photometer. Tests have shown that the error in approximating the exact integral of solar energy between λ_1 and λ_2 nm by the equivalent filter is less than about 1% for the solar spectrum or modifications of it that gradually absorb rapidly increasing energy at shorter wavelengths across the filter. Hence, we can say to good accuracy that

$$\int I(l,J,j)\,\mathrm{Rel}_{spec}(l)\,dl = 0.8571\int_{350\,nm}^{475\,nm} I(l,J,j)\,dl = 0.8571\, I_{350}^{475}(J,j) \qquad (40.)$$

Thus, we have

$$DN - DNdark = 0.8571\,\mathrm{Resp}_{peak}\int I_{350}^{475}(J,j)\,\mathrm{Rel}_1(J,j)\,d\Omega \qquad (41.)$$

Now we replace the integrated intensity in direction (J,j) with <I>, the integrated intensity averaged over all directions (weighted with the relative spatial response function). Then the average wavelength integrated intensity, <I> is given by

$$< I >= \frac{DN - DNdark}{0.8571 \mathrm{Resp}_{peak} \int \mathrm{Rel}_1(J, j)\, d\Omega} \tag{42.}$$

Recall that when the responsivity of the instrument was measured, the integral of the spatial response function was not known, and was set to unity. Thus the measured responsivity, $\mathrm{Resp}_{\mathrm{meas}}$ was determined by

$$\mathrm{Resp}_{meas} = \frac{DN - DNdark}{\int I(l)\mathrm{Rel}_{spec}(l)\, dl} \tag{43.}$$

where $I(\lambda)$ is the intensity at wavelength λ which is essentially constant over directions in the integrating sphere. From (43) and (39) we see that

$$\mathrm{Resp}_{\mathrm{peak}} = \mathrm{Resp}_{meas} \Big/ \int \mathrm{Rel}_1(J, j)\, d\Omega \tag{44.}$$

where Rel_1 is the relative spatial response function during the absolute calibration tests, that is, without any external filters on the DISR sensor head.

Substituting (44) into (42) gives

$$< I >= \frac{(DN - DNdark)}{0.8571 \mathrm{Resp}_{meas}}. \tag{45.}$$

Note that for the ULV,

$$\int \mathrm{Rel}_1(J, j)\, d\Omega = 0.6702, \tag{46.}$$

while for the DLV,

$$\int \mathrm{Rel}_1(J, j)\, d\Omega = 0.8175. \tag{47.}$$

Thus,

$$< I >= \frac{(DN - DNdark)}{(0.8571)\,\mathrm{Resp}_{meas}}. \tag{48.}$$

The intensity <I> above is properly averaged over the field of view of the instrument, and integrated over wavelengths from λ_1 to λ_2 nm.

The above value of <I> refers to the field of view of the instrument centered at one location (azimuth) of the ULV or DLV. For the DLV, two measurements are made,

approximately 180° apart in azimuth. These values at 178° and 358° can simply be averaged to give the average intensity, Iave in azimuth. Thus we have

$$I\mathit{ave} = 0.5(< I_{178} > + < I_{358} >) \tag{49.}$$

Finally, the upward flux, Fup between λ_1 and λ_2 nm is given by

$$\text{Fup} = \pi \text{ Iave} \tag{50.}$$

For the downward diffuse flux, measurements are made at azimuths relative to the sun of 5.5°, 140°, and 180°. It is possible to estimate Iave by averaging the measurements at 5.5° and 180°, or alternatively, to use the average value of a cosine (azimuth) function fit to the three measurements. Here

$$DN(j\ ) = \text{A} + \text{B}\cos(j\ ) \tag{51.}$$

The cosine function needs to be determined to get the direct beam flux, so this is available for use in the diffuse downward flux. In that case, the diffuse downward flux, F down dif, is given by

$$\text{Fdowndif} = \frac{p\,(\text{A} - DN\mathit{dark})}{(0.8571)\text{Resp}_{meas}} \tag{52.}$$

Determination of Direct Flux

When the sun is located at a zenith angle J_s and the instrument is pointed at an azimuth j_S relative to the sun, the instrument produces a response

$$\begin{aligned} &DN - DN\mathit{dark} = (DN_{diffuse}(j_s) - DN\mathit{dark}) \\ &+ \text{Resp}_{peak}\iint Isun(l, J_s, j_s)\text{Rel}_{spec}(l)\,dl\,\text{Rel}_1(J_s, j_s)\,d\Omega \end{aligned} \tag{53.}$$

Here $\text{DN}_{\text{diffuse}}$ is the signal due to diffuse sky light on the field of view of the instrument when centered at azimuth j_S relative to the sun. The intensity of the sun can be thought of as the flux from the direct solar beam divided by $\Delta\Omega_s$, the solid angle of the sun. The limits of integration of the direct solar beam, $d\Omega$, are also the solid angle of the sun. Thus, we have

$$DN - DNdark = (DN_{diffuse}(j_s) - DNdark) + \mathrm{Resp}_{peak} \int \frac{F_{sun}(l, J_s, j_s)}{\Delta\Omega_s} \mathrm{Rel}_{spec}(l) dl \, \mathrm{Rel}_1(J_s, j_s) \Delta\Omega_s \quad (54.)$$

This becomes

$$DN - DNdark = (DN_{diffuse}(j_s) - DNdark) + \mathrm{Resp}_{peak} \mathrm{Rel}_1(J_s, j_s) 0.8571 F_{350}^{475} \quad (55.)$$

Now we write the diffuse counts at the azimuth of the direct flux measurement as the cosine function determined from the measurements where the direct beam was shaded, from (51). This gives

$$DN - DNdark = (A + B\cos(j) - DNdark) + \mathrm{Resp}_{peak} \mathrm{Rel}_1(J_s, j_s) 0.8571 F_{350}^{475} \quad (56.)$$

Substituting for the peak response and solving for the integrated flux of the direct beam gives

$$F_{350}^{475} = \frac{[DN(j_s) - DNdark - (A + B\cos(j_s) - DNdark)] \iint \mathrm{Rel}_1(J, j) d\Omega}{0.8571 \mathrm{Resp}_{meas} \mathrm{Rel}_1(J_s, j_s)} \quad (57.)$$

Substituting the values of the terms determined above gives

$$F_{350}^{475} = \frac{[DN(j_s) - DNdark - (A + B\cos(j_s) - DNdark)] 0.6702}{(0.8571) \mathrm{Resp}_{meas} \mathrm{Rel}_1(J_s, j_s)} \quad (58.)$$

The downward flux carried by the direct solar beam is Fdown dir and is given by

$$\mathrm{Fdowndir} = \cos(J_s) F_{350}^{475} \quad (59.)$$

The total downward flux is the sum of the direct downward flux and the diffuse downward flux. The total downward flux minus the upward flux is the net flux. The change in the net flux between two altitudes is the flux absorbed by the intervening layer and is available for heating the layer.